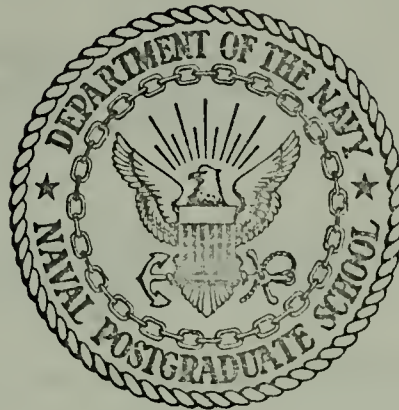


HOLOGRAPHIC INTERFEROMETRY OF THE FLOW
FIELD BETWEEN A FIN AND FLAT PLATE

Robert Ward Heyer

NAVAL POSTGRADUATE SCHOOL

Monterey, California



THESIS

Holographic Interferometry of The Flow
Field Between a Fin And Flat Plate

by

Robert Ward Heyer

Thesis Advisor:

D. G. Collins

March 1972

Approved for public release; distribution unlimited.

T147653

Holographic Interferometry of The Flow
Field Between a Fin And Flat Plate

by

Robert Ward Heyer
Lieutenant, United States Navy
B.S.E.E., Duke University, 1964

Submitted in partial fulfillment of the
requirements for the degree of

MASTER OF SCIENCE IN AERONAUTICAL ENGINEERING

from the

NAVAL POSTGRADUATE SCHOOL
March 1972

thesis
H/52635
c 1

ABSTRACT

This study was an attempt to map the density field in a fin-flat plate junction three-dimensionally using holographic interferometry. This investigation has extended the density studies by Matulka [12, 13] and Jagota [3, 4] to include, for the first time, interferometric fringe information obtained through a transparent model in supersonic flow. The fringe information was then inverted by a FORTRAN computer program to produce a plot of the density field around the model. The feasibility of the method was demonstrated.

The factors which are thought to have limited the success of the experiment include vibration of the model, fluctuations of the tunnel flow and the fact that the model was somewhat too large in relation to the size of the wind tunnel test section. Schlieren photography was used to look through and around the model and to verify that the same flow was established as was reported by Thomas [23, 24] and Winkelmann [26, 27].

The data reduction of holographic interferograms was, for the first time, accomplished using photographic enlargements. This technique is considered to be much easier and more accurate than the one used in the previous investigations. However, the data reduction step, because of the time and labor involved, is considered to be the rate controlling process of the whole analysis.

TABLE OF CONTENTS

I.	INTRODUCTION -----	6
II.	EXPERIMENTAL APPARATUS -----	7
	A. THE WIND TUNNEL -----	7
	B. THE HOLOGRAPHIC ARRANGEMENT -----	7
	C. THE WIND TUNNEL MODELS -----	8
III.	ANALYTICAL EVALUATION OF THE DENSITY FIELD ----	9
	A. THE BASIC INTERFEROMETRIC EQUATION -----	9
	B. THE INTEGRAL INVERSION -----	11
	C. THE NUMERICAL PROCEDURE -----	14
IV.	EXPERIMENTAL PROCEDURE -----	15
	A. LABORATORY TECHNIQUES -----	15
	1. Model Considerations -----	15
	2. Holographic Techniques -----	16
	a. Direct Fin-Root Flow Method -----	18
	b. Total Model Flow Method -----	18
	3. Schlieren Analysis -----	19
	B. PHOTOGRAPHIC TECHNIQUES -----	19
	C. DATA REDUCTION -----	20
V.	EXPERIMENTAL RESULTS AND DISCUSSION -----	22
VI.	CONCLUSIONS AND RECOMMENDATIONS -----	35
APPENDIX A:	Reduction Of An Interferogram To Obtain Fringe Shift Data -----	98
APPENDIX B:	Calculation Of Tunnel Wall And Grid Plastic Refraction Correction -----	101

APPENDIX C: Application Of Computer Program "Holofer"	125
BIBLIOGRAPHY -----	175
INITIAL DISTRIBUTION LIST -----	177
FORM DD-1473 -----	178

ACKNOWLEDGEMENTS

This writer wishes to gratefully acknowledge Dr. D. J. Collins for his most valuable guidance and assistance during the course of this investigation; Dr. T. H. Gawain for his valuable assistance and recommendations in the writing of this report; the technical staff of the Department of Aeronautics under R. Besel and T. Dunton, particularly N. Lechenby, J. Multon, and G. Middleton, for their able assistance in the fabrication and assembly of the models and equipment used in this study; Mrs. John B. Coleman Jr. for her considerable effort in the final preparation; and my wife and family for their noble patience and encouragement.

I. INTRODUCTION

The determination of the flow field in the wing-body junction of an aircraft in supersonic flight presents many problems. The typical approach has been to measure the static pressure on the surface using many small pressure taps [23, 24] and to determine the velocity field in the junction using translatable pressure probes [18, 19, 25]. Thomas [23, 24] and Winkelmann [26, 27] used azobenzene and oil-smear tests to view the flow field around a flat plate-fin junction. From the streak patterns on the plate and fin, they were able to illustrate the three-dimensional flow field, although in a partially speculative fashion. This study has attempted to map the density field in a fin-flat plate junction three-dimensionally using holographic interferometry. Although this objective was not fully achieved, the feasibility of the method has been demonstrated.

By using a Q-switched laser with exposure times of about twenty nanoseconds, it was possible to obtain three-dimensional holographic interferograms of the density field in the fin-flat plate junction. From holograms taken at a number of viewing angles the fringe shifts in different planes could be obtained. By integrating this information using a FORTRAN computer program, the density field can be determined. This technique has been previously demonstrated for the flow field of a free jet by Matulka [12, 13] and for the supersonic flow field around a cone at angle of attack by Jagota [3, 4].

The tests were performed at the Naval Postgraduate School, using the four-inch supersonic wind tunnel.

II. EXPERIMENTAL APPARATUS

A. THE WIND TUNNEL

The investigation was conducted in the Naval Postgraduate School blowdown-to-atmosphere supersonic wind tunnel. The test section is four inches by four inches in cross section and six inches long with two different sets of side walls. The two-inch thick plexiglas side walls, which have a refraction index of 1.49, present a complete field of view of the flow from the nozzle throat to aft of the test section mounting bracket (Figure 1 (a)). The second set of sidewalls used are aluminum with high quality optical glass portholes located in the test section area (Figure 1 (b)). The interchangeable nozzle for a test section Mach number of 2.8 was used for all tests. The nominal run time is five minutes at Mach 2.8 with the maximum stagnation pressure of about 105 pounds per square inch.

B. THE HOLOGRAPHIC ARRANGEMENT

The holographic arrangement is illustrated in Figure 2 and shown in photographs included as Figures 3, 4, and 5. The equipment stand was rested on a portion of the building floor that was vibrationally isolated. A Konrad K-1 pulsed ruby laser with a Pockels cell Q-switching unit was used to produce monochromatic light at a wave length of 6943 Angstroms and exposure time of twenty nano-seconds. The laser cavity length was seventy-three cm. giving a coherence length of about ten cm. To maintain the laser head and output etalon at a constant temperature of 27.5 degrees centigrade, a Lauda constant temperature circulator Model N was used. This was controlled by an electronic relay type R-10 coupled with a Culligan de-ionizer.

Holograms were obtained by routing the reference beam under the wind tunnel and the scene beam through the test section, and intersecting the two beams on the hologram plate at an intersecting angle of approximately 50 degrees. The beam sizes were controlled by translating the concave lenses located between the beam splitter and hologram plate in each beam (Figure 2). The Q-switched laser and optics were aligned using a continuous wave helium-neon laser. For reference purposes, grids were mounted on the outside tunnel walls and aligned using a surveyor's transit. The holographic stand and test section were completely enclosed in a wooden box to enable holograms to be taken in the daylight (Figure 6).

C. THE WIND TUNNEL MODELS

The fin-flat plate models used are shown in Figures 7 (a), (b), (c), and (d). The metal portions of both models were stainless steel. The center section, part of one strake, and all of the other strake of the first model in Figure 7 (a) were made of epoxy while the center section of the second model, Figures 7 (b) and 7 (c), was fabricated from plexiglas. The flat plate grids in both models were etched into the plastic surface and coated with a clear plastic to achieve a smooth surface.

The models were rotated about their sting mounts as shown in Figure 7 (d). Alignment for the desired rotation angle was accomplished by aligning prescribed lines on the sting mount collar with a scribed mark on the sting stand using a surveyor's transit.

III. ANALYTICAL EVALUATION OF THE DENSITY FIELD

A. THE BASIC INTERFEROMETRIC EQUATION

Interferograms are created when two coherent light beams are superimposed on each other and projected on a viewing screen. The light and dark regions observed correspond to the relative phase difference between the two beams which are caused by a difference in the two optical path lengths. Consider a coherent beam which is split and then recombined on a viewing screen. A difference in optical path lengths of the two beams may be achieved in two ways in order to create an interferogram. The first is to make the physical distance traveled by the two beams different. In a vacuum this path length difference is expressed as $L = C_0 \Delta t$ where C_0 is the speed of light in a vacuum. The second way is to maintain equal physical path lengths but to have the beams traverse through different media prior to recombining. In this case each light beam will travel at a speed $\frac{C_0}{n}$ where n is the index of refraction for the medium traversed. The optical path length difference then becomes:

$$\Delta L = L (n_2 - n_1) = C_0 \Delta t \quad (1)$$

The interference pattern or fringes observed may be expressed as a function of the optical path length difference or

$$g = \frac{\Delta L}{\lambda} \quad (2)$$

where: g = fringe shift

λ = wave length of the light source

ΔL = change in optical path

Combining equations (1) and (2), the fringe shift is then

$$g = \frac{L}{\lambda} (n_2 - n_1) \quad (3)$$

The index of refraction is known to be a function of density. Since the speed of light is only slightly less in gases than in a vacuum, the index of refraction could be closely approximated by the series expansion [8]

$$n = 1 + \beta \frac{\rho}{\rho_s} \quad (4)$$

where

β = dimensionless constant related to the Gladstone-Dale
constant by $K = \beta/\rho_s$

ρ_s = reference density of 0° C, 760 mm. Hg.

The variation of β with wavelength is small and has a value of 0.000292 for $\lambda = 5893$ angstroms.

Considering a fixed difference in the index of refraction between the two beams in Equation (3), then

$$g = \beta \frac{L}{\lambda} \left(\frac{\rho_2 - \rho_\infty}{\rho_s} \right) \quad (5)$$

If the density varies in a beam path, the net change in the optical path length will be the integrated effect along the beam path or

$$g = \frac{\beta}{\lambda \rho_s} \int_0^L (\rho - \rho_\infty) ds = Q \int_0^L f(x, y, z_c) ds \quad (6)$$

where

$$Q = \frac{\beta \rho_\infty}{\lambda \rho_s} \quad (6a)$$

$$f(x, y, z_c) = \frac{\rho(x, y, z_c)}{\rho_\infty} - 1 \quad (6b)$$

z_c = a plane of constant z

ds = incremental distance along the ray

In order to determine the density along the beam path where the fringe shift is known from an interferogram, Equation (6) must be inverted.

B. THE INTEGRAL INVERSION

The integral inversion technique was first reported by C. D. Maldonado et al in 1965 [9, 10, 11]. R.D. Matulka [12, 13] and R. C. Jagota [3, 4] used this method to determine the density variation in an asymmetric free jet and about a cone at angle of attack, respectively. The technique involves representing the function, $f(x, y, z_c)$ in Equation (6) by a complete set of orthogonal functions where the unknown coefficients are evaluated using the orthogonality relationship between the set of functions. The functions are orthogonal over the entire plane and also have the property of being invariant in form to any rotation of the coordinate system. Figure 8 illustrates the coordinate system for the inversion where x and y are the fixed laboratory coordinates and x' and y' are the coordinates in which the fringe number function is defined. As the view through the test section is varied the primed coordinates are rotated with respect to the fixed coordinates x and y .

The fringe shift expressed in Equation (6) may be written as the transform

$$g(\xi, y, z_c) = f(x, y, z_c) \quad (7)$$

or, inverting the equation, the density function, f , is equal to:

$$f(x, y, z_c) = T_g^{-1}(\xi, y, z_c) \quad (8)$$

The density function can be expanded in the following manner using a set of polynomial functions, $U_{m+2k}^{\pm m}(\alpha x, \alpha y)$, and unknown complex coefficients, $C_{m+2k}^{\pm m}(\alpha)$

$$f(x, y, z_c) = \sum_{m=0}^{\infty} \sum_{k=0}^{\infty} \epsilon_m \left[C_{m+2k}^m(\alpha) U_{m+2k}^m(\alpha x, \alpha y) + C_{m+2k}^{-m}(\alpha) U_{m+2k}^{-m}(\alpha x, \alpha y) \right] e^{-(\alpha^2 x^2 + \alpha^2 y^2)} \quad (9)$$

where

$$\epsilon_m = \begin{cases} 1/2 & m=0 \\ 1 & m=1, 2, 3, \dots \end{cases}$$

α = arbitrary scale factor

The polynomial functions, $U_{m+2k}^{\pm m}(\alpha x, \alpha y)$, are invariant in form to a rotation of the coordinate system [10, 12, 13]. They also have a Gauss transform which makes them adaptable to the physical situation and to manipulating into the form of Equation (7). The functions are defined as:

$$U_{m+2k}^{\pm m}(\alpha x, \alpha y) = (-1)^k \alpha \left[\frac{k! (\alpha^2 x^2 + \alpha^2 y^2)^m}{\pi (m+k)!} \right]^{\frac{1}{2}} e^{\pm i m \phi} L_k^m(\alpha^2 x^2 + \alpha^2 y^2) \quad (10)$$

where $\phi = \tan^{-1}\left(\frac{y}{x}\right) - \frac{\pi}{2}$ (10a)

L_k^m = Laguerre polynomial

$$= \sum_{s=0}^k \left[\frac{(m+k)!}{(k-s)!(m-s)!s!} \right] [(-1)^s (\alpha^2 x^2 + \alpha^2 y^2)]^s \quad (10b)$$

And the Gauss Transform of $U_{m+2k}^{\pm m}$ is:

$$I_{m+2k}^{\pm m}(\alpha y'; \xi) = \int_{-\infty}^{\infty} U_{m+2k}^{\pm m}(\alpha x, \alpha y) e^{-\alpha^2 x'^2} dx' = \frac{e^{\pm i m \xi} H_{m+2k}(\alpha y')}{[k! (m+k)!]^{\frac{1}{2}} 2^{m+2k}} \quad (11)$$

where $H_{m+2k}(\alpha y') =$ Hermite polynomials

By applying the transform above to Equation (9), the fringe function in

Equation (7) can be written as:

$$g(\xi, y, z_c) = \sum_{m=0}^{\infty} \sum_{k=0}^{\infty} \frac{\epsilon_m [C_{m+2k}^m(\alpha) e^{im\xi} + C_{m+2k}^{-m}(\alpha) e^{-im\xi}] H_{m+2k}(\alpha) e^{-\alpha^2 y'^2}}{[k!(m+k)! 2^{2(m+k)}]^{1/2}} \quad (12)$$

using the following orthogonality relationship on Equation (12)

$$\int_{-\pi}^{\pi} e^{\pm im\xi} e^{\mp in\xi} d\xi \int_{-\infty}^{\infty} H_{m+2k}(\alpha y') H_{n+2l}(\alpha y') e^{-\alpha^2 y'^2} dy' = \frac{2\pi}{\alpha} \left[(m+2k)!(n+2l)! 2^{m+2k} 2^{n+2l} \delta_{mn} \delta_{(m+2k)(n+2l)} \right] \quad (13)$$

where δ is the kroneker delta, the expansion coefficients $C_{m+2k}^{\pm m}$, can be determined by:

$$C_{m+2k}^{\pm m}(\alpha) = \frac{\alpha}{2\pi^{3/2}} \left[\frac{(k!(m+k)!)^{1/2}}{(m+2k)!} \right] \int_{-\pi}^{\pi} g(y', \xi, z_c) H_{m+2k}(\alpha y') e^{\mp im\xi} dy' d\xi \quad (14)$$

Substitution of the coefficients in Equation (14) back into Equation

(9) results in the density variation being expressed as:

$$f(x, y, z_c) = \left(\frac{\alpha}{\pi}\right)^2 \sum_{m=0}^{\infty} \sum_{k=0}^{\infty} \epsilon_m [k!(m+k)!]^{1/2} e^{-(\alpha^2 x^2 + \alpha^2 y^2)} \cdot \text{REAL} \left[\int_{-\pi}^{\pi} \int_{-\infty}^{\infty} g(y', \xi, z_c) e^{-im\xi} H_{m+2k}(\alpha y') dy' d\xi \right] U_{m+2k}^m(\alpha x, \alpha y) \quad (15)$$

or by inserting Equation (10):

$$f(x, y, z_c) = \left(\frac{\alpha}{\pi}\right)^2 \sum_{m=0}^{\infty} \sum_{k=0}^{\infty} \epsilon_m \frac{(-1)^k k!}{(m+2k)!} (\alpha^2 x^2 + \alpha^2 y^2)^{m/2} L_k^m(\alpha^2 x^2 + \alpha^2 y^2) \cdot [B_{m+2k}^m(\alpha) \cos(m\phi) + D_{m+2k}^m(\alpha) \sin(m\phi)] e^{-(\alpha^2 x^2 + \alpha^2 y^2)} \quad (16)$$

where:

$$B_{m+2k}^m(\alpha) = \int_{-\pi}^{\pi} \int_{-\infty}^{\infty} g(y', \xi, z_c) \cos(m\xi) H_{m+2k}(\alpha y') dy' d\xi \quad (17)$$

$$D_{m+2k}^m(\alpha) = \int_{-\pi}^{\pi} \int_{-\infty}^{\infty} g(y', \xi, z_c) \sin(m\xi) H_{m+2k}(\alpha y') dy' d\xi \quad (18)$$

Equations (16), (17), and (18) are the basic equations used to calculate the density distribution from the experimentally determined fringe variations.

C. THE NUMERICAL PROCEDURE

The form of the density distribution in Equations (16), (17), and (18) must be modified in order to input the experimentally determined fringe distribution. First from Figure 8 and Equation (6b) it can be seen that it is only necessary to integrate Equations (17) and (18) over an area where the density is changing from a known density, ρ_{∞} . Outside of this region where there is no change in density, the function $f(x,y,z_0) = 0$, i.e. outside the test section. Also since the fringe distribution is taken in small increments over the test area the coefficients, B and D, can be approximated as

$$B_{m+2k}^m(\alpha) = \sum_{i=1}^{I-1} \sum_{j=0}^{J-1} g(\xi_j + \Delta\xi_j, x_i + \Delta x_i) \int_{\xi_j}^{\xi_{j+1}} \cos(m\xi) d\xi \int_{x_i}^{x_{i+1}} H_{m+2k}(\alpha x) dx \quad (19)$$

$$D_{m+2k}^m(\alpha) = \sum_{i=1}^{I-1} \sum_{j=0}^{J-1} g(\xi_j + \Delta\xi_j, x_i + \Delta x_i) \int_{\xi_j}^{\xi_{j+1}} \sin(m\xi) d\xi \int_{x_i}^{x_{i+1}} H_{m+2k}(\alpha x) dx \quad (20)$$

The integral of ξ is easily determined and by using the derivative formula for Hermite polynomials the integral of x may be manipulated to yield

$$B_{m+2k}^m(\alpha) = \left[\frac{1}{2\alpha m(m+2k+1)} \right] \sum_{i=0}^{I-1} \sum_{j=0}^{J-1} g(\xi_j + \Delta\xi_j, x_i + \Delta x_i) \cdot [\sin(m\xi_{j+1}) - \sin(m\xi_j)] [H_{m+2k+1}(\alpha x_{i+1}) - H_{m+2k+1}(\alpha x_i)] \quad (21)$$

$$D_{m+2k}^m(\alpha) = - \left[\frac{1}{2\alpha m(m+2k+1)} \right] \sum_{i=0}^{I-1} \sum_{j=0}^{J-1} g(\xi_j + \Delta\xi_j, x_i + \Delta x_i) \cdot [\cos(m\xi_{j+1}) - \cos(m\xi_j)] [H_{m+2k+1}(\alpha x_{i+1}) - H_{m+2k+1}(\alpha x_i)] \quad (22)$$

In the computation of the density function from Equation (16), obtaining the infinite summations experimentally is not plausible or

possible. It has been demonstrated that by using a finite number of terms and by adjusting the values of $\Delta \xi$, Δx and α , it is possible to obtain the density distribution with very good accuracy [3, 4, 12, 13]. Equation (16) then becomes:

$$\begin{aligned} f(x, y, z_c) = \left(\frac{\alpha}{\pi}\right)^2 \sum_{k=0}^K \sum_{m=0}^M \epsilon_m (-1)^k \left[\frac{k!}{(m+2k)!} \right] (\alpha^2 x^2 + \alpha^2 y^2) \cdot \\ L_k^m(\alpha^2 x^2 + \alpha^2 y^2) \left[B_{m+2k}^m(\alpha) \cos(m\phi) + D_{m+2k}^m(\alpha) \sin(m\phi) \right] \cdot \\ e^{-(\alpha^2 x^2 + \alpha^2 y^2)} \end{aligned} \quad (23)$$

IV. EXPERIMENTAL PROCEDURE

A. LABORATORY TECHNIQUES

The analysis of a free jet by Matulka [12, 13] illustrated how holographic interferometry can be used to obtain a complete three dimensional plot of the density within a moving transparent flow field. Jagota [3, 4] in his study of a cone at angle of attack in supersonic flow went one step further by introducing an opaque object into an assumed steady state flow field and describing the density field three-dimensionally.

This investigation has attempted to determine the three-dimensional density field around a transparent object in a supersonic flow field by passing a light beam through the object. Specifically the interest was to describe the flow field existing in the junction of a fin-root intersection.

1. Model Considerations

In order to obtain uniform flow around the fin-root area, a model of the form shown in Figure 9 was selected. The flat plate has a knife

edge and is intended to remain at zero degrees angle of attack so as to establish the flow conditions illustrated. The fin edges were made circular in order to approach flow conditions similar to those established in Winkelmann's [26, 27] investigation. Plastic and metal strakes were added on the model sides so as to maintain two-dimensional flow as well as to add strength to the flat plate. In the first model constructed (Figure 7(a)), maximum visibility of the plastic fin-flat plate center section was achieved by bolting the leading edge and aft plate together through the plastic center section. Due to model flexure, this design was found to be unsuitable and the second model in Figures 7(b) and 7(c) was constructed. The model was made from a single piece of stainless steel. The model rigidity was satisfactory but unfortunately the strengthening borders around the plastic center section reduced the holographic visibility somewhat.

Since the wind tunnel blocks were fixed, it was possible to make multiple test runs with the same flow conditions over the model provided supersonic flow had been established over the model.

2. Holographic Techniques

In order to obtain holographic interferograms it was necessary to ensure that the optical path lengths of the scene and reference beams remained approximately equal. Since the ruby laser is believed to have a coherency length of approximately ten centimeters, the equality of lengths is far less critical than in the classical Mach-Zehner interferometric approach. Consequently a string was used in the experiment to trace the reference beam and then adjust the scene beam. This method kept the two beam lengths within one centimeter of each other. Since the scene beam traversed approximately 4.5 inches of plastic tunnel walls and

grids which the reference beam did not, it was necessary to compensate by making the scene beam physically 2.25 inches shorter than the reference beam. The reference beam varied in length from 61 inches to 68 inches during the experimentation.

To determine the fringe/density field, finite fringe interferograms were made by three different techniques. In the direct fin-root flow approach the diffuser plate was part of the model. Either the mirror, M_5 , in Figure 2 or the hologram plate holder was translated between the no-flow exposure and the flow-established exposure. In the total model flow method the diffuser plate was located between scene beam lens, L_3 , and the test section (See Figure 2) and it was translated horizontally or vertically. Translations were varied from .001 inches to .006 inches with the translation distance of .003 inches yielding the best fringe separation.

Most of the holograms taken using basically the holographic arrangement shown in Figure 2 gave well-defined fringe patterns. In order to improve upon the fringe definition, a variety of techniques was attempted. The transverse mode selector was varied from 1.0 mm. to 2.5 mm. in increments of 0.5 mm. to determine the best lighting of the model. The hologram plate holder was rotated horizontally to various positions. These positions varied between being perpendicular to the scene beam to being perpendicular to the bisection of the angle between the scene and reference beams. Polarization plates were added in both the scene and reference beams between the test section and hologram plate in the scene beam and between the last mirror, M_4 , and the hologram plate in the reference beam. A one-quarter wave plate was also placed between the first lens, L_1 , and the beam splitter as recommended by Okayama and Emori [14].

The holograms were taken using 4" x 5" Agfa-Gavaert 8E-75 hologram plates. The developing process involved:

1. Five minutes in Kodak D-19 developer
 2. Thirty seconds in an acetic acid stop bath
 3. Five minutes in standard fixer
 4. Five minutes in a flowing water bath
 5. One minute emersion in Kodak Photo Flo wetting agent
 6. Drying using blowing cool air
- a. Direct Fin-Root Flow Method

Since the flow field in the fin-root junction is assumed to be identical on either side of the fin, then it is only necessary to determine the density on one side of the fin. To accomplish this it is necessary to obtain holograms for 180° of view as shown in Figure 10. The holograms for the views from 0° to 90° can be obtained by using a frosted fin and flat plate as shown in Figure 11. The advantage of having the frosted plate as part of the model is that the fringe/density information obtained by the interferogram is believed to be only for the area between the fin-root intersection to the tunnel wall vice the whole test section, but this was not verified. In order to obtain the fringe information for angles greater than 90° but less than 180° the fin would be exchanged for one containing a stainless steel reflective surface. The scene beam would then enter the test area from the viewing port below the tunnel and be reflected to the hologram plate as shown in Figure 12.

- b. Total Model Flow Method

In this method the diffuser plate was located in the scene beam outside the test section as shown in Figure 14 and the flat plate

center section and fin were made of optically clear plexiglas. By translating the diffuser plate between exposures of the hologram, an interferogram of the whole density field in the test section about the model was obtained. From Figure 13 it can be seen that due to symmetry only 90° of view was required to obtain the density field. This makes it much easier experimentally to take the holograms than the previous method described.

3. Schlieren Analysis

A standard Schlieren knife-edge system was used to verify the establishment of the supersonic flow network around the model as shown in Figure 9. Photographs were also taken of the flow with the model at 0° and 90° rotation in order to compare the fin shock conditions with those obtained by Winkelmann [26, 27].

B. PHOTOGRAPHIC TECHNIQUES

By illuminating the holograms with a helium-neon laser beam which has a wave length of 6328 Angstroms, the original scene was reconstructed. Since the original scene beam and the reconstructed beam were of different wave lengths, there is actually a small distortion in the reconstructed scene but of neglectable effect because the hologram plate emulsion in the development process also shrinks.

The typical method for reconstructing the scene is to illuminate the hologram as illustrated in Figure 15. The diffuse glass used in the construction of the hologram appears to act as an infinite light source of non-parallel rays which illuminates the scene. If a small aperture is positioned at the focal plane of the imaging lense, an almost parallel set of rays may then be selected as shown in Figure 16. A third method

illustrated in Figure 17 uses a small diameter conjugate beam to illuminate the hologram. A large depth of field is achieved because the narrow beam acts as an aperture. This effect was of considerable advantage since it enabled both the front and rear grids, the model, and the fringe patterns to be simultaneously projected on the screen. The best photographs were obtained by focusing on the plane of the fringes.

C. DATA REDUCTION

Photographic interferograms were obtained by illuminating the hologram scene with a thin laser beam and using a camera with a viewing screen located in the film plane as shown in Figure 15. The line of sight in the plane desired was achieved by translating the hologram until common points on the front and rear grids were aligned. The camera, with the aperture set wide open at $f/7.7$, was then adjusted to give the best focus on the fringe plane. The best photographic results were achieved by using an exposure time of $1/10$ second with Polaroid Type 55 P/N film.

It was felt that the density field could be well defined three-dimensionally along the fin if the density fields were determined in four planes perpendicular to the Z-axis and equally spaced along the fin as shown in Figure 18. In obtaining the fringe data across a constant Z-plane it would be necessary to take six photographs per rotation angle, aligned at appropriate intervals down the y' axis, and then graphically mate the fringe data to form one complete set. The six photos across the field were felt necessary because the optical path length from the model to the hologram plate varied for those points not on the aligned plane.

The fringe shift reduction was accomplished using two different techniques. The first was to project the negative, using a photo enlarger,

onto a sheet of paper and trace out the fringe pattern, model surfaces and grid lines. The light fringes were traced out since it was much easier to judge their center line. From the fringe lines forward of the fin in the region of uniform flow one fringe line which appeared the straightest and compatible with most others was selected as the bench mark. A straight line was then drawn over that fringe and extended past the aligned Z plane (i.e. y' axis). Lines parallel to the bench mark line were then drawn likewise over the remaining fringe lines. The fringe displacements were then read relative to the lines drawn at the points of intersection of the fringes with the y' axis. The radius of the inversion circle was selected so that the fin-root intersection was the origin and the fin tip was the 100 percent point.

In the second technique an enlarged positive photograph was made from the negative. Again one fringe line in the uniform flow region just forward of the fin which appeared to be parallel with the majority of the fringes was selected as the bench mark. The remaining fringes were likewise traced over with lines parallel to the first. The fringe displacements were then measured relative to the lines drawn. For further details see Appendix A.

The locations at which reference lines crossed the y' axis in both techniques above were further adjusted to account for the tunnel wall refraction displacement as shown in Figure 19 and computed by a computer program in Appendix B. Once these corrections were made, the radial variation of the fringe number could then be plotted for the various y' alignment planes and a smooth curve drawn through the data points. The fringe number at 201 equidistant points across the field can then be obtained for input into the computer program, HOLOFER, in MODE 3. For

further details on how to use the computer program, HOLOFER, see Appendix C. Once the data from all the rotation angles of the model have been put into the computer program, the program will then calculate the density field across the inversion circle for that Z-plane. After the density has been calculated for all four Z-planes in Figure 18, a three-dimensional plot of the density field can be made by connecting points of equal density across the fin.

V. EXPERIMENTAL RESULTS AND DISCUSSION

The initial attempts to establish uniform flow over the flat plate shown in Figure 7(a) were unsuccessful due to model vibration and flexure. Movement of the model sting within its holder and flexure of the model plastic center section allowed the model leading edge to establish a little over 1° angle of attack upward when flow was established. Due to various modifications made in attempts to eliminate the vibration, the sting finally fractured.

In an attempt to eliminate these problems, the second model shown in Figures 7(b) and 7(c) was made of a single piece of stainless steel and the sting was mated to its holder to within .001 inches. The model center section was made of poured epoxy and the strakes were both made of stainless steel with plexiglas inserts. The model rotation about the sting was reduced to approximately 0.3° angle of attack upward. Due to the vibration in passing through the transonic range and a weak glue seal between the metal strakes and plexiglas inserts, the inserts were found to break loose. They were subsequently removed and not replaced.

In order to determine the flow field using the direct fin-root approach, the epoxy fin and model center section were frosted on one side using fine

emery paper (see Figure 20). Holograms were taken of the model at rotation angles of 0° , 12° , 45° and 90° using the holographic arrangement in Figure 2 excluding the diffuser plate between lens, L_3 , and the test section. The mirror, M_5 , was translated in various directions from towards to parallel to the test section between the exposures without flow and with flow established. Fringe patterns were obtained around the model, but only at 0° and 12° rotation could any fringe patterns be observed across the fin. It was found that the fin fringe pattern appeared to remain almost unchanged no matter how or how much the mirror, M_5 , was translated while the fringe around the model changed appropriately. For instance, in Figure 21 the mirror was not translated and in Figure 22 the mirror was translated .006 inches horizontally parallel to the tunnel.

Since fringes could not be observed across the flat plate at 45° and 90° , it was felt that the epoxy center section might be too imperfect optically. Consequently double-exposed holograms were taken with no flow through the test section and various translation distances from 0 to .005 inches. The fringe patterns were excellent across the whole model and their spacing decreased according to the increase in the translation of M_5 . Next the diffuser plate in the scene beam in Figure 2 was inserted with the model at 0° rotation angle and translated between no flow and flow exposures of the hologram. The fringes about the model were of excellent quality but the double diffusion of the scene beam through the model caused all fringe patterns on the model (fin) to disappear.

It was felt at this point that the fringe pattern obtained across the fin was caused by the movement of the model to an angle of attack and possibly by model vibration, although none was observed visually. The

lack of any fringes across the flat plate center section is not well understood but is believed to be caused by vibration of the model.

Since it was not possible to obtain acceptable interferograms with the diffuser plate as part of the model due to model motion, it was felt that the effect of minor model movements could be eliminated by using an optically clear model and an external translating diffuser plate. Therefore the fin and model center sections were replaced with optically clear plexiglas. With these changes it was found that the flat-plate leading-edge angle of attack had been reduced to approximately 0.1° .

Initially double-exposure holograms were taken using the arrangement in Figure 2 and translating the diffuser horizontally. At 0° model rotation the holographic interferograms were excellent. But as observed in Figure 23 it would be extremely difficult to determine the fringe change across the fin since no free stream reference fringes were available, due to the flat plate leading edge Prandtl-Meyer expansion and fin shock intersecting the tunnel top just above the fin. With a larger tunnel or smaller model this would be an excellent technique.

The diffuser plate was then translated vertically between exposures and excellent horizontal fringe patterns were obtained as shown in Figure 24. The model was then rotated to $22\frac{1}{2}^\circ$ and the same holographic technique was used. Excellent fringe patterns were obtained above and below the flat plate center section. Fringe patterns across the flat plate center section and fin in this area were very light and usable interferograms could not be photographed with the polaroid camera. In an attempt to improve on the fringe quality, polarizer plates were inserted in the reference beam between the mirror, M_4 , and the hologram plate and in the scene beam between the lens, L_3 , and the diffuser plate in order to ensure

polarization of both beams. No significant improvement could be noticed and they were subsequently removed. A one-quarter wave polarizer plate was then placed between the lens, L_1 and the beam splitter in order to utilize circularly polarized light for the reference and scene beams. Okayama and Emori [14] found that their image resolution improved considerably; however, with this particular arrangement little to no improvement in the fringe resolution was observed and the approach was abandoned.

The transverse mode selector was then varied from 2.0 mm. to 1.5 mm. and later to 1.0 mm. in an effort to improve the coherency length of the laser light and consequently the image resolution. Due to the decrease in output light intensity, up to six exposures were taken during a run with flow established. Image and fringe definition were not found to increase possibly due to model vibration which was not visible to the eye.

The model was rotated to 45° and $67\frac{1}{2}^\circ$ and double exposure holograms were taken with a 2.5 mm. transverse mode selector. There were no observable fringe patterns in any portion of the test section. Consequently it was believed that supersonic flow was not established due to tunnel blockage caused by the shock wave from the model and by slight model vibrations in passing through the transonic range. In the transition to supersonic flow, the model leading edge would sometimes flex as much as 0.2° depending upon the transition time.

The test section walls were changed from the total plexiglas side walls shown in Figure 1(a) to the aluminum walls with the optical quality glass port holes (Figure 1(b)). The better quality glass would hopefully improve the viewing and the port holes made the model much more accessible. The metal strakes were also removed from the model since they appeared to have a minimal effect on the flow, were an interference optically,

and appeared to add very little structurally. Flow tests were run and the model was found to attain an angle of attack of about 0.14° upward when flow was established at Mach 2.84. The angle of attack was tolerable, however the model also maintained a visible high frequency vibration of about $\pm 0.05^\circ$. Double exposure holograms were taken with the model at 0° rotation and fringes could only be observed forward of the Prandtl-Meyer expansion on the top of the model and forward of the flat plate leading edge shock on the bottom. The tunnel seals were found to leak and were replaced and resealed. The same angle of attack and high frequency model vibration still persisted. Double exposure holograms were again taken and a very faint fringe pattern was observed across the model. In reproducing the scene when aligned along a constant Z-plane passing through the fin, it was impossible to photograph the fringe pattern across the fin because of a bad speckle effect. Double exposure holograms were made at model rotation angles of 45° and 90° without and with flow. The holograms taken without flow gave excellent fringe patterns across the model however no fringes could be observed with flow.

At this point a knife edge Schlieren system was set up to determine just what the flow conditions were in the tunnel and around the model. The first runs were made at a model rotation angle of 90° and presented the shock knee in front of the fin (Figures 25(a) and 25 (b)) which was pointed out by Thomas [23, 24] and Winkelman [26, 27]. Due to the model vibration, the shock extending out from the shock knee was observed to flutter about $\pm \frac{1}{2}$ cm.

The model was then rotated back to 0° and Schlieren photographs were taken as shown in Figure 26. During all but one of the runs at this rotation angle, the model would pitch up approximately 0.14° angle of attack and continue to vibrate about $\pm 0.05^\circ$ at a high frequency when

flow was established. The plate leading edge shock and fin shock appeared quite fuzzy and light. Due to oil from the tunnel supply reservoir mixing in the flow, a light oil smear pattern can be observed across the fin in Figure 26. During one run, which could not be duplicated, the model pitched up as flow was established but did not vibrate. The plate shock and Prandtl-Meyer waves, fin shock system, and tunnel Mach lines became very distinct and well defined as seen in Figure 27. The schematic of the Schlieren photographs in Figure 28 points out the cause for the various flow lines observed. The non-uniformity of the free stream caused by tunnel leakage can be easily seen. Consequently the experimental work was discontinued due to tunnel conditions and time considerations.

It was felt at this point that if the holographic interferogram taken of the clear plexiglas fin at 0° rotation angle could be reduced to useful data for the computer program then the holographic method would be to a certain extent verified even though the actual density field could not yet be determined.

In obtaining interferograms from the hologram, the reconstruction technique shown in Figure 15 was used. The plane of constant Z across the model to be reduced was chosen to be the forward most vertical grid line crossing the fin. It should be pointed out that in order to simplify the hologram alignment process, all four reduction planes across the model should have been scribed on the exterior grids. The three photographic points across the Z plane on the y' axis were, for convenience, chosen to be where horizontal exterior grid lines crossed the y' axis on the fin. Five interferogram photographs were taken at points A, B, and C as shown in Figure 29. Photographs 2 and 5 were taken using a Kodak Wratten Gelatin Filter N.D. 2.0 placed in the reconstruction beam in order to reduce the

beam intensity and increase the fringe definition. These two photographs were also used to provide a check on the consistency of the reduction process.

All five negatives were blown up on the photo enlarger in the dark room and the plate, fin, grid lines and fringes were traced out on a sheet of white paper as shown in Figures 30-34. It was very difficult to trace the fringes in the region of the fin tip and fin root due to the photographic resolution and the fin tip shadow. Also fringes were not visible in the region of the fin leading edge shock. Consequently, connecting the fringe in front of the fin to the correct fringe on the fin was a best guess effort. Typical of the problem was that fringe lines in two of the drawings were initially improperly connected across the fin leading edge shock. After being checked against the photograph negatives, the fringes were reconnected and the data taken correlated well with the data from other drawings. The fringes in the fin root area were extremely light in some photographs which made it quite difficult to determine their centerline crossing the y' axis. Another point of difficulty was determining the location of the top and bottom of the fin. An error in drawing here will have an effect later when the fringe locations are normalized with respect to the fin height.

Enlarged positives were then made from the negatives as shown in Figures 35-39 to see if the data accuracy could be improved by eliminating the difficulties of tracing the fringes in the dark room. This method also made it possible usually to reassess the assumed path of the fringe lines at a later time if the data did not appear to correlate properly. The same problems of locating the fringe lines in the region of the fin tip and of connecting the fringe lines across the fin shock are readily apparent in the figures.

To obtain the fringe change across the fin one of the straightest fringes in the free stream region which paralleled the majority of other free stream fringes was selected. A straight line was drawn through its centerline and extended to cross the y' axis. The other free stream reference lines were then drawn parallel to the first and adjusted so as to best follow the centerline of the selected fringe. This method actually averages the free stream conditions and is only valid if the free stream is essentially uniform. Since it was not possible to obtain in the photographs the free stream fringe pattern forward of the leading edge Prandtl-Meyer expansion for the lower fin region, the fringe reference lines in photo enlargements were drawn over the fringes just prior to the fin shock. In order to adjust them to free stream conditions their location was moved downward a distance equal to 1.1 times the average fringe interval for that photograph. The figure 1.1 was observed in all the enlarged photographs to be the approximate fringe change across the Prandtl-Meyer expansion. In the drawings (Figures 30-34), fringe reference lines for the lower fringes (generally $y' \leq .8$) were initially aligned along the straightest portion of the fringe prior to intercepting the fin shock. By comparing the reference line location on the drawing with the fringe pattern in the photographic enlargements the reference line location and fringe change were adjusted by an appropriate portion or all of the 1.1 fringe change caused by the Prandtl-Meyer expansion. All of the reference lines were then corrected for the tunnel wall and grid plastic parrallax shown in Figure 19 and computed in Appendix B. The reference fringe locations were then normalized with respect to the wing height and the fringe numbers calculated by dividing the fringe change by the average fringe interval. For further details and calculations see Appendix A.

The data obtained for alignment points A and C by the two different reduction processes are plotted in Figures 40-43. The data obtained from the photo enlargements aligned at point C and shown in Figure 43 gave the best data agreement between two photographs. The worst data agreement was obtained from the reduction of the drawings aligned at the same point. The inconsistency in the data was probably caused by connecting the wrong fringe lines across the fin leading edge shock. The data fluctuations and discrepancies between the curves in the figures could have been caused by a number of things. It could have been caused, for instance, by not drawing the fringe reference line parallel to or exactly on the free stream fringe center line or slightly missing the fringe center as it crosses the y' axis or by misconnecting fringe lines across the fin shock as was illustrated in Figure 42. Fringe location errors could be caused by misdrawing the fin tip and root lines as was mentioned earlier. Another contributor would be measurement errors.

To analyze these sources for error, first consider that the typical fin size in the drawings and photo enlargements averaged about 2.5 inches high and 2.75 inches wide and that the fringe spacing averaged about 0.10 inches. All measurements were taken using a ruler graduated in 0.01 inches and readings were made to the nearest .005 inches. Since the average difference between the data points and curves ran around $\frac{1}{4}$ fringe, some figures were calculated to determine what measurement errors could produce this fringe error. It was found that an error of .025 inches in alignment of the fringe reference line with the free stream fringe center line and/or fringe center line crossing the y' axis could produce $\frac{1}{4}$ fringe error. This fringe error will also occur if the fringe reference line differs from the free stream center line by more than 1.4° when drawn 1 inch from the y' axis or by more than 0.36° when drawn 4 inches from the

y' axis. A difference of .01 inches in the average fringe interval could also produce a $\frac{1}{4}$ -fringe error; however, this is not too likely since it is an average of fifteen to twenty-five intervals. By comparing the actual height-to-width ratio with those found in all the drawings and photo enlargements it was found that average error was around 2% or a distance of .02 on the y'-axis.

In order to compare the interferogram negative quality and the two different reduction techniques, a plot of the data for each negative was made as shown in Figures 44-48. Photographs 1 and 3 in Figures 44 and 46 gave the smoothest curves indicating the highest interferogram resolution. Photograph 5 (Figure 48) gave the worst dispersion indicating poor interferogram resolution; yet looking at the enlargement in Figure 39, the fringe line contrast is very good. In comparing Figures 40-48 it appears that the reduction technique using the photographic enlargements gave the most consistent data. This technique also provides a much easier and faster recheck on the proper tracing of fringe lines because it is extremely difficult and tedious to duplicate the fringe pattern to the same scale over the drawings using the photo-enlarger in the dark room.

All the data obtained by either method for one alignment point were then plotted in Figures 49 and 50 in order to observe the dispersion. A fringe number dispersion of about 0.6 fringes was observed in the data taken from the negatives aligned at point A and a dispersion of about 0.8 fringes for the data about point C. The dispersion is attributable to the inaccuracies in the drawings, to the photographic quality of the interferograms, and to the inaccuracies in correcting the lower fringe reference lines to free stream conditions. The last point is based upon the increased dispersion between the fin tip and fin root data.

Figures 51 and 52 show an integrated curve of the fringe change across the wing as determined by each reduction method. In constructing the curve, the data from the three aligned points was plotted so as to just overlap each other. These two curves were then compared in Figure 53. The maximum variation in the fringe number is about $\frac{1}{2}$ a fringe but the variations in the location of the fringe maximums and minimums average about 0.1 inches on the fin. The location difference is probably due to improper drawing of the fringe reference lines compounded with not being able to measure the wing height accurately. Due to the inaccuracies introduced in tracing the negative and then reducing the data it is felt that the photo enlargement method is the more accurate reduction method.

With fringe data from only one field of view, the density field, obviously, could not be obtained. It was felt useful to consider the flow field axisymmetric in order to exercise the computer program and to provide a check on the program's ability to handle these particular curve shapes. Fringe data at 101 equidistant points across the fin from $0 \leq Y' \leq 1.0$ was obtained from Figure 53 for both curves and fed in HOLOFER in Mode 3 for the axisymmetric case. For further details on HOLOFER see Appendix C. The scale factor, α , in Equation 9 was then varied from 0.2 to 2.5 and a value to 1.0 was determined to yield the most accurate density solutions. This value was verified by feeding the function data, $(\frac{\rho}{\rho_\infty} - 1)$, calculated by Mode 3 back into the program in Mode 1 and comparing the fringe data calculated with the original fringe data obtained from Figure 53.

The density distribution for both the drawing and photographic reduction cases is plotted in Figure 54. The density as Y' approaches zero actually goes as the drawn lines even though the points indicate a dip.

Matulka [12, 13] pointed out that the computer program accuracy does not converge at the origin. The large variations of the density curves at values of $Y' > 0.8$ are caused by the program trying to adapt to a step or shock wave type function at $Y' = 1.0$. If the remainder of the fringe data in Figure 53 for values of $Y' > 1.0$ had been included as input data the density curves would have smoothed out. This shock wave step function effect was demonstrated and analyzed by Matulka [12, 13].

The low values of density for the photographic data curve around $Y' = 0.38$ were unexpected but not surprising. First, the photographic fringe data curve is more extreme than the drawing fringe data curve and second, the density curves are not true values anyway since the field was considered axisymmetric and this is not the case in reality.

In general the density curves are felt to be reasonable under the assumed conditions. Consequently it is believed that the computer program could very easily and accurately handle a complete analysis of the flow field around the fin-flat plate.

In completing the analysis there are some data reduction problems which would have been encountered in reducing the interferograms at other model rotation angles which merit discussion. With no model rotation, adjusting the fringe reference lines close to the fin root to account for the leading edge Prandtl-Meyer expansion was relatively easy. However, when the model is rotated, the fringe shift across the Prandtl-Meyer expansion can no longer be considered a constant and it will be very difficult to adjust the fringe lines at lower values of Y' to free stream conditions. The best solution would be to increase the scene beam diameter and/or reduce the model size in order to photograph the free stream fringe lines forward of the plate leading edge. The free

stream lines could be connected to the appropriate fringe lines forward of the fin and this would eliminate the numerical correction and increase the fringe data accuracy.

Also at the rotated angles, fringe information will not be available for portions of the reduction plane due to shadows cast by the model sides as shown in Figure 55. In the lower portion of the hologram the fringe curve can be connected with a smooth line because the density field in that portion should be essentially constant. Care must be taken in completing the curve, though, since this information will be used in the integration of other rotation angles. The fringe curve in the upper portion must also be completed carefully but should be easier since the shadow will be smaller. For this particular model it was calculated that for angles greater than 46.6° the upper shadow would not penetrate the fin.

There are two more problems to be coped with which do not have apparent solutions at this time. The first has to do with the superimposing of fringe information from different locations onto one scene beam line as illustrated in Figure 56. In case I the superimposing of the fringe change in Region A onto that in Region C and locating the fringe reference line at point C' is tolerable because the density field in Region A should be fairly constant and uniform. However in case II where the fringe change in all three regions are superimposed and located at point C'', the answer is not readily apparent. If the plate and fin were of equal thicknesses then points A'' and C'' would be the same and the error would be somewhat reduced. If, in addition, the thicknesses were made as thin as structurally possible, the error would be reduced to a minimum. Also it might be possible to integrate the model geometry into the computer program but this has not been attempted.

With the model at rotation angles between 0° and 90° scene beam defraction at the fin root and tip areas would also present problems as seen in Figure 57. A minimization of the problem could again be achieved by minimizing the fin and plate thicknesses.

VI. CONCLUSIONS AND RECOMMENDATIONS

The investigation, although not totally successful, has demonstrated the feasibility of using holographic interferometry to determine the flow field around a transparent model by looking through the model. The problems of model vibration and movement, of superimposing different fringe information on one beam, and of scene beam divergence through the fin root and tip regions must still be solved. The model vibrations and rotation to an angle of attack are attributable to the tunnel pressure fluctuations caused by tunnel leaks and to possible movement of the sting holder. It is felt that all three problems could be decreased to neglectable effects by reducing the overall model size and by incorporating the model geometry into the computer program.

The basic holographic arrangement was found to work quite well for this type of experiment. The holograms were generally high quality except when unfavorable tunnel flow conditions existed. The use of circularly polarized light recommended by Okayama and Emori [14] did not increase the hologram resolution appreciably but the method merits further considerations because of their excellent results.

The data reduction process was found to be the rate-controlling step in the investigation due to the time and labor involved. Reducing the data from enlarged photographs of the interferogram saved some time and appeared to increase the data accuracy. The data scatter of $\pm 1/8$ fringe

was considered acceptable considering the fringe resolution in the holograms. It was felt that this could be reduced by using either a larger tunnel or a smaller model. With either of the changes it would be possible either to use the free stream fringe pattern forward of the model as the reference conditions across the whole model or to use a vertical fringe pattern, since the leading edge Prandtl-Meyer expansion and fin shock would not block out the free stream fringes above the fin. It appears that the use of vertical fringes would also considerably reduce the data reduction time.

With the use of Schlieren the flow network described by both Thomas [23, 24] and Winkelmann [26, 27] was verified to exist. From the top view (90° model rotation) the fin shock and its fluctuations were observed and photographed through the flat plate plastic center section.

The computer program, HOLOFER, was found to be quite capable of handling the type of flow field fringe data which would be generated in a complete analysis of this type. As pointed out before it is believed that the program should be modified to incorporate the model geometry.

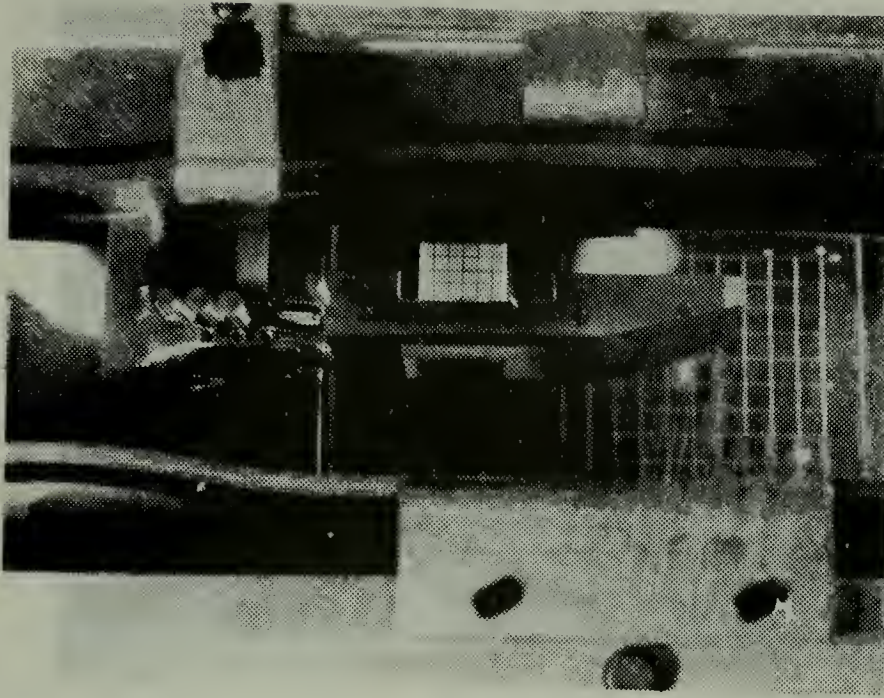


Figure 1(a). Wind Tunnel Test Section with Clear Plastic Side Walls

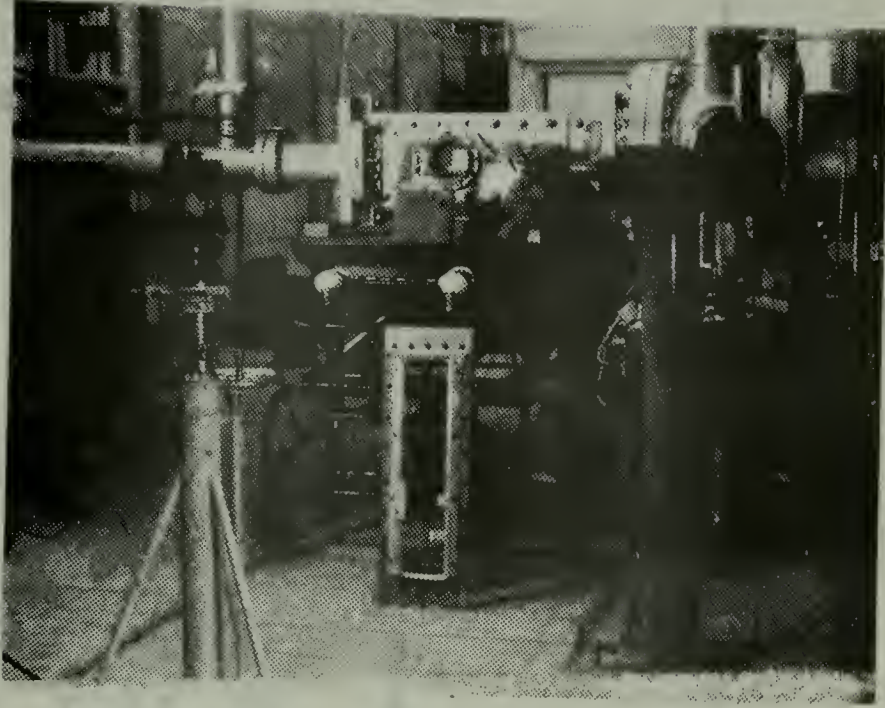


Figure 1(b). Wind Tunnel Test Section with Aluminum Side Walls

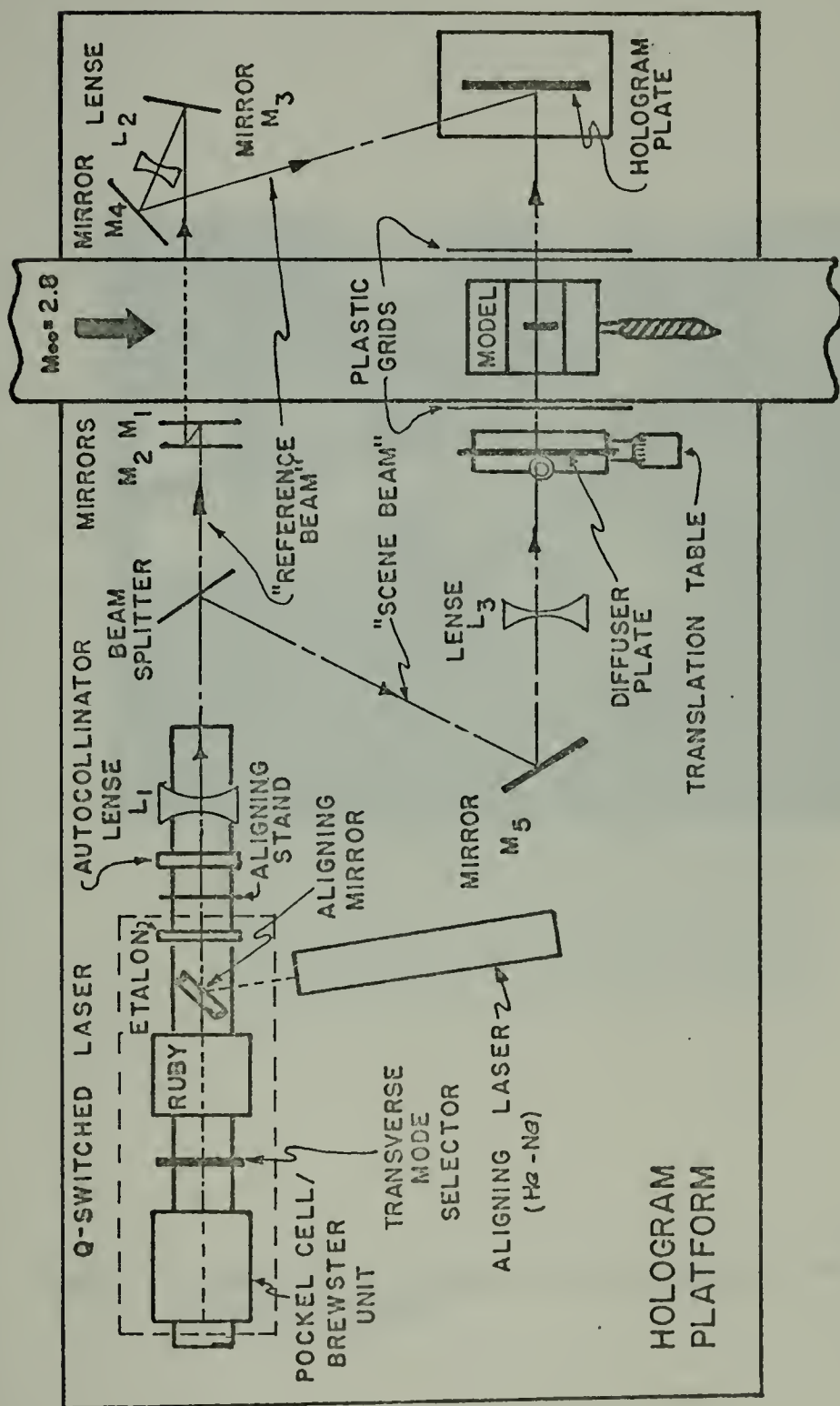


Figure 2. Schematic Representation of the Holographic Arrangement

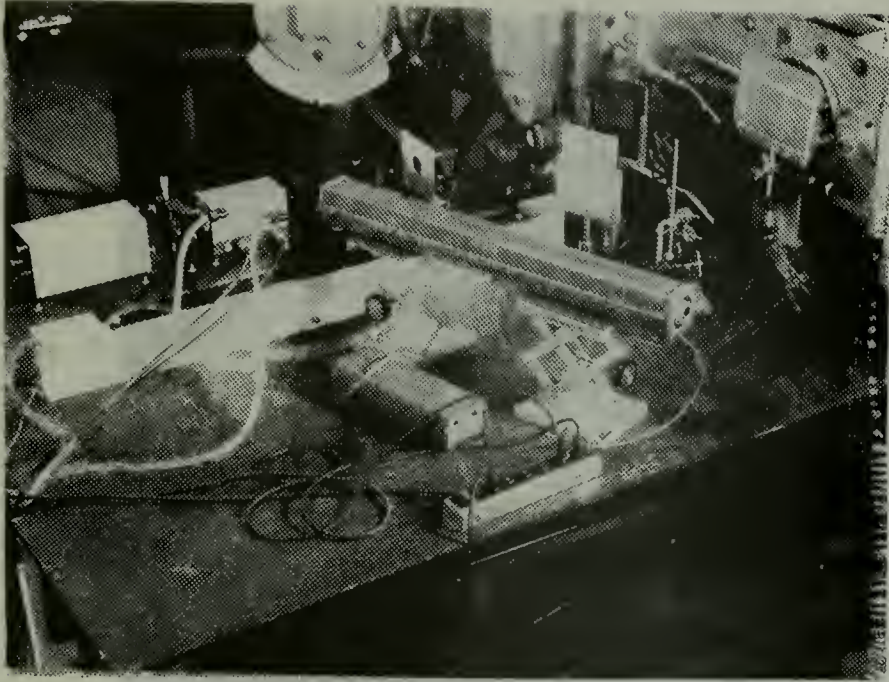


Figure 3. Holographic Arrangement Including the Laser Cooling and Aligning Equipment

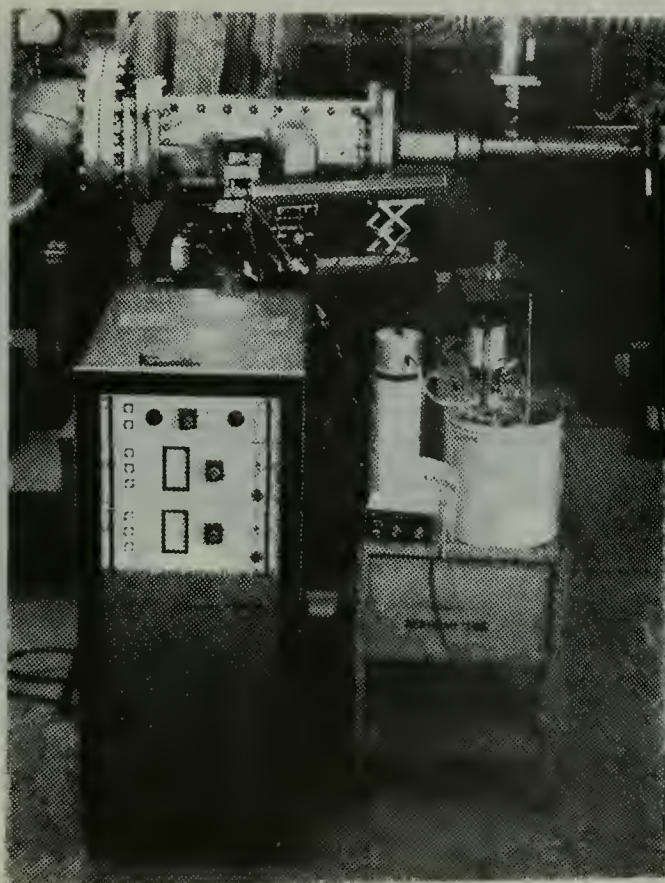


Figure 4. Ruby Laser Power Supply and Cooling Unit



Figure 5. Hologram Plate Holder and Mirrors on the Reverse Side of the Wind Tunnel

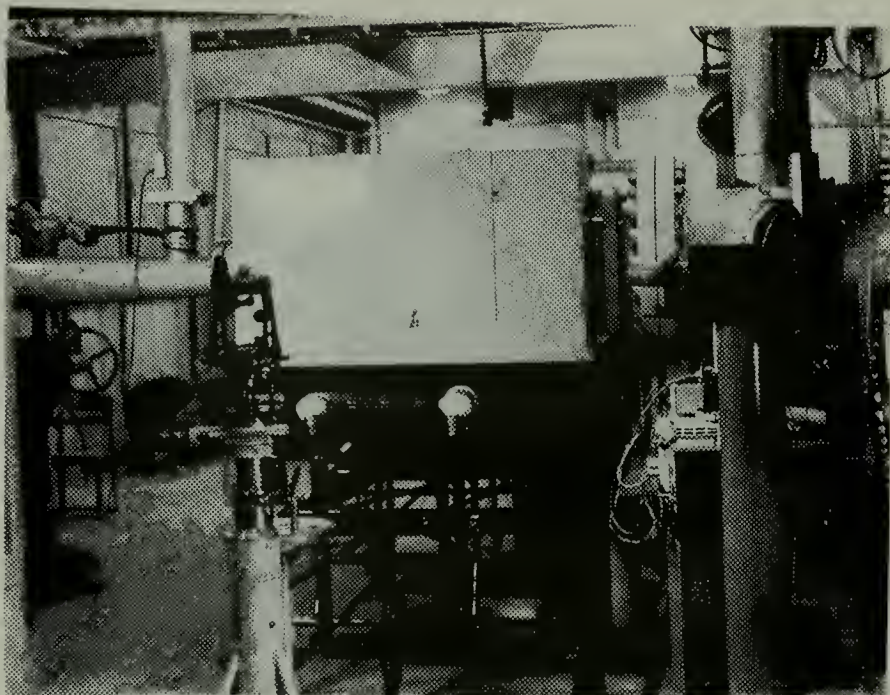


Figure 6. Hologram Platform Box Cover for Daylight Photography

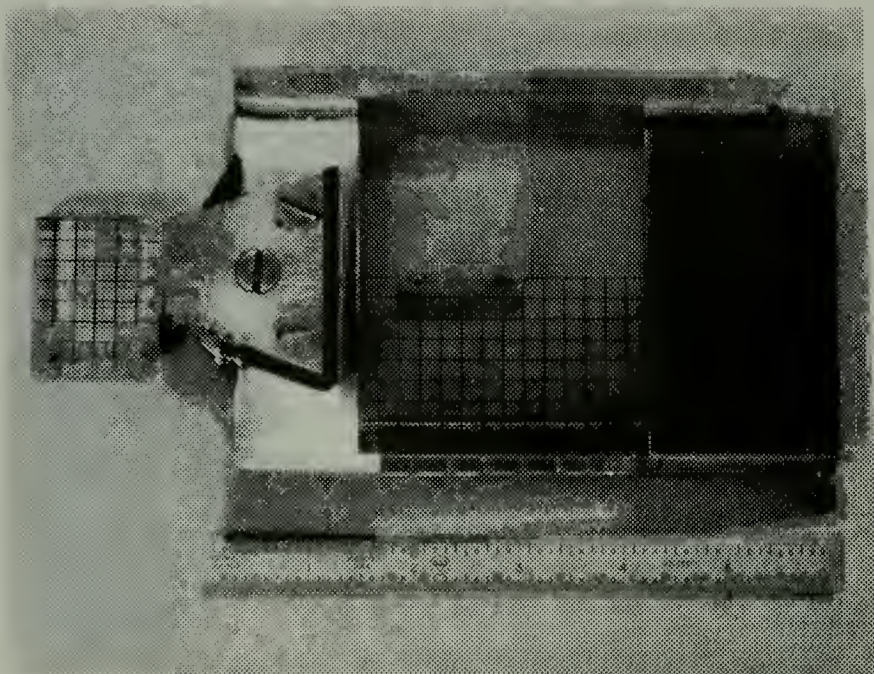


Figure 7(a). Initial Fin-Flat Plate Model Used in the Experiment

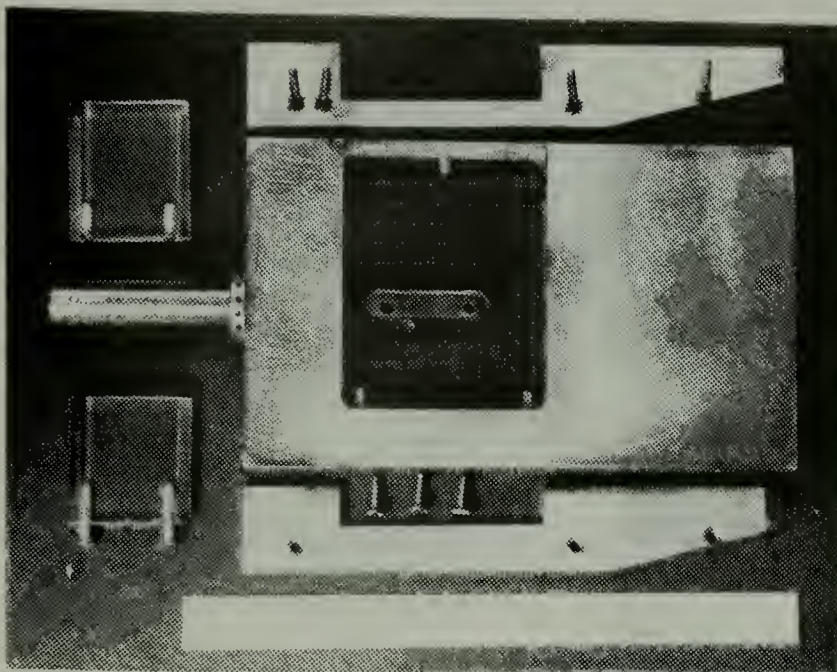


Figure 7(b). Second Fin-Flat Plate Model Used in the Experiment

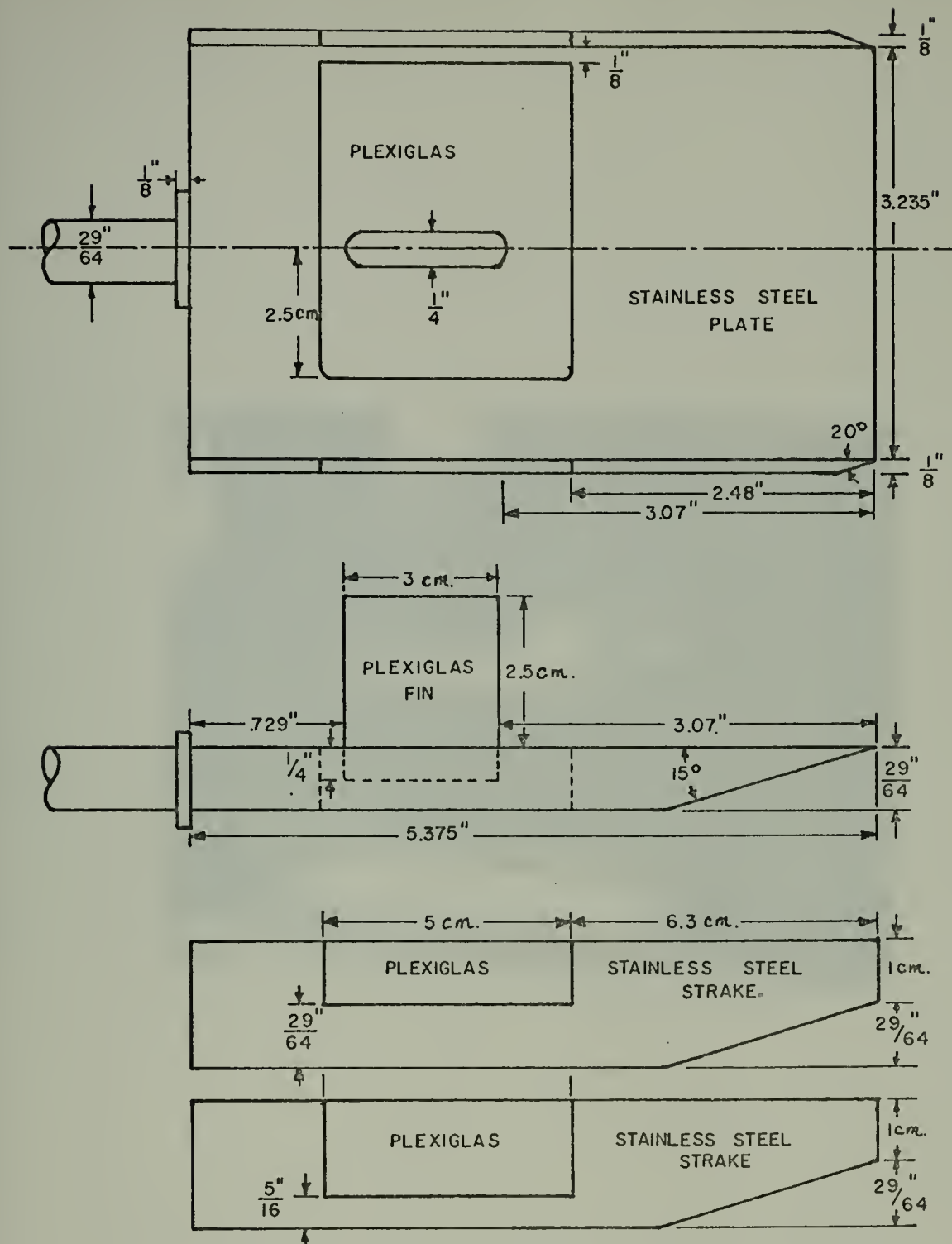


Figure 7(c). Details of the Second Fin-Flat Plate Model

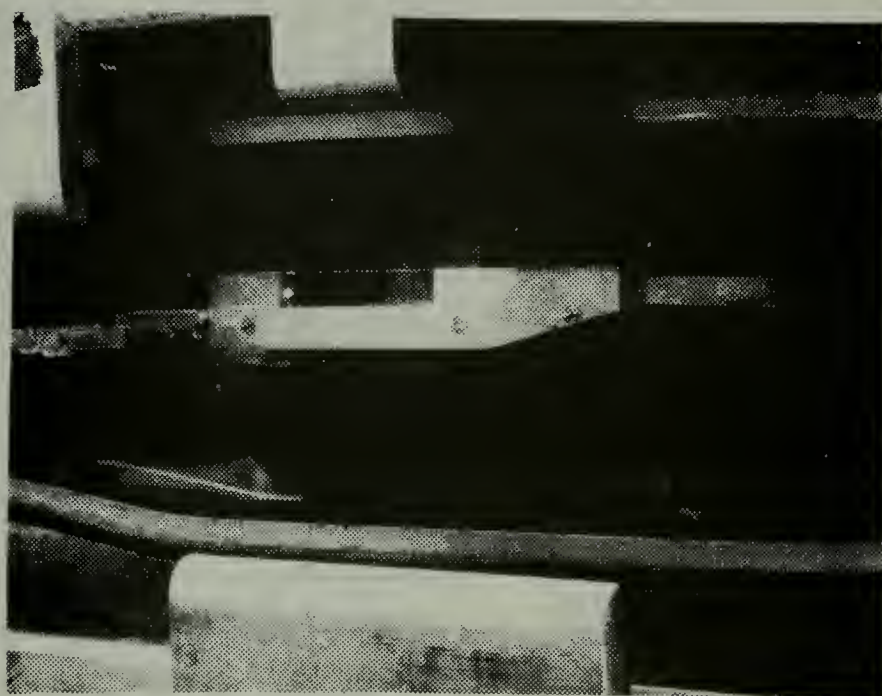


Figure 7(d). Model Mounting in the Wind Tunnel Test Section

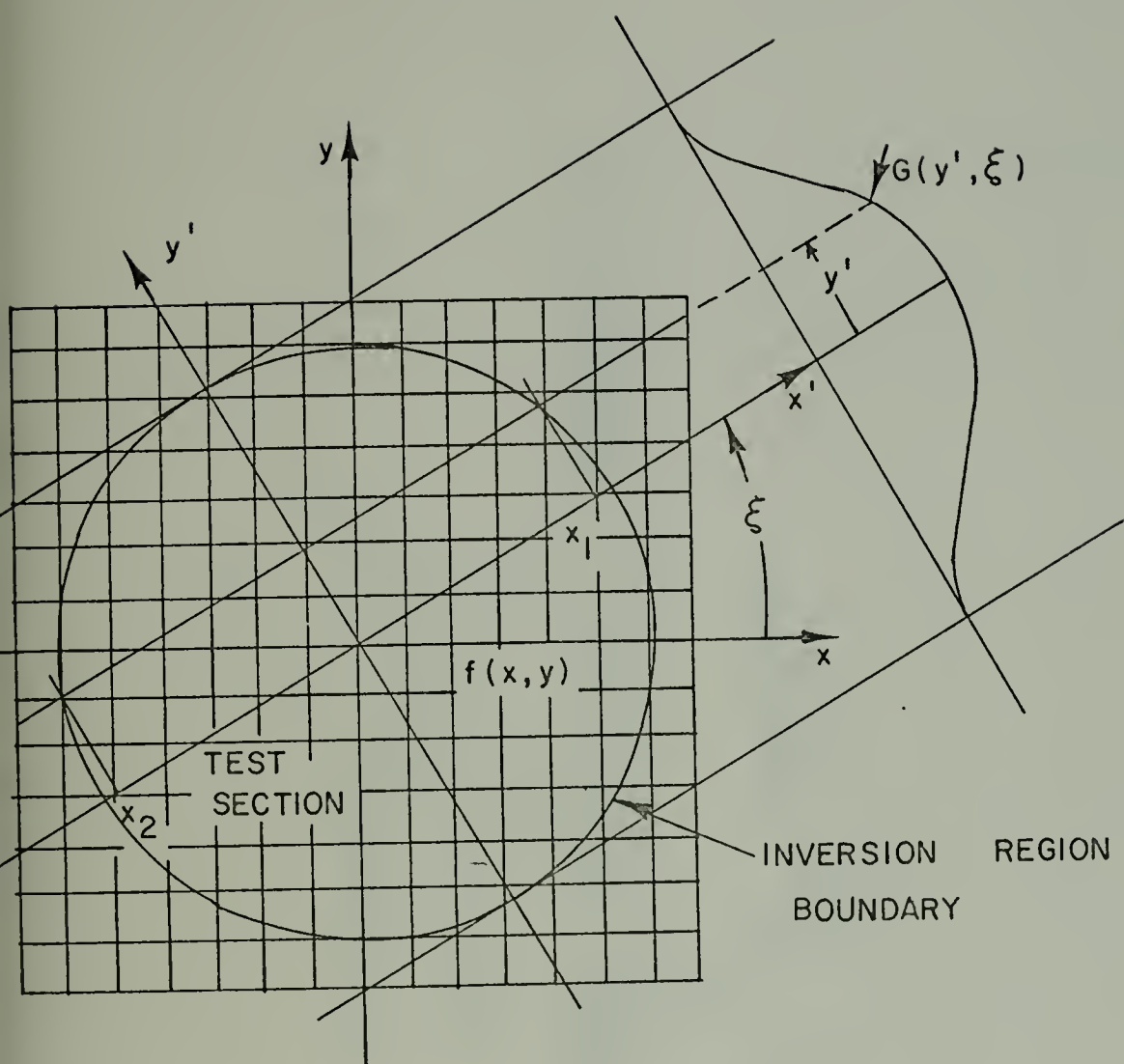


FIGURE 8. CO-ORDINATE SYSTEM USED FOR THE INVERSION OF FRINGE NUMBER TO DENSITY

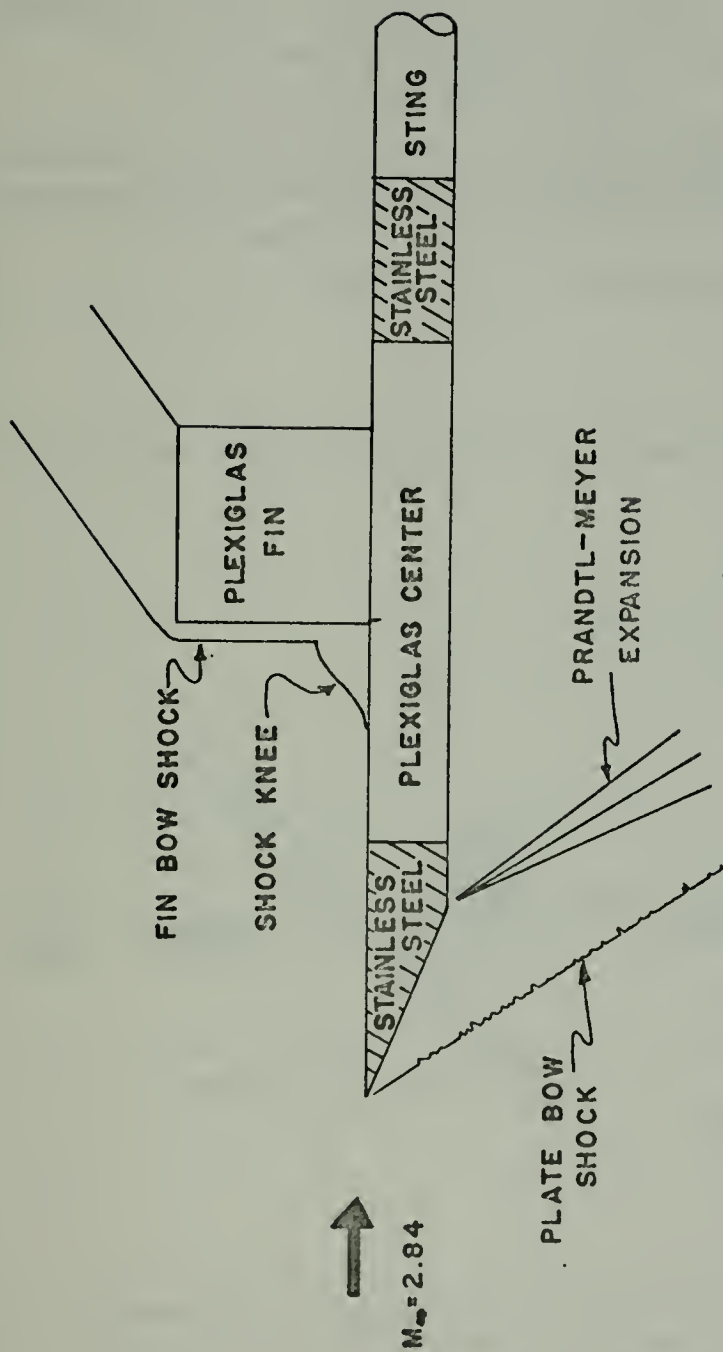


Figure 9. Schematic of the Desired Model Flow Network

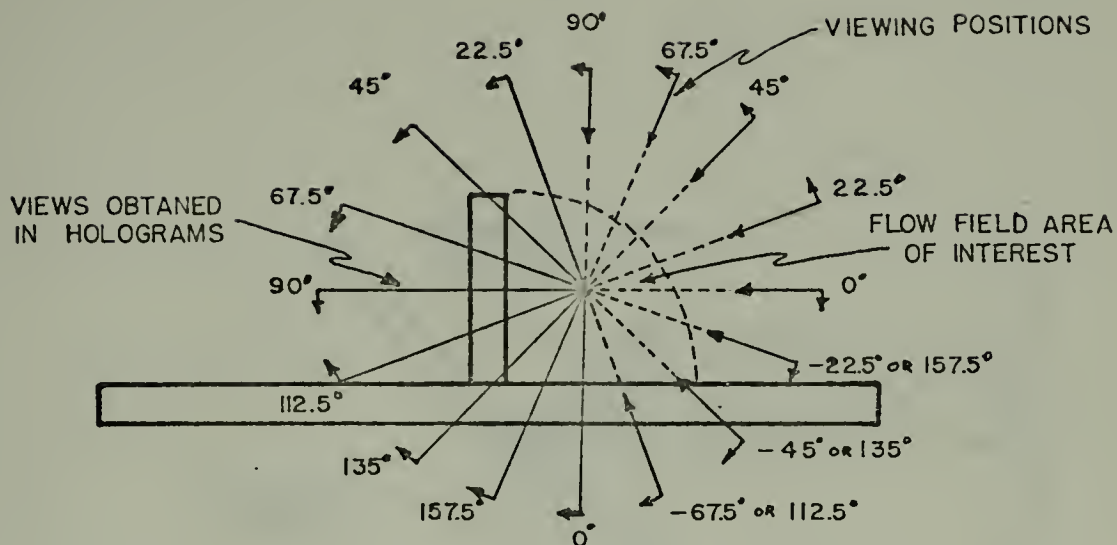


Figure 10. Desired Holographic Views in the Direct Fin-Roof Method

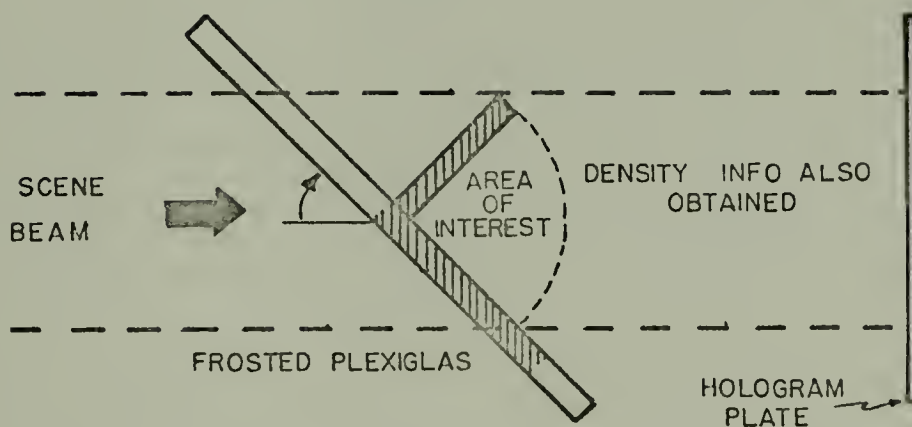


Figure 11. Schematic of the Model Used to Obtain Holographic Views Between 0° and 90° in the Direct Fin-Roof Method

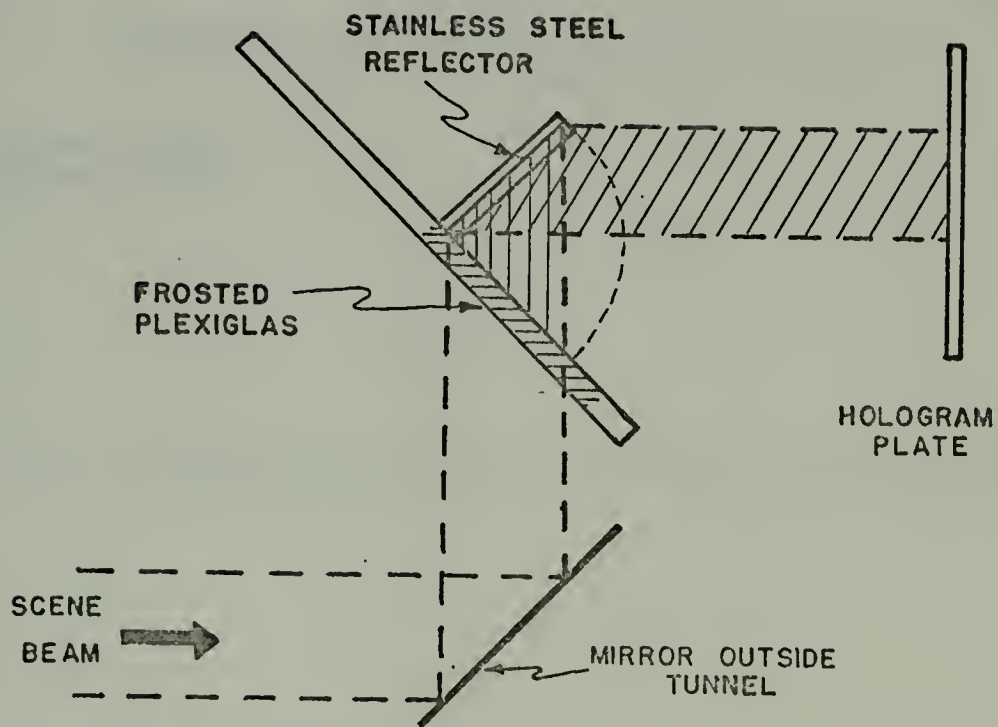


Figure 12. Schematic of the Model Used to Obtain Holographic Views Between 90° and 180° in the Direct Fin-Root Method

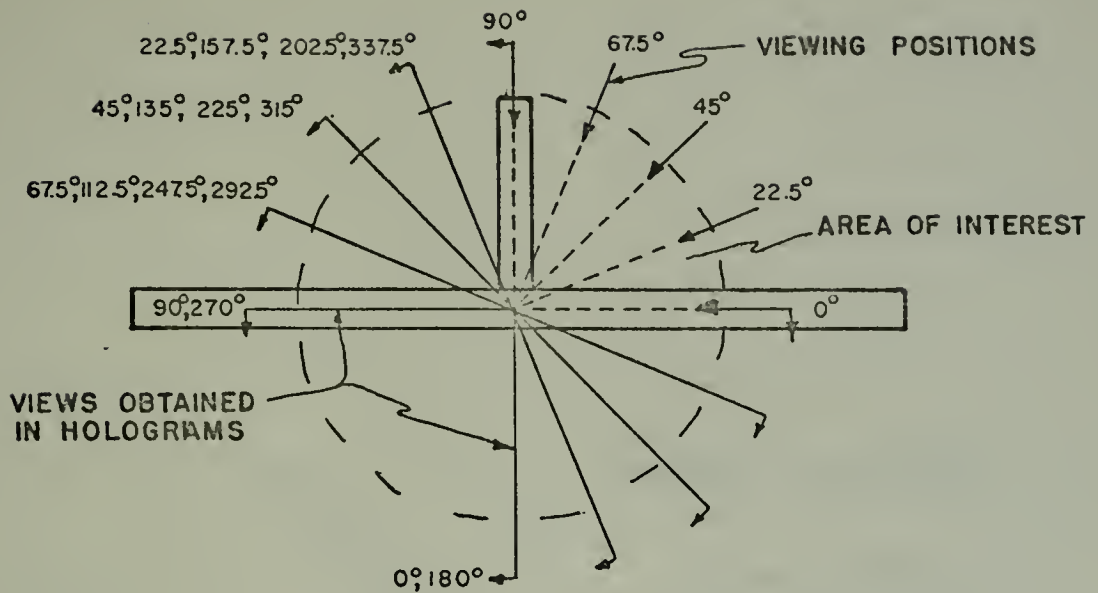


Figure 13. Holographic Viewing Angles Required in the Total Model Flow Method

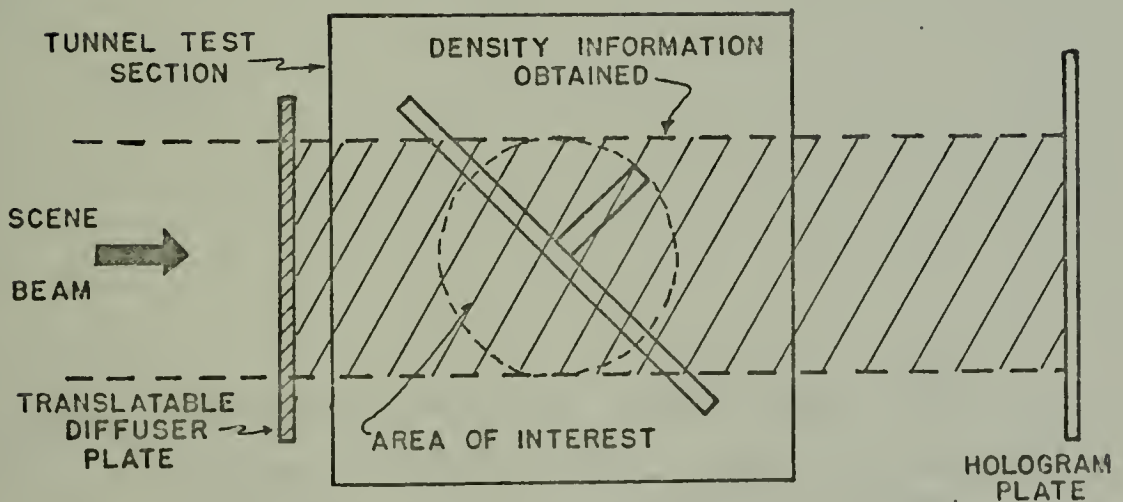


Figure 14. Schematic of the Technique Used to Obtain Holograms in the Total Model Flow Method

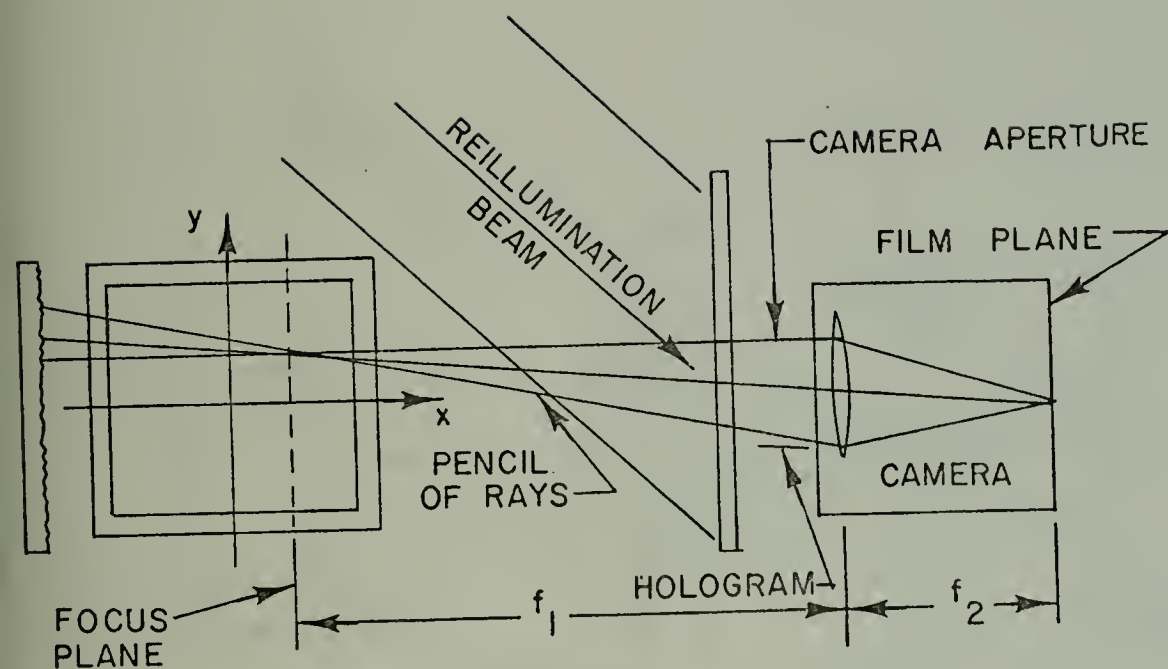


FIGURE 15. EFFECT OF APERTURE SIZE FOCUS PLANE POSITION ON THE PENCIL SIZE OF RAYS ABOUT A LINE OF SIGHT RECORDED BY CAMERA

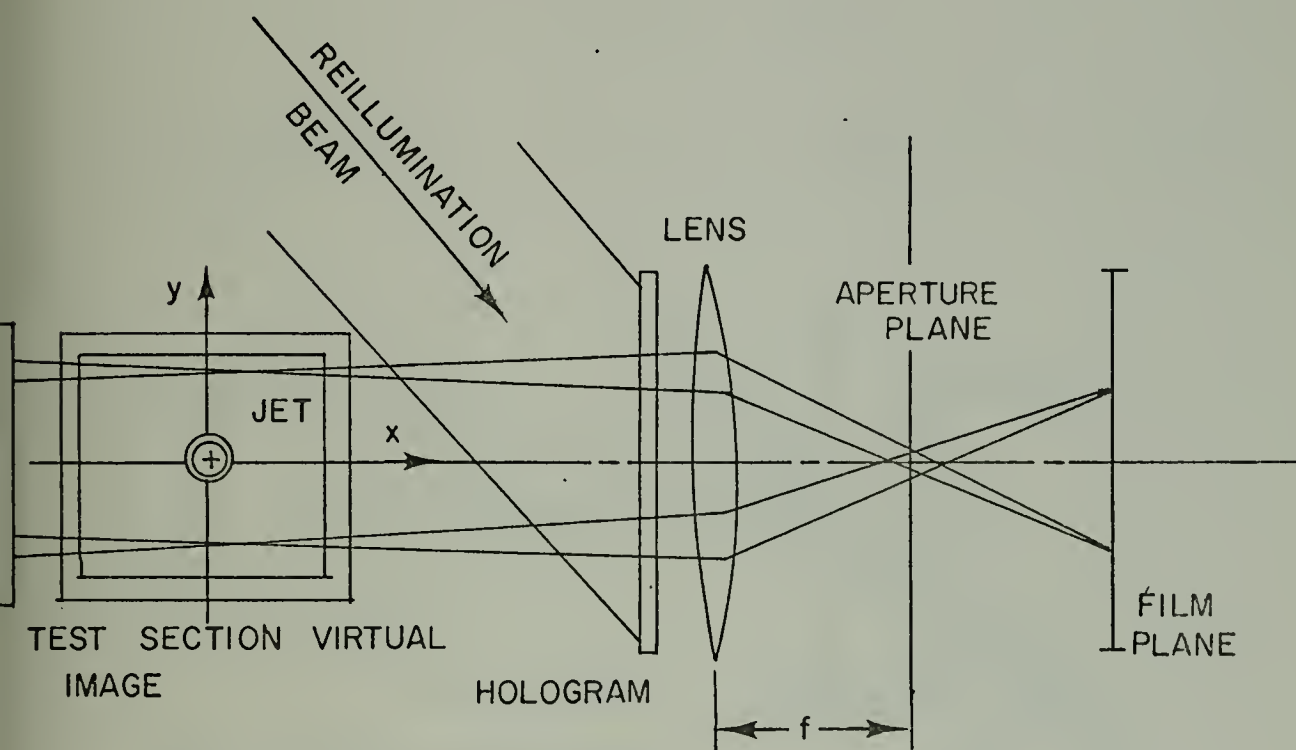


FIGURE 16. SPATIAL FILTERING TECHNIQUE FOR SELECTING PHOTOGRAPH OF CONSTANT ANGLE LINES OF LIGHT

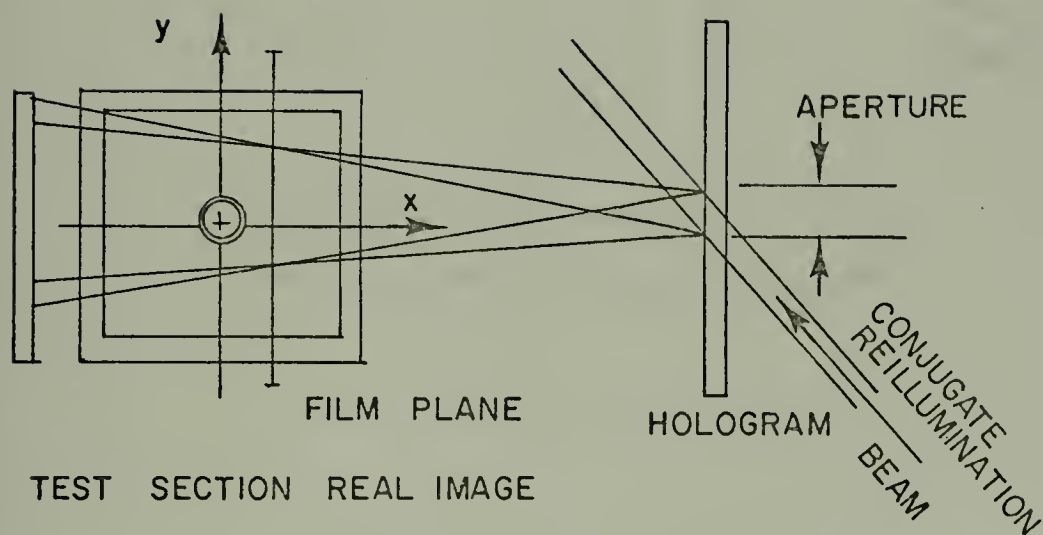


FIGURE 17. LENSLESS PHOTOGRAPHIC TECHNIQUE USING A CONJUGATE REFERENCE BEAM OF SMALL DIAMETER

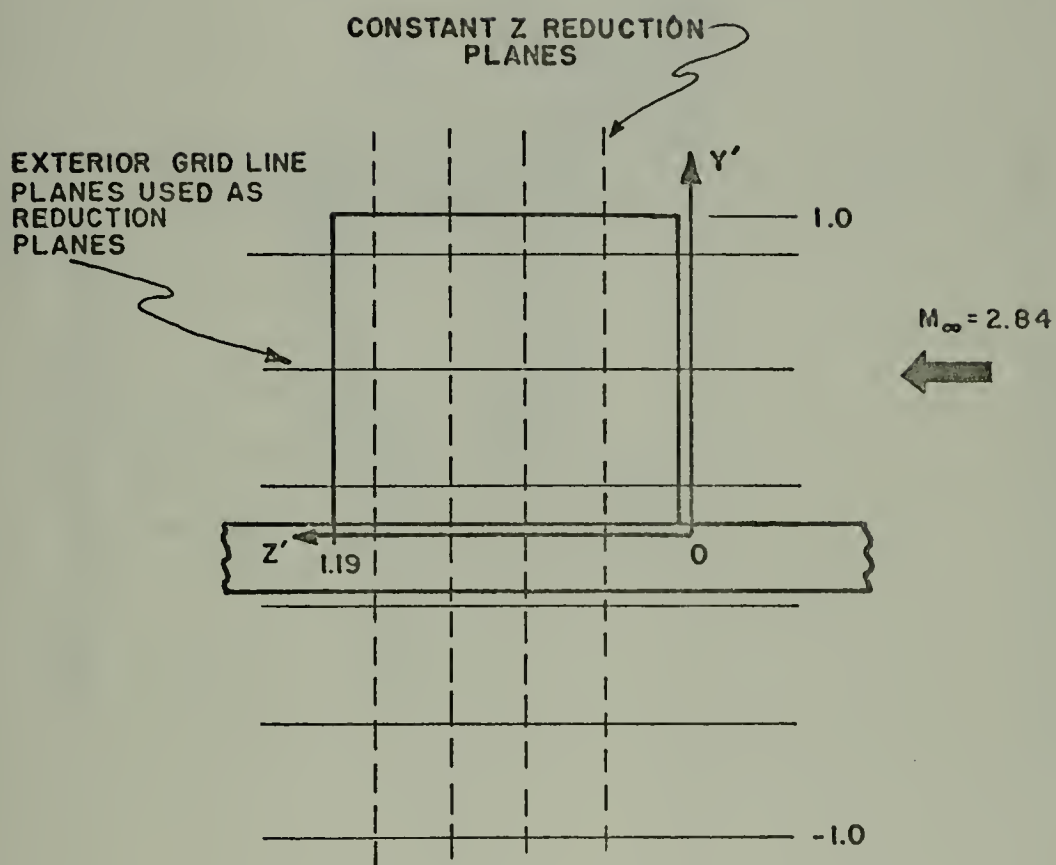


Figure 18. Data Reduction Planes Desired to Describe the Density Field Down the Fin

PLASTIC GRID AND TUNNEL WALL

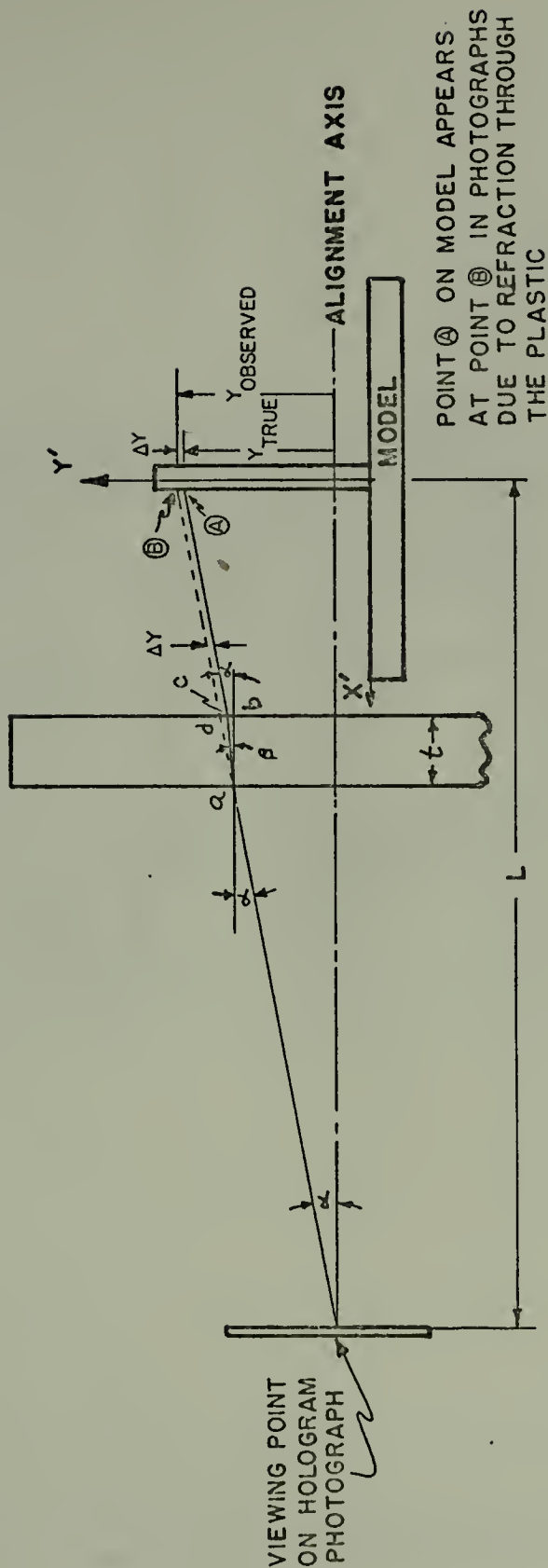


Figure 19. Schematic of the Refraction Displacement in the Photographs of Points Not Located on the Aligned Axis Caused by the Plastic Grid and Tunnel Wall

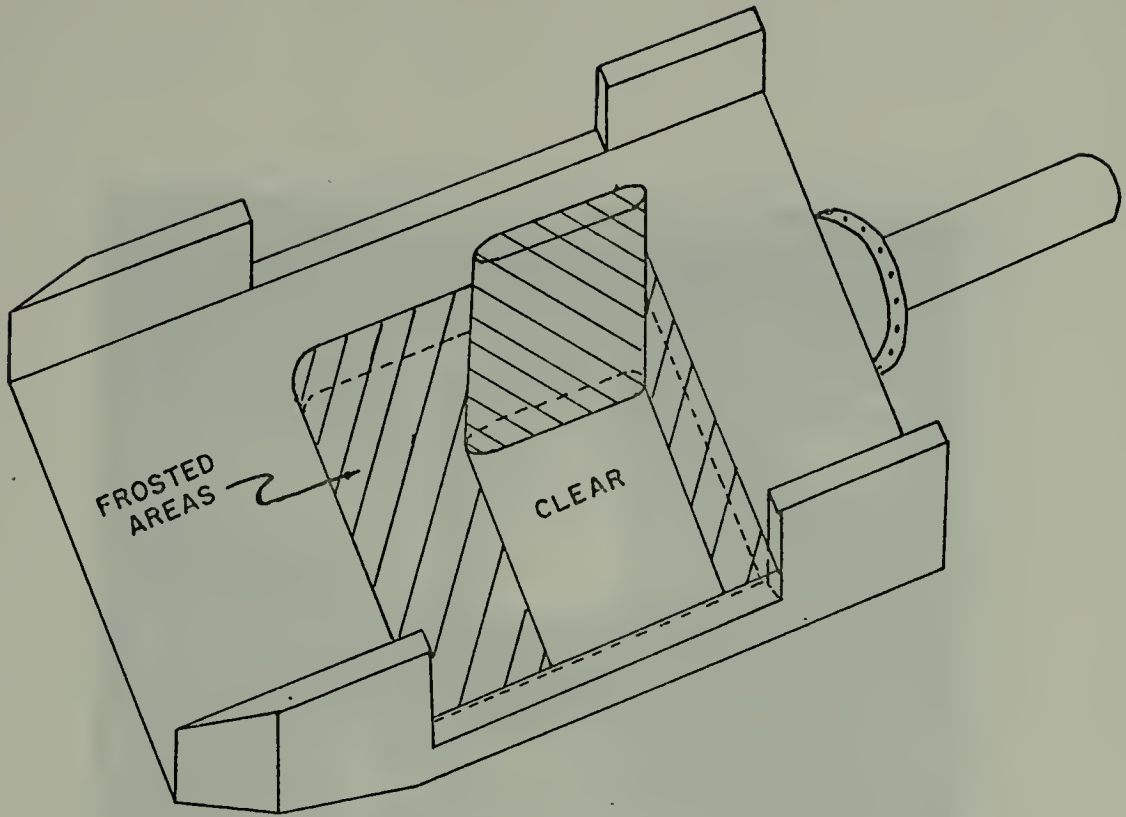


Figure 20. Schematic of the Diffused Plastic Portion of the Model
Required in the Direct Fin Flow Method

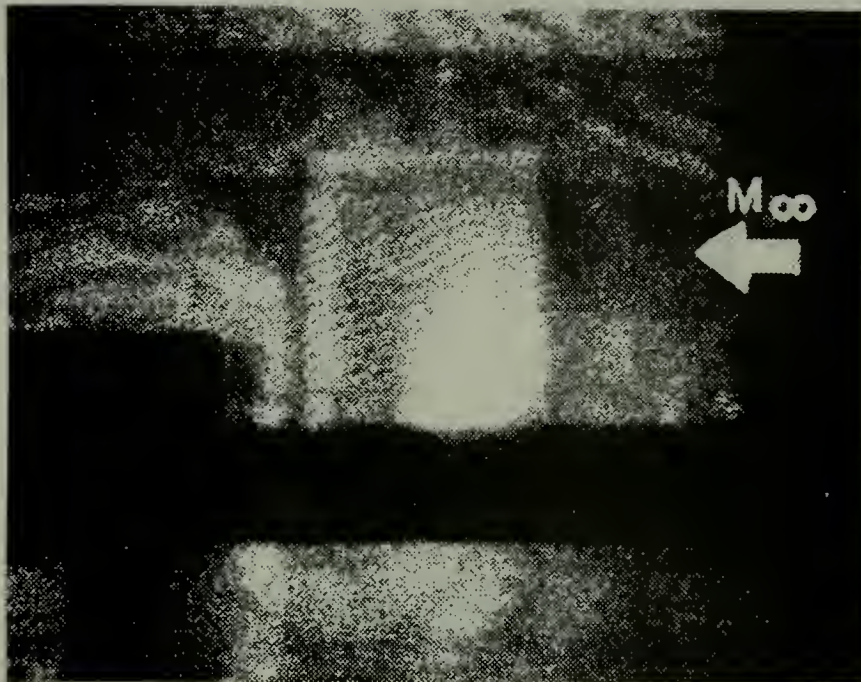


Figure 21. Interferogram Obtained in the Direct Fin Flow Method with the Model at 0° Rotation, Mach 2.84 and no Translation of Mirror, M_5

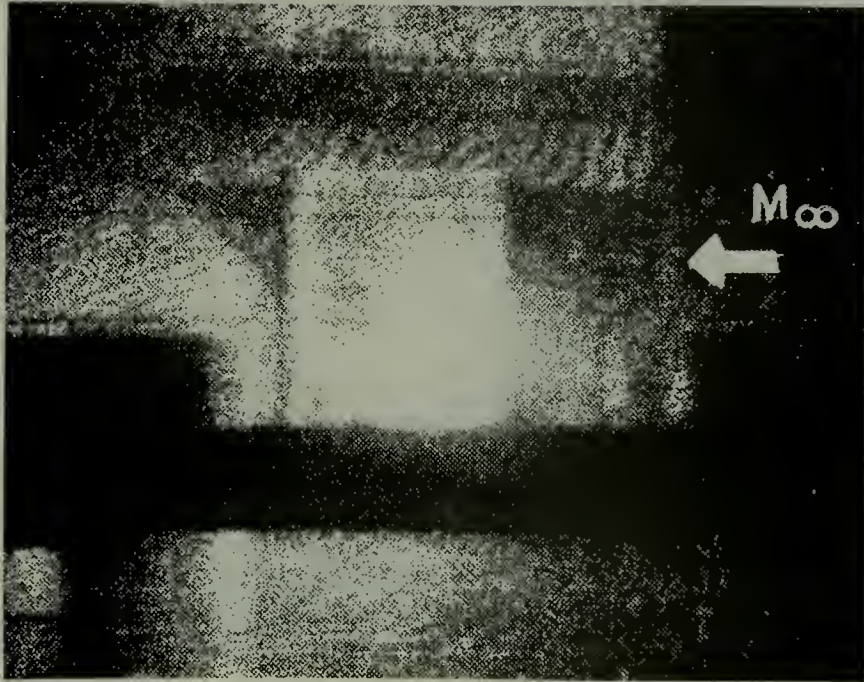


Figure 22. Interferogram Obtained in the Direct Fin Flow Method with the Model at 0° Rotation, Mach 2.84 and a .006 inches Translation of Mirror, M_5 , Parallel to the Test Section



THE UNIVERSITY OF CHICAGO PRESS
CHICAGO, ILL. 60637
1980

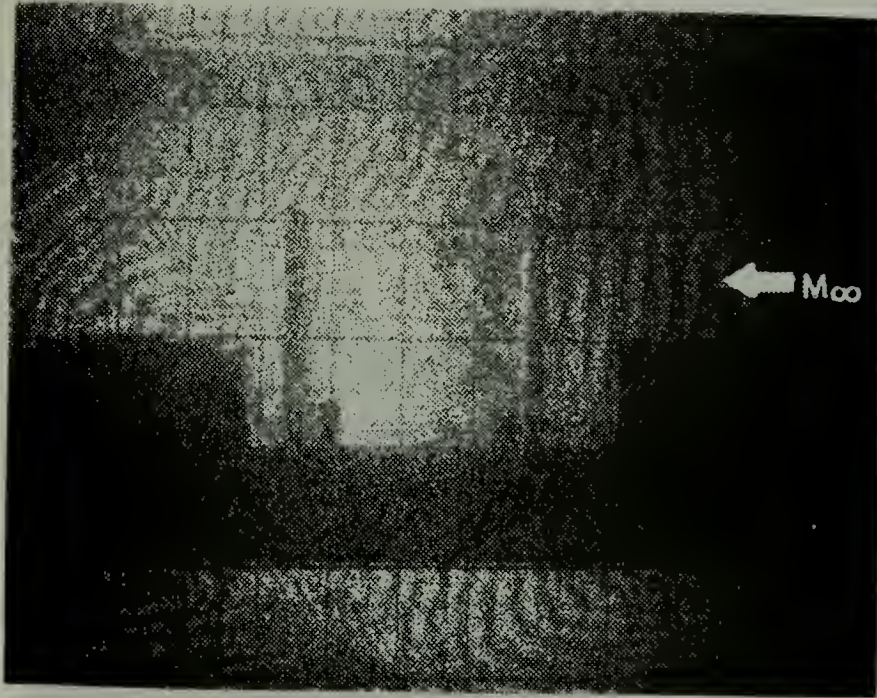


Figure 23. Interferogram Obtained in the Total Flow Method with the Clear Plexiglas Fin Model at 0° Rotation, Mach 2.84 and a .0015 inches Horizontal Translation of the Diffuser Plate Parallel to the Test Section



THE UNIVERSITY OF CHICAGO
LIBRARY
1100 EAST 58TH STREET
CHICAGO, ILL. 60637
TEL. (312) 937-1234
FAX (312) 937-1234
WWW.CHICAGO.EDU

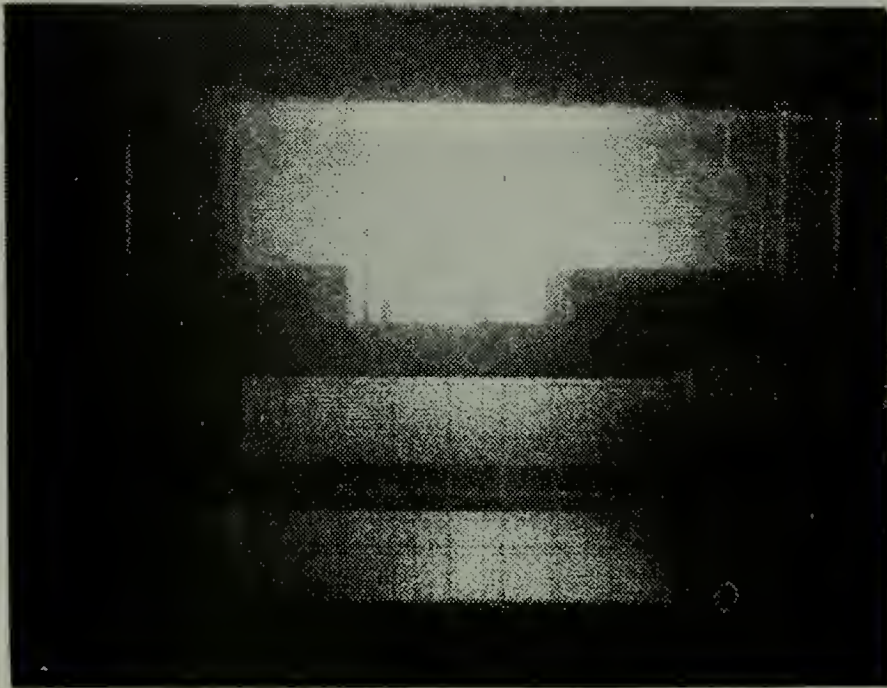


Figure 24. Interferogram Obtained in the Total Flow Method with the Clear Plexiglas Fin Model at 0° Rotation, Mach 2.84 and a .0045 Vertical Translation of the Diffuser Plate Parallel to the Test Section

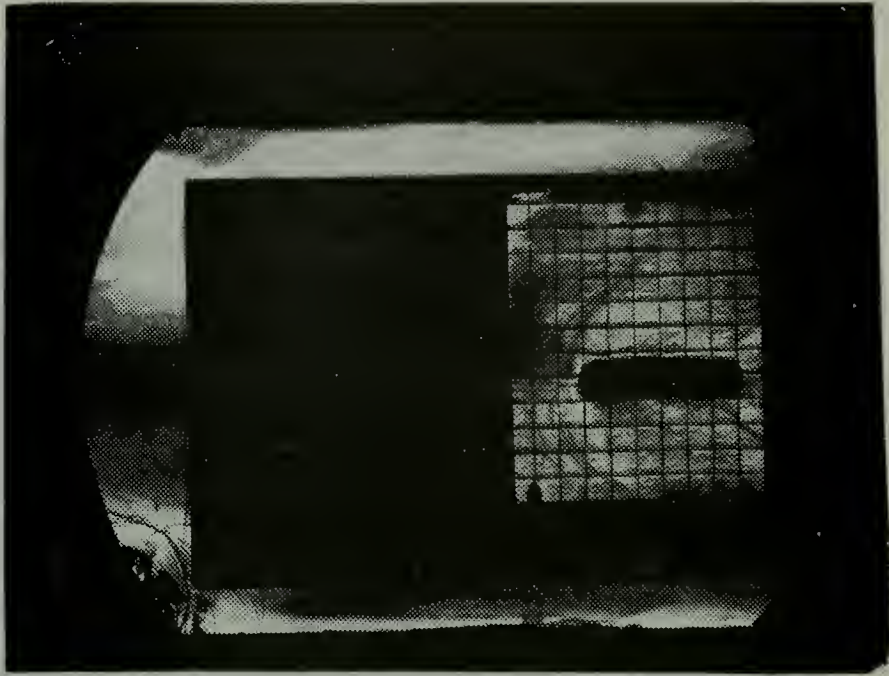


Figure 25(a). Illustration of the Shock Network Around the Fin at Mach 2.84 with a 90° Model Rotation Angle Using a Horizontal Knife Edge Schlieren System



Figure 25(b). Illustration of the Shock Network Around the Fin at Mach 2.84 with a 90° Model Rotation Angle Using a Vertical Knife Edge Schlieren System



Figure 2.10.1. A photograph of a small, dark, rectangular object, possibly a piece of wood or a small box, resting on a light-colored surface. The object is oriented horizontally and has a slightly irregular shape. The background is a plain, light-colored surface.

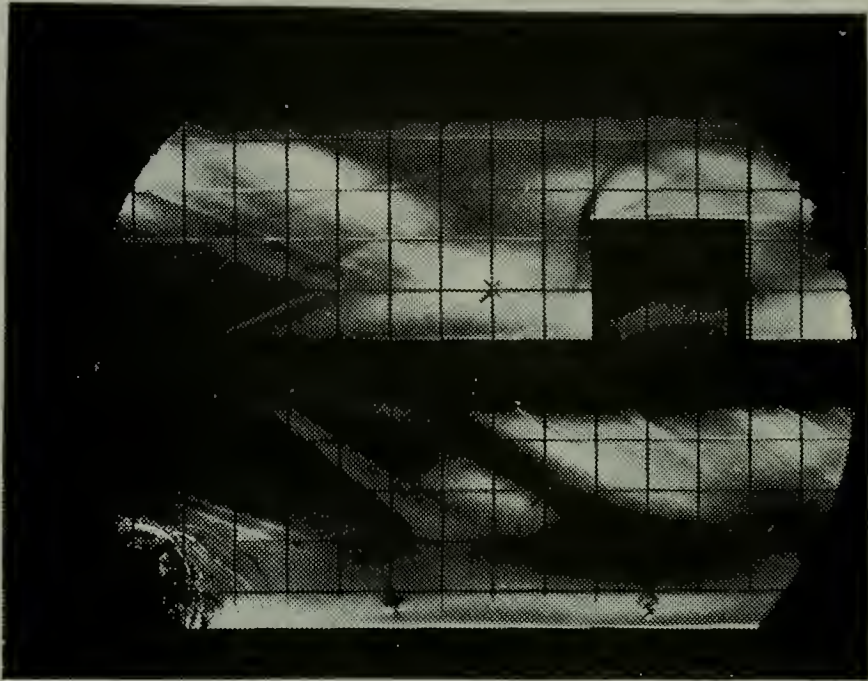


Figure 26. Illustration of the Model Flow Network at Mach 2.84, 0° Model Rotation and a Plate Vibration of $\pm .05^\circ$ Angle of Attack Using a Schlieren System

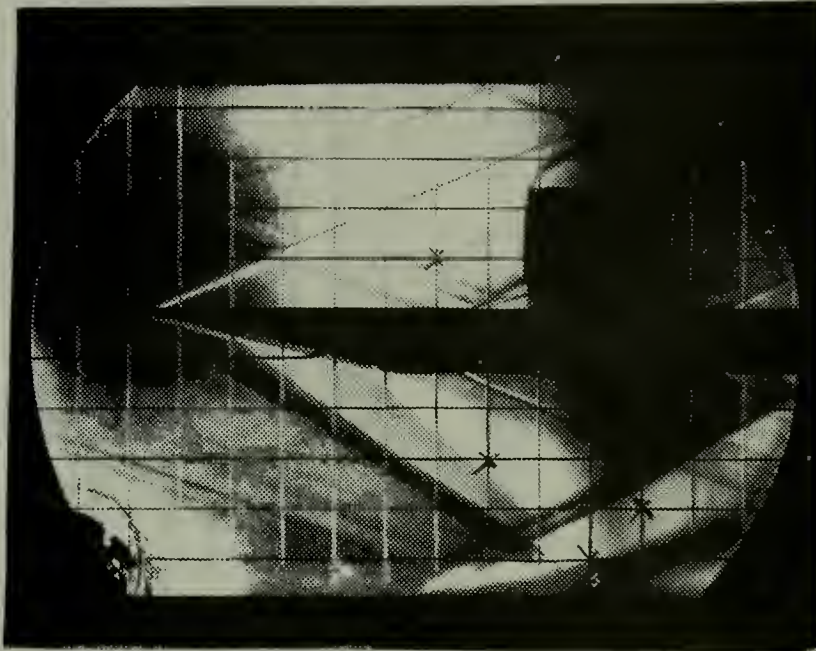


Figure 27. Illustration of the Model Flow Network at Mach 2.84, 0° Model Rotation and No Plate Vibration Using a Schlieren System

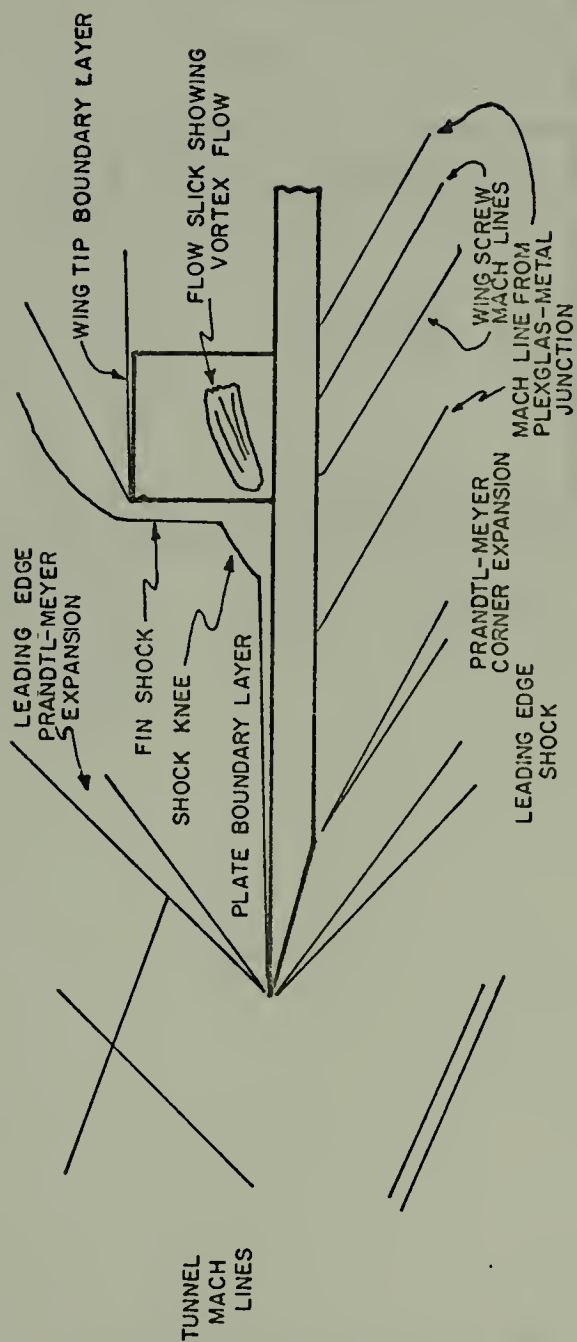


Figure 28. Schematic of the Flow Observed in the Schlieren Photographs

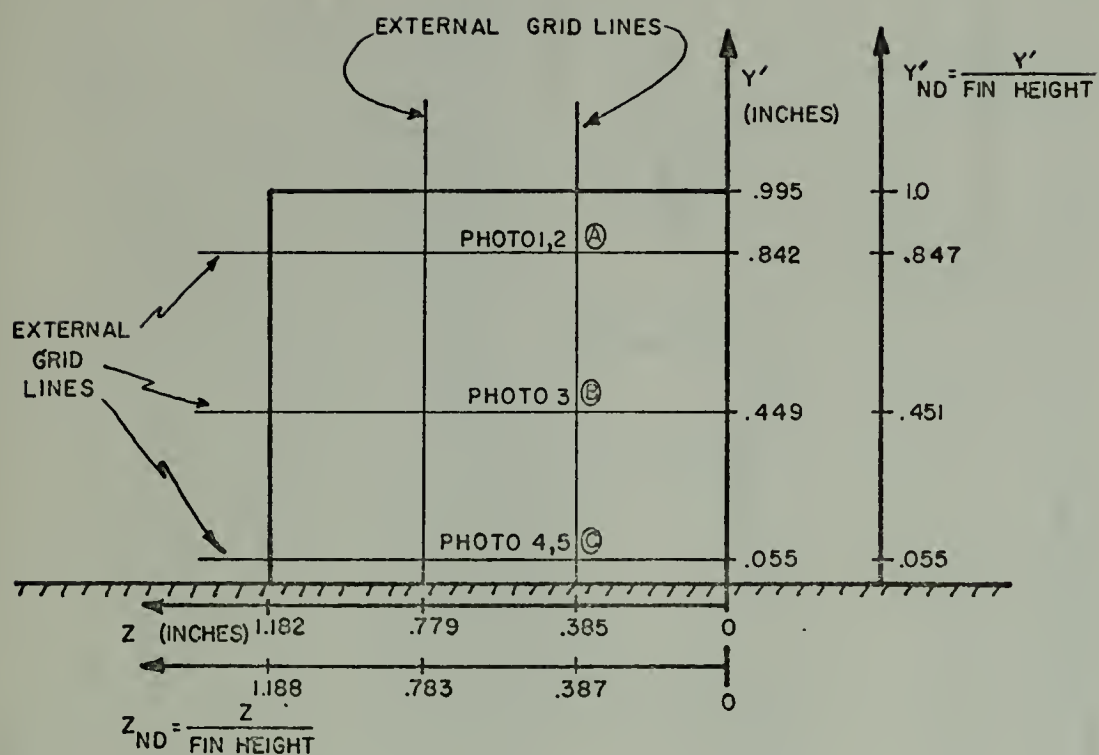


Figure 29. Schematic of the Fin at 0° Rotation Showing the Locations of the External Grid Lines and of the Interferogram Photographic Points

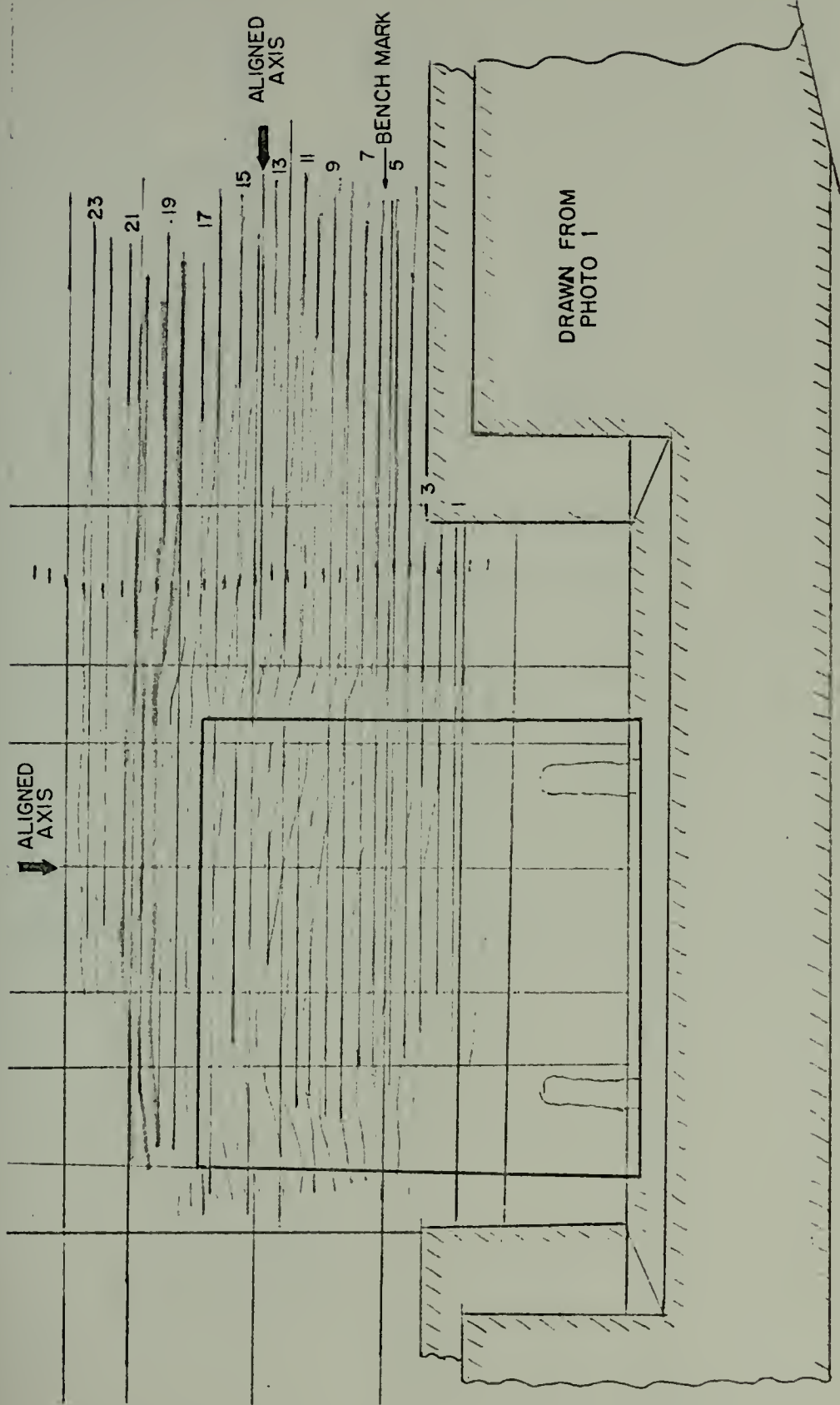


Figure 30. Actual Drawing and Data Reduction of Interferogram Photograph 1 Aligned at $Z = 0.387$, $Y' = 0.847$ for Mach 2.84 and 0° Model Rotation Angle

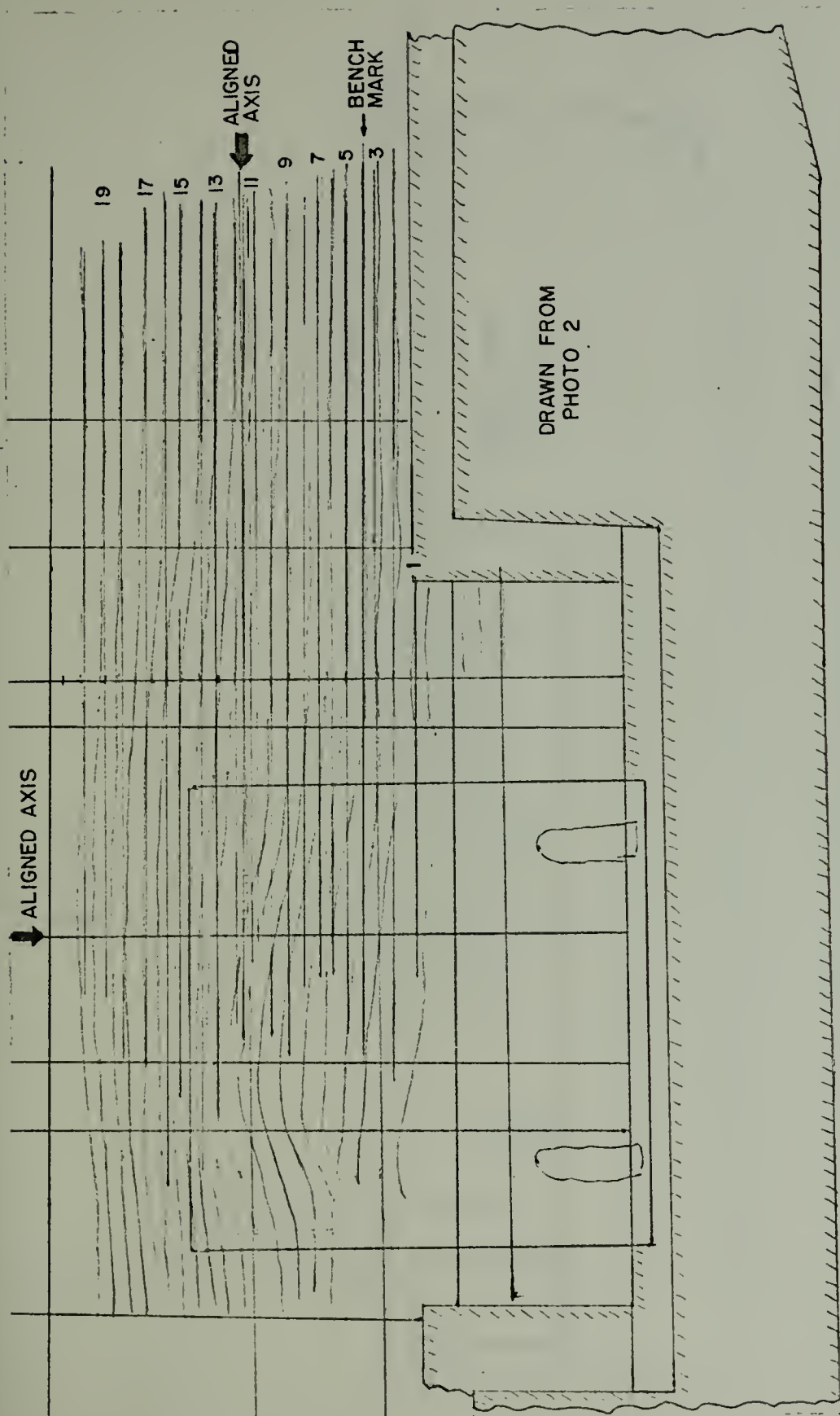


Figure 31. Actual Drawing and Data Reduction of Interferogram Photograph 2 Aligned at $Z = 0.387$, $Y' = 0.847$ for Mach 2.84 and 0° Model Rotation Angle

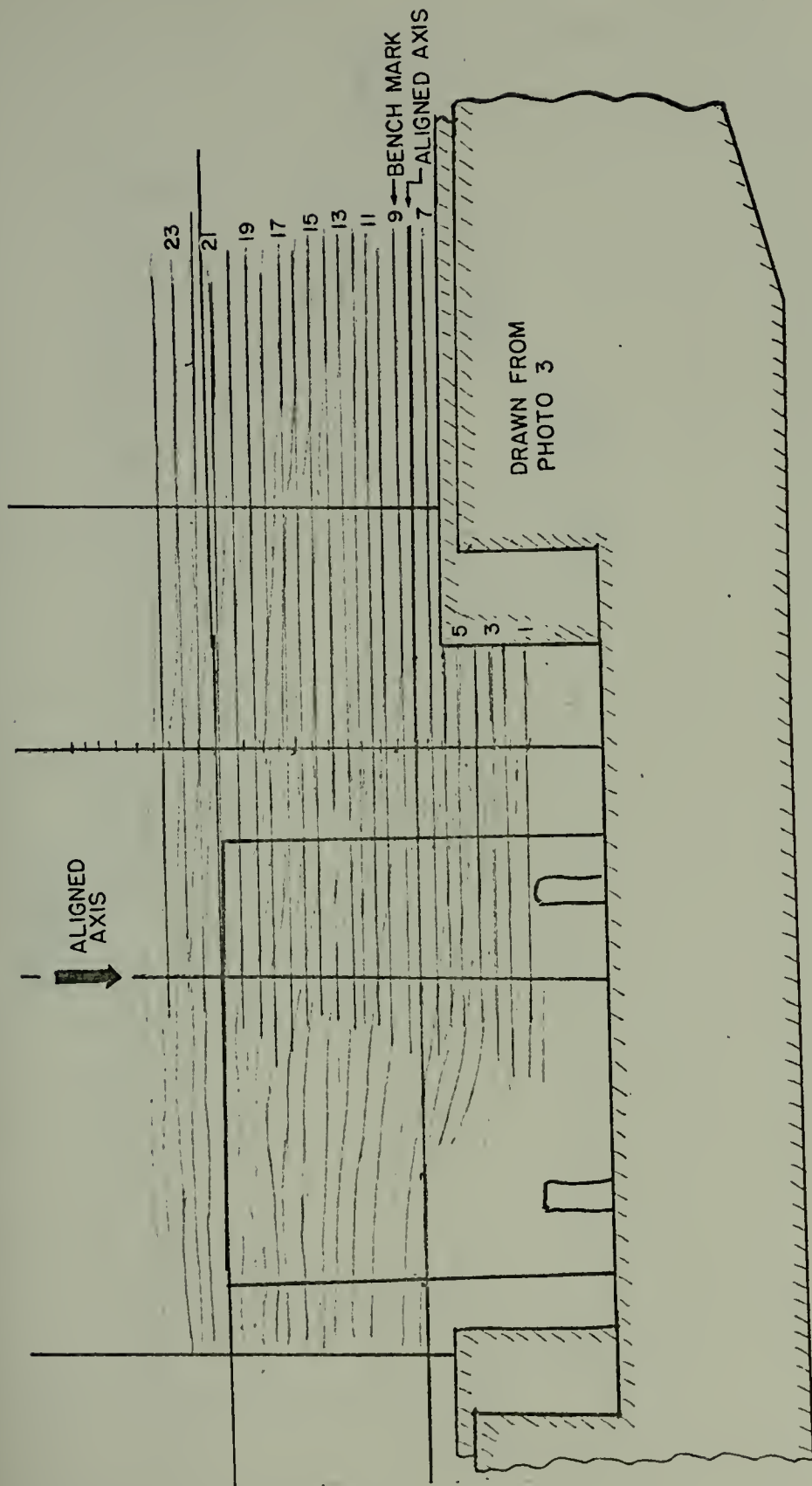


Figure 32. Actual Drawing and Data Reduction of Interferogram Photograph 3 Aligned at $Z = 0.381$, $y' = 0.451$ for Mach 2.84 and 0° Model Rotation Angle

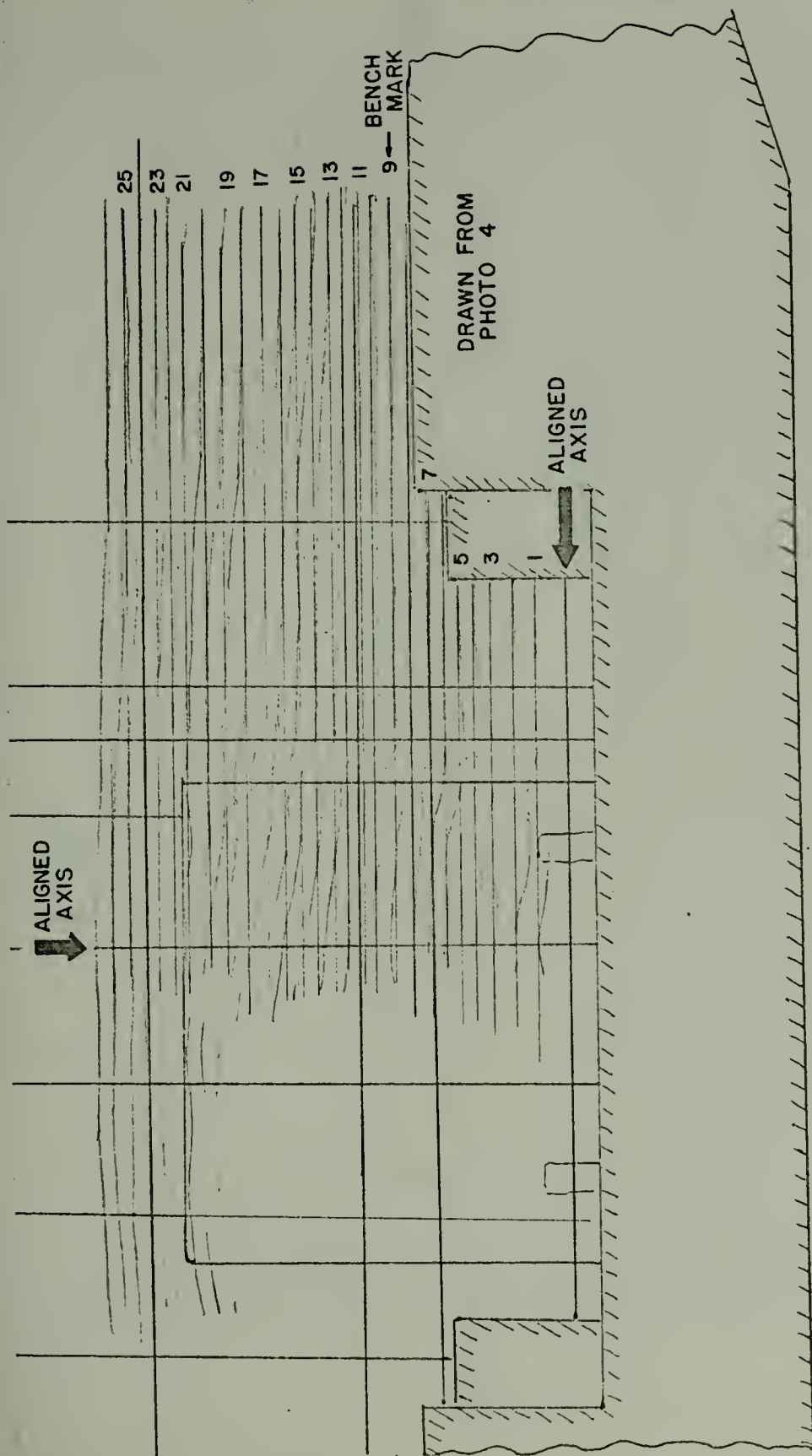


Figure 33. Actual Drawing and Data Reduction of Interferogram Photograph 4 Aligned at $Z = 0.387$, $y' = 0.055$ for Mach 2.84 and 0° Model Rotation Angle

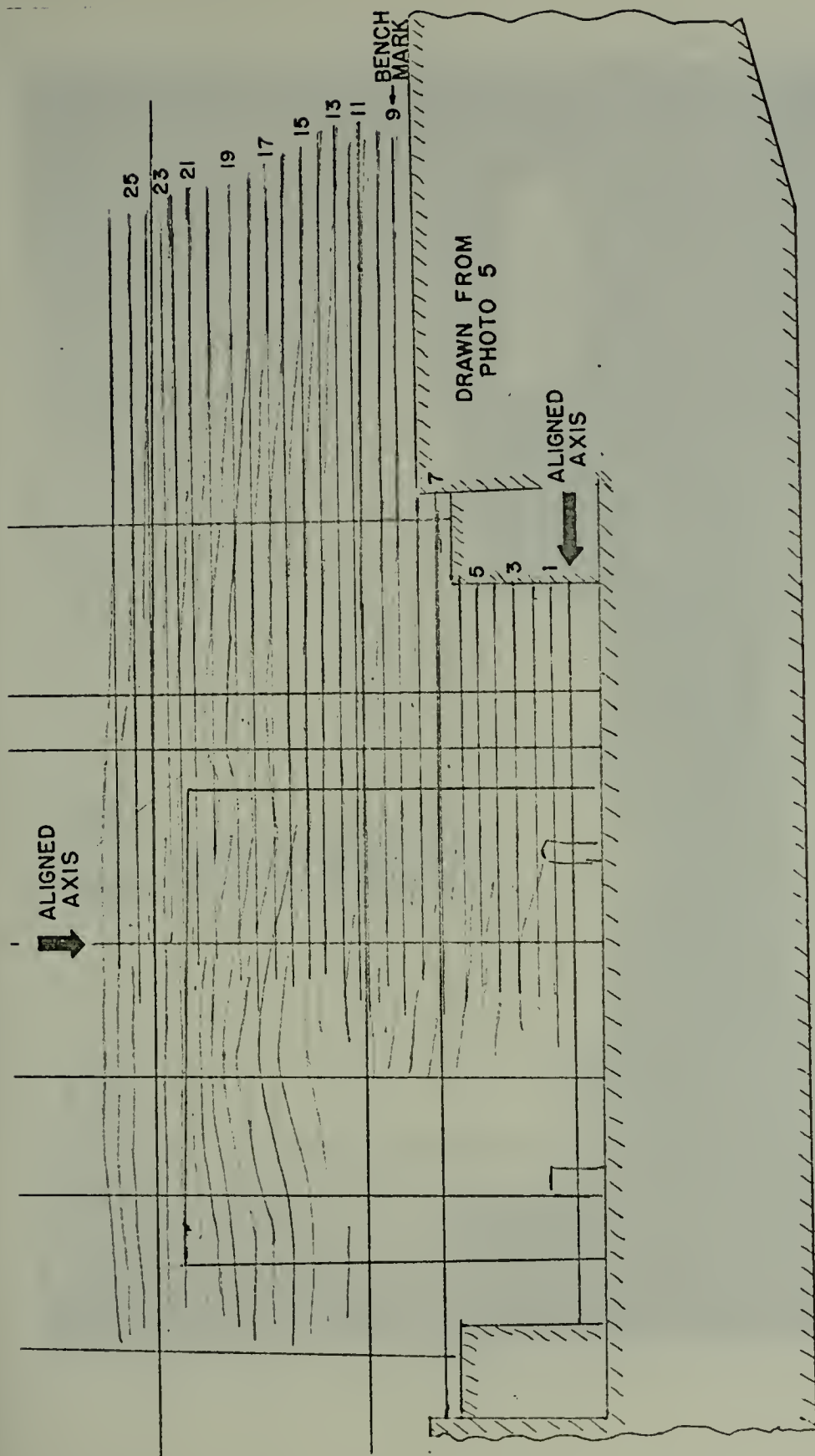


Figure 34. Actual Drawing and Data Reduction of Interferogram Photograph 5 Aligned at $Z = 0.387$, $y' = 0.055$ for Mach 2.84 and 0° Model Rotation Angle

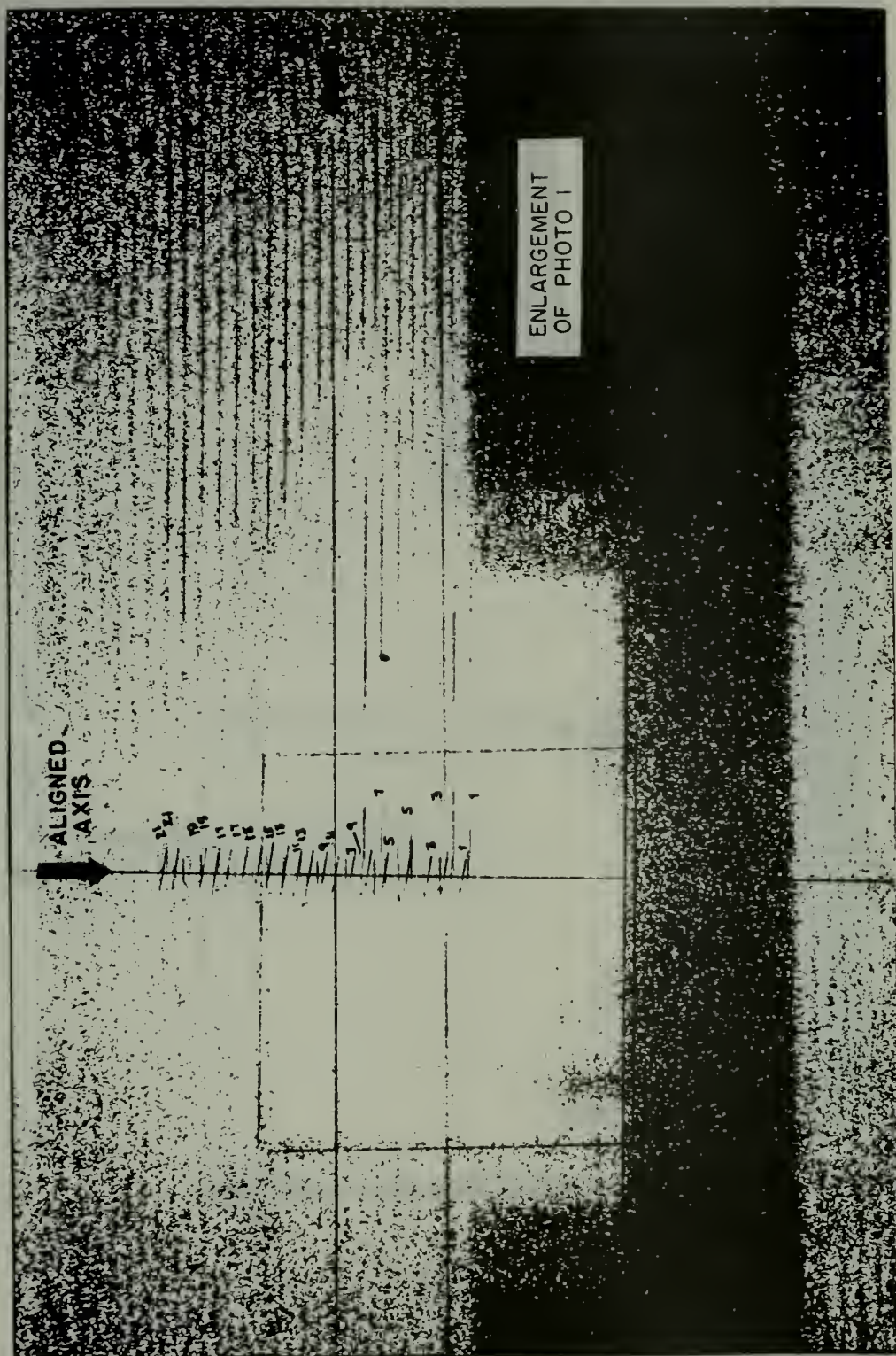


Figure 35. Actual Enlarged Photograph Used for the Data Reduction of Interferogram Photograph 1
 Aligned at $Z = 0.387$, $Y' = 0.847$ for Mach 2.84 and 0° Model Rotation Angle

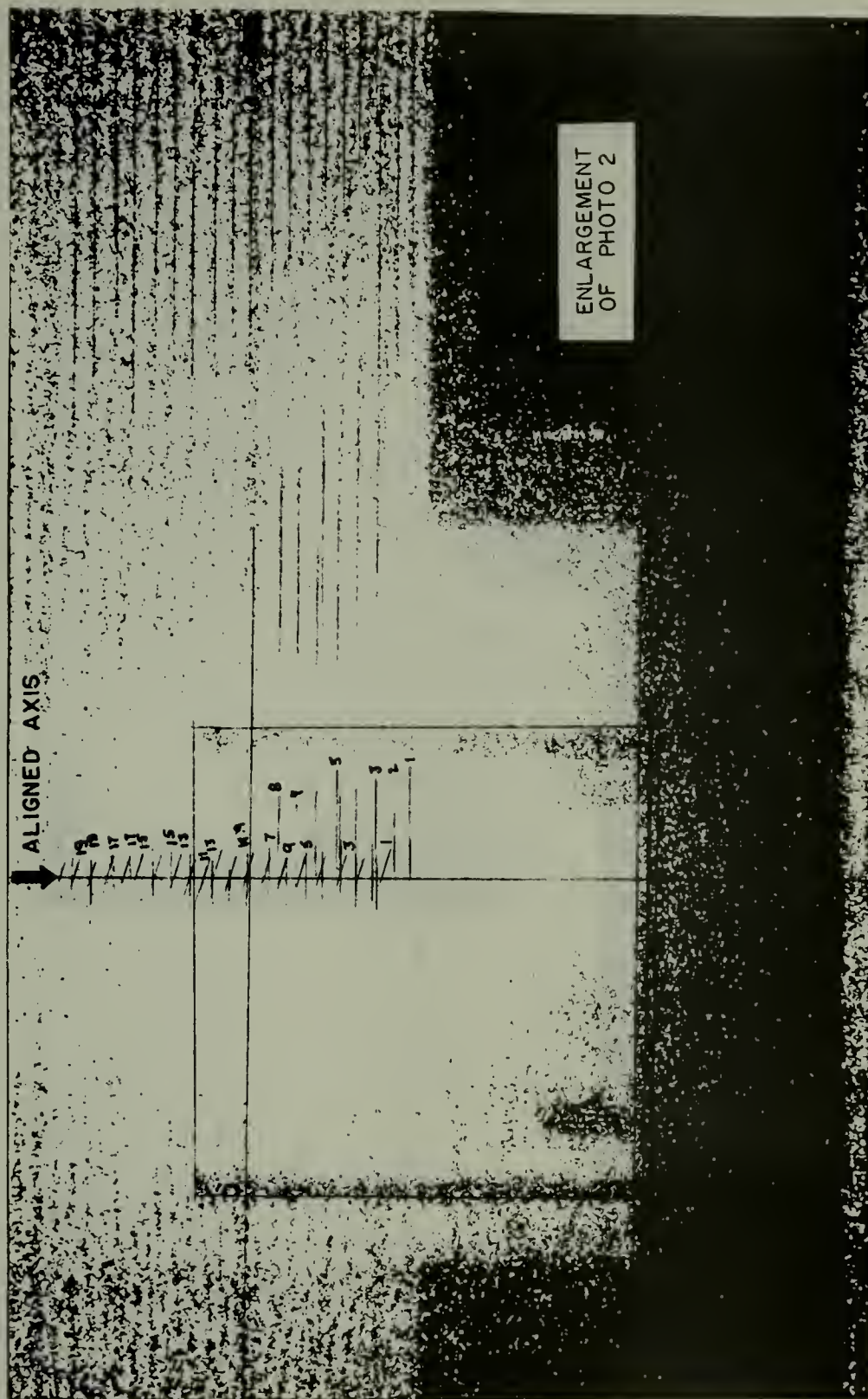


Figure 36. Actual Enlarged Photograph Used for the Data Reduction of Interferogram Photograph 2
 Aligned at $Z = 0.387$, $Y' = 0.847$ for Mach 2.84 and 0° Model Rotation Angle

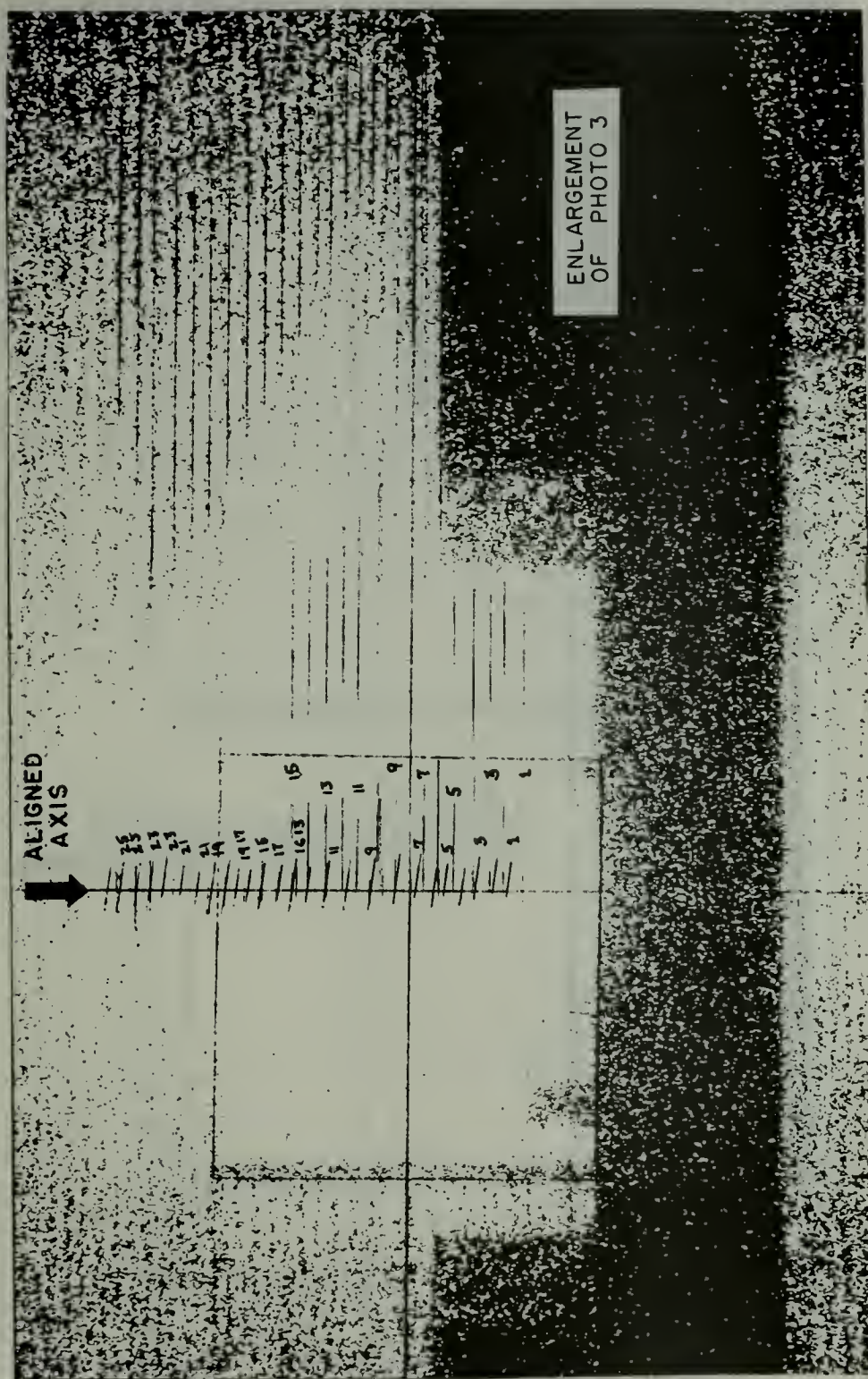


Figure 37. Actual Enlarged Photograph Used for the Data Reduction of Interferogram Photograph 3
 Aligned at $Z = 0.387$, $Y' = 0.451$ for Mach 2.84 and 0 Model Potation Angle

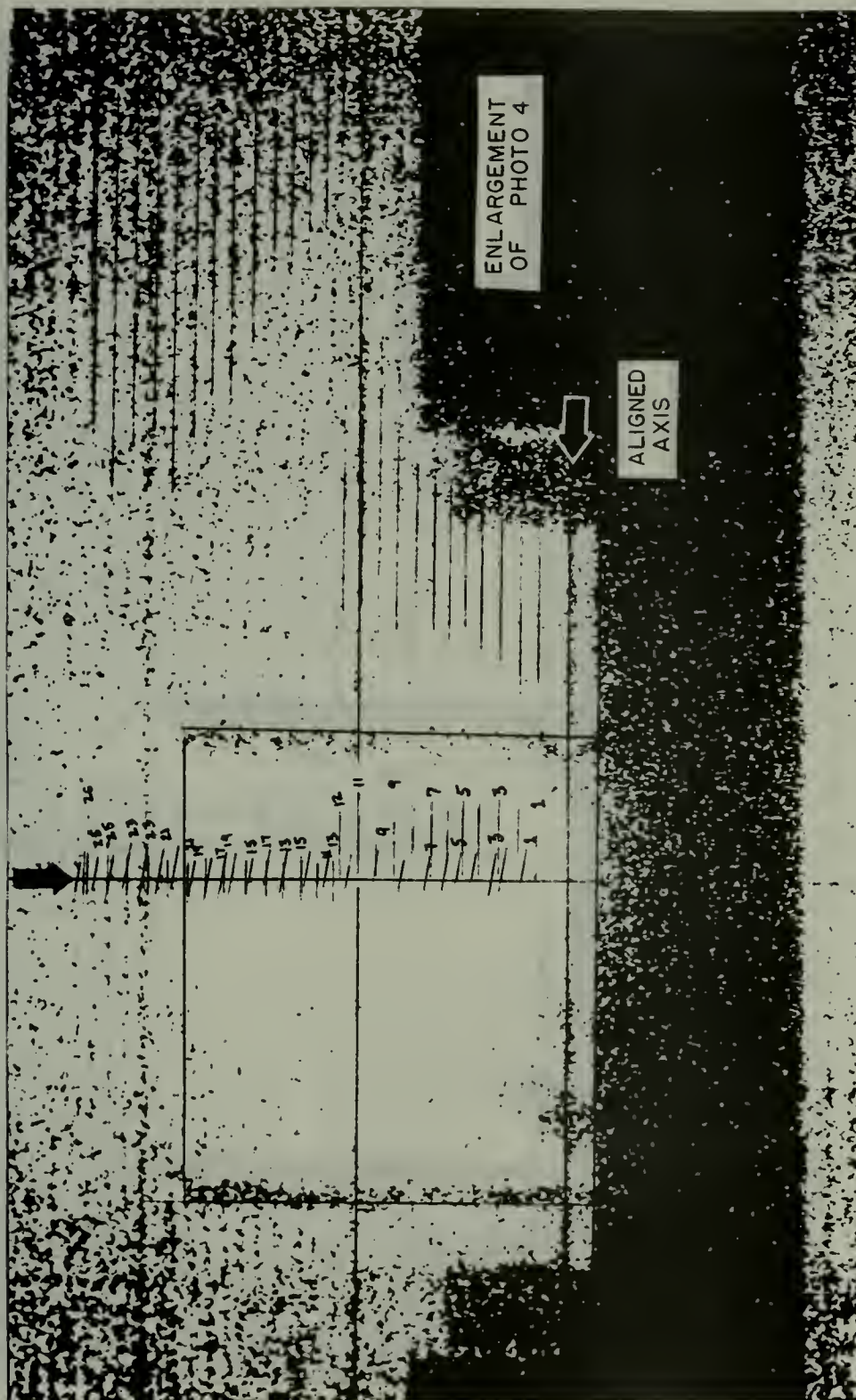


Figure 38. Actual Enlarged Photograph Used for the Data Reduction of Interferogram Photograph 4
 Aligned at $Z = 0.387$, $Y' = 0.055$ for Mach 2.84 and 0° Model Rotation Angle

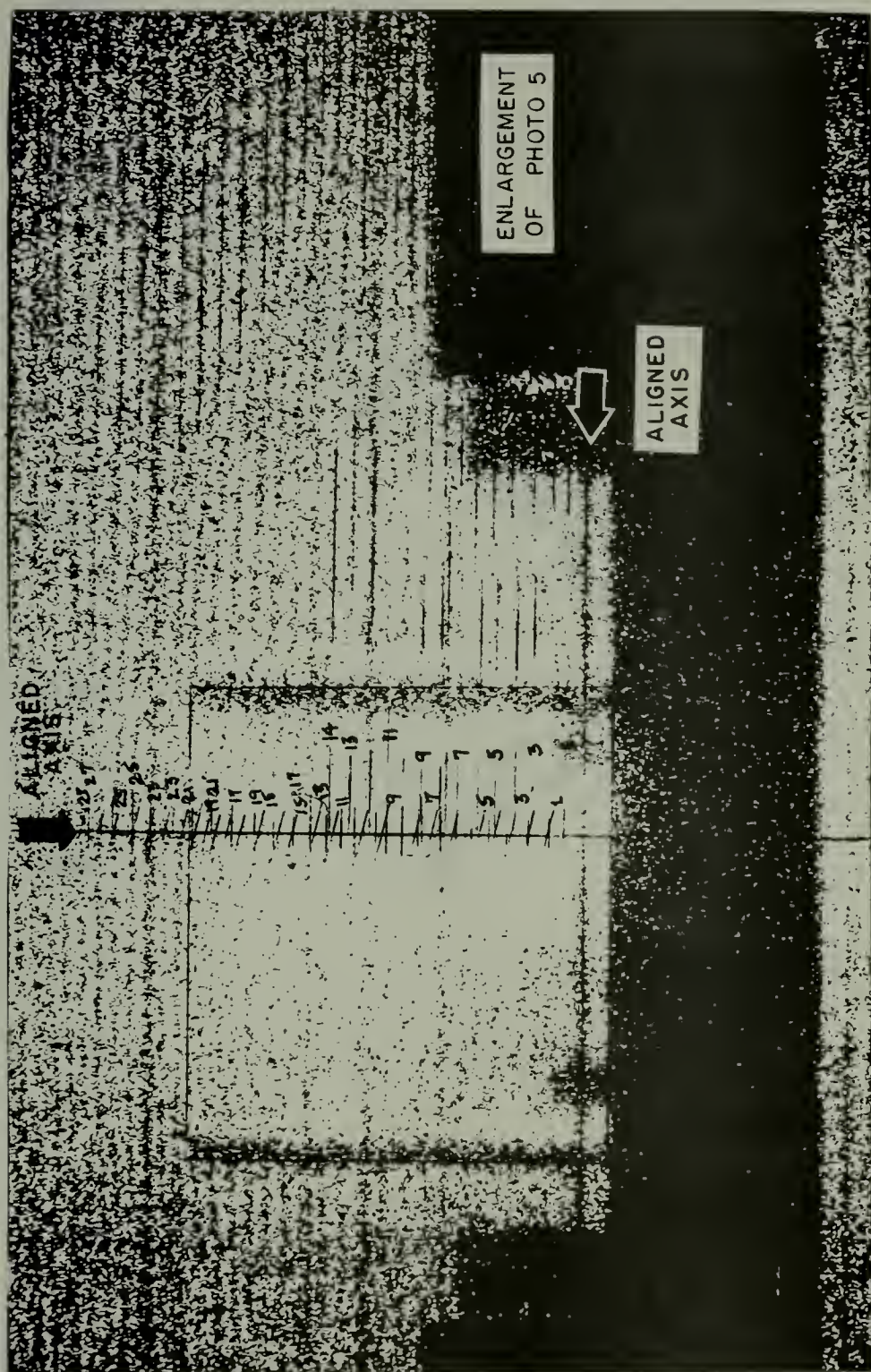


Figure 39. Actual Enlarged Photograph Used for the Data Reduction of Interferogram Photograph. 5
 Aligned at $Z = 0.387$, $Y' = 0.055$ for Mach 2.84 and 0° Model Rotation Angle



Figure 40. Comparison of Fringe Data Obtained from Drawings of Interferogram Photographs 1 and 2 Aligned at $Y' = 0.847$



Figure 41. Comparison of Fringe Data Obtained from Photographic Enlargements of Interferogram Photographs 1 and 2 Aligned at $Y' = 0.847$

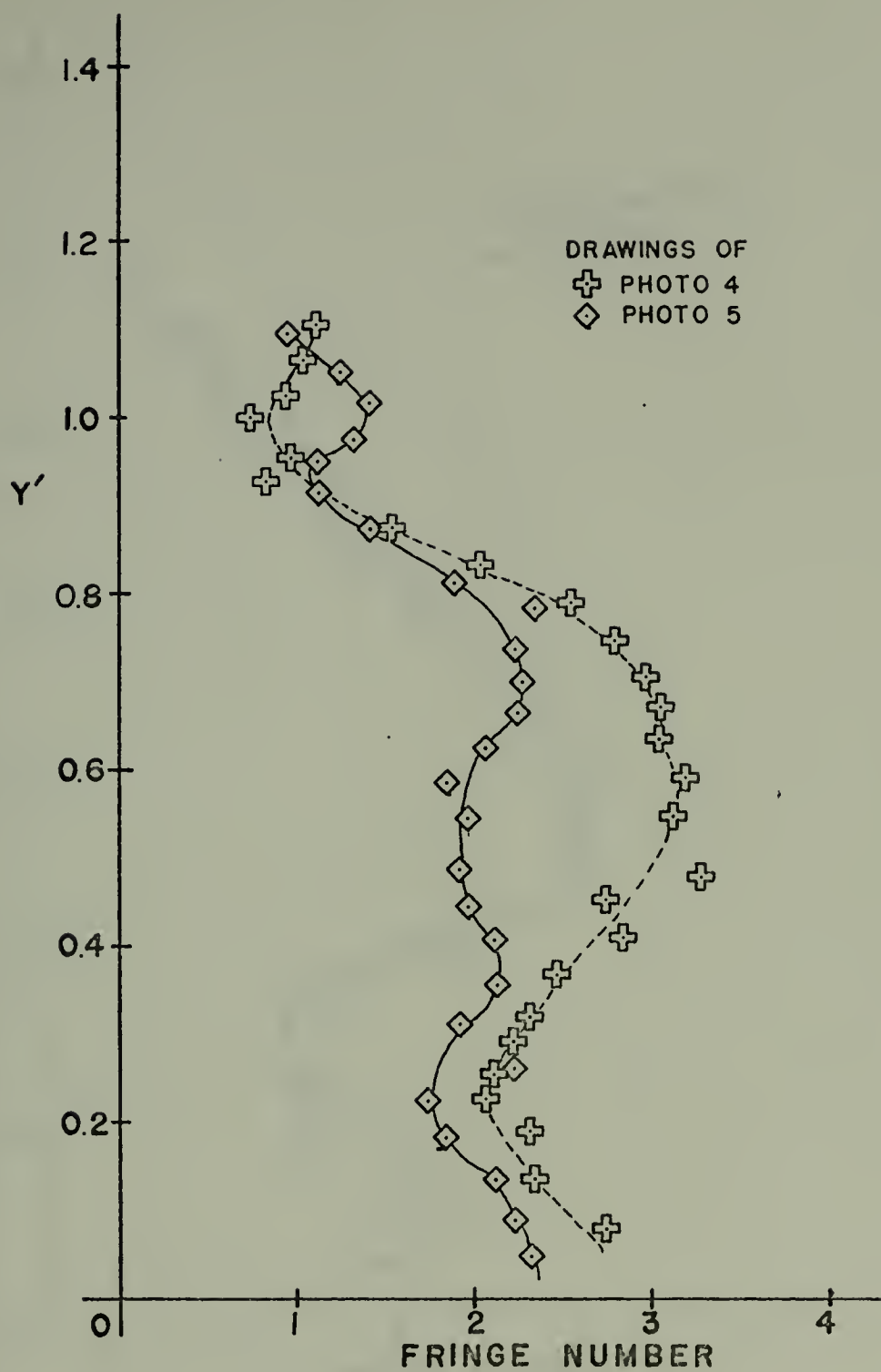


Figure 42. Comparison of Fringe Data Obtained from Drawings of Interferogram Photographs 4 and 5 Aligned at $Y' = 0.055$

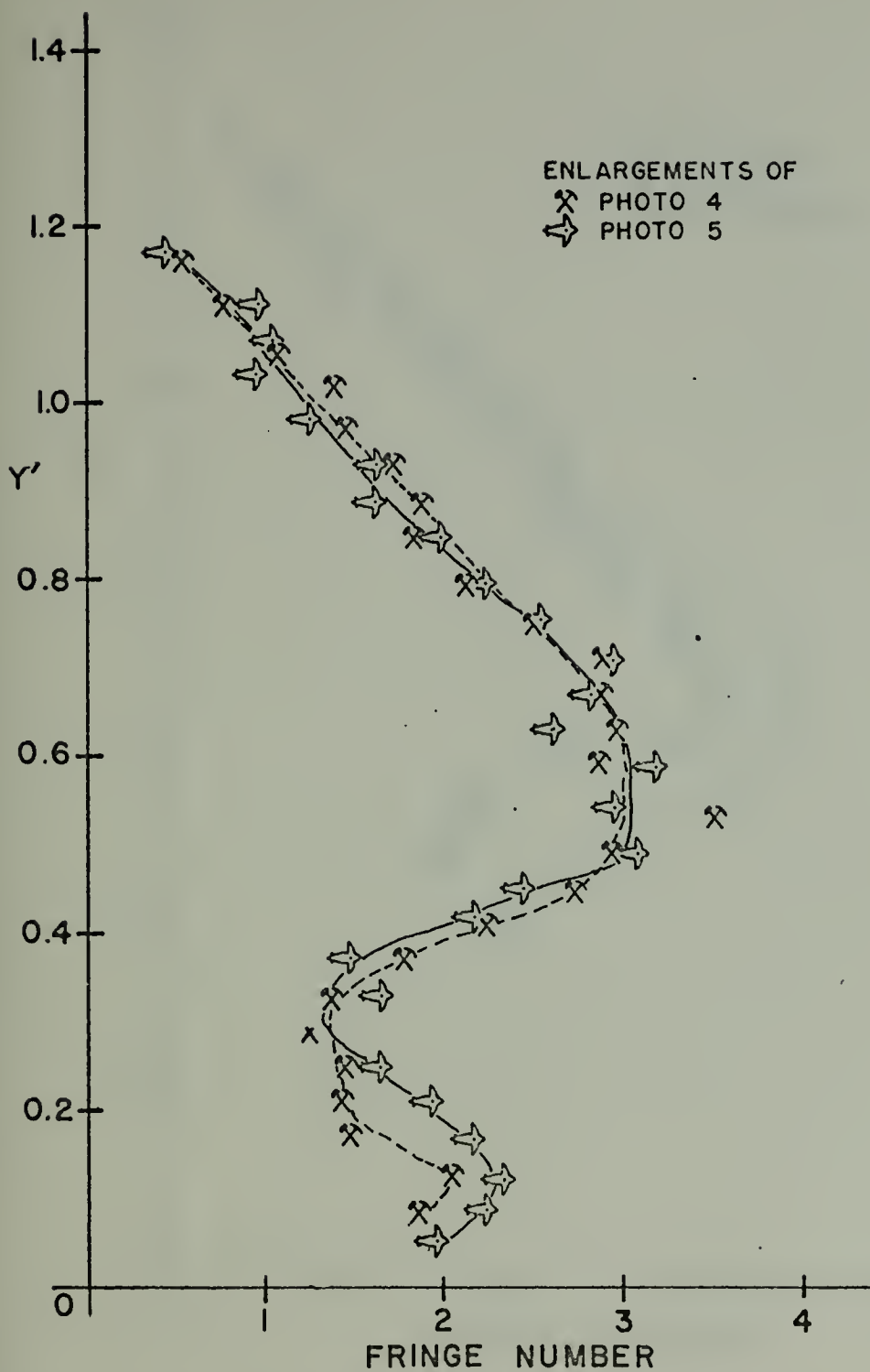


Figure 43. Comparison of Fringe Data Obtained from Photographic Enlargements of Interferogram Photographs 4 and 5 Aligned at $Y' = 0.055$

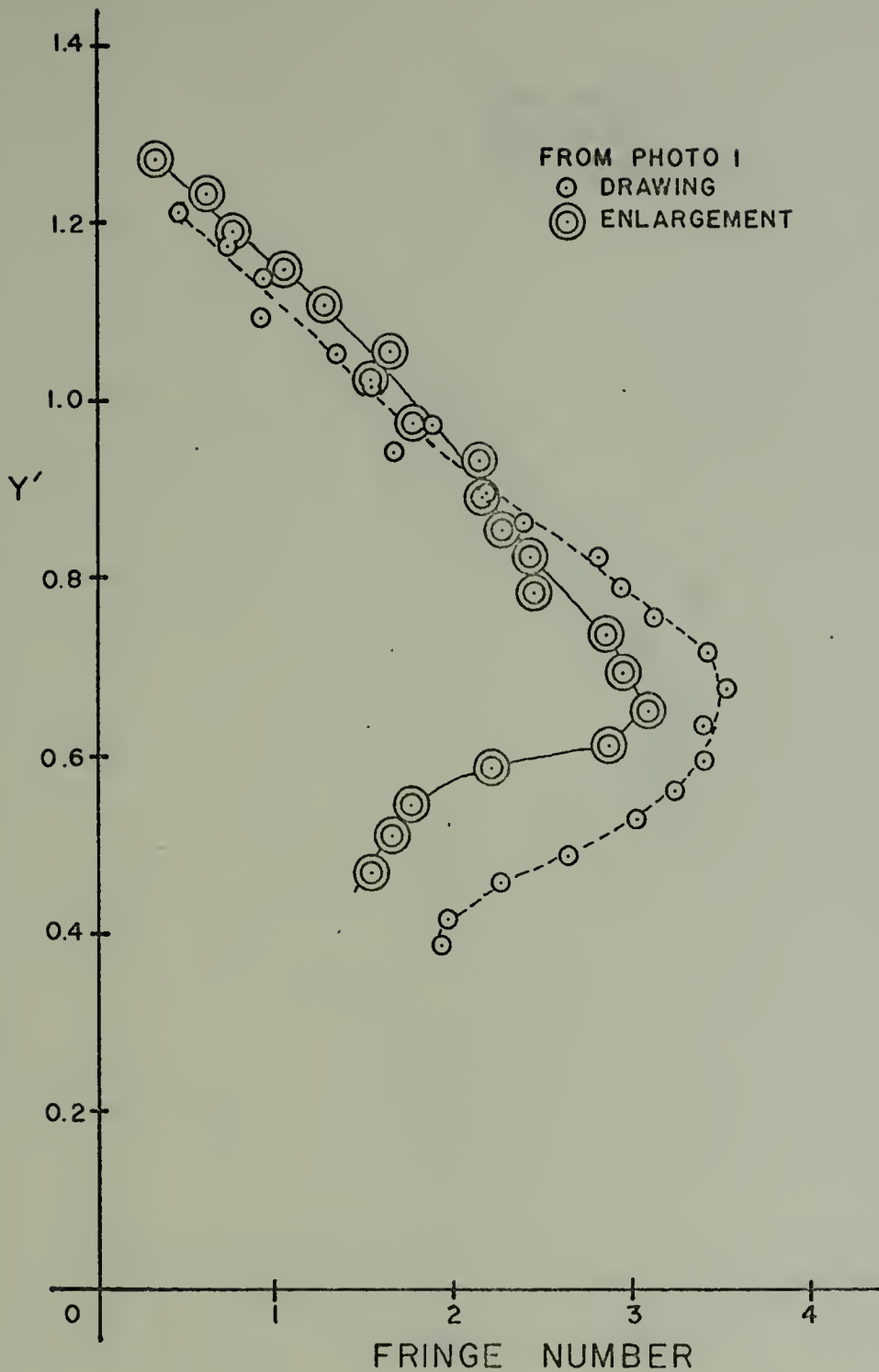


Figure 44. Comparison of Fringe Data Obtained from the Drawing and Photographic Enlargement of Interferogram Photograph 1 Aligned at $Y' = 0.847$

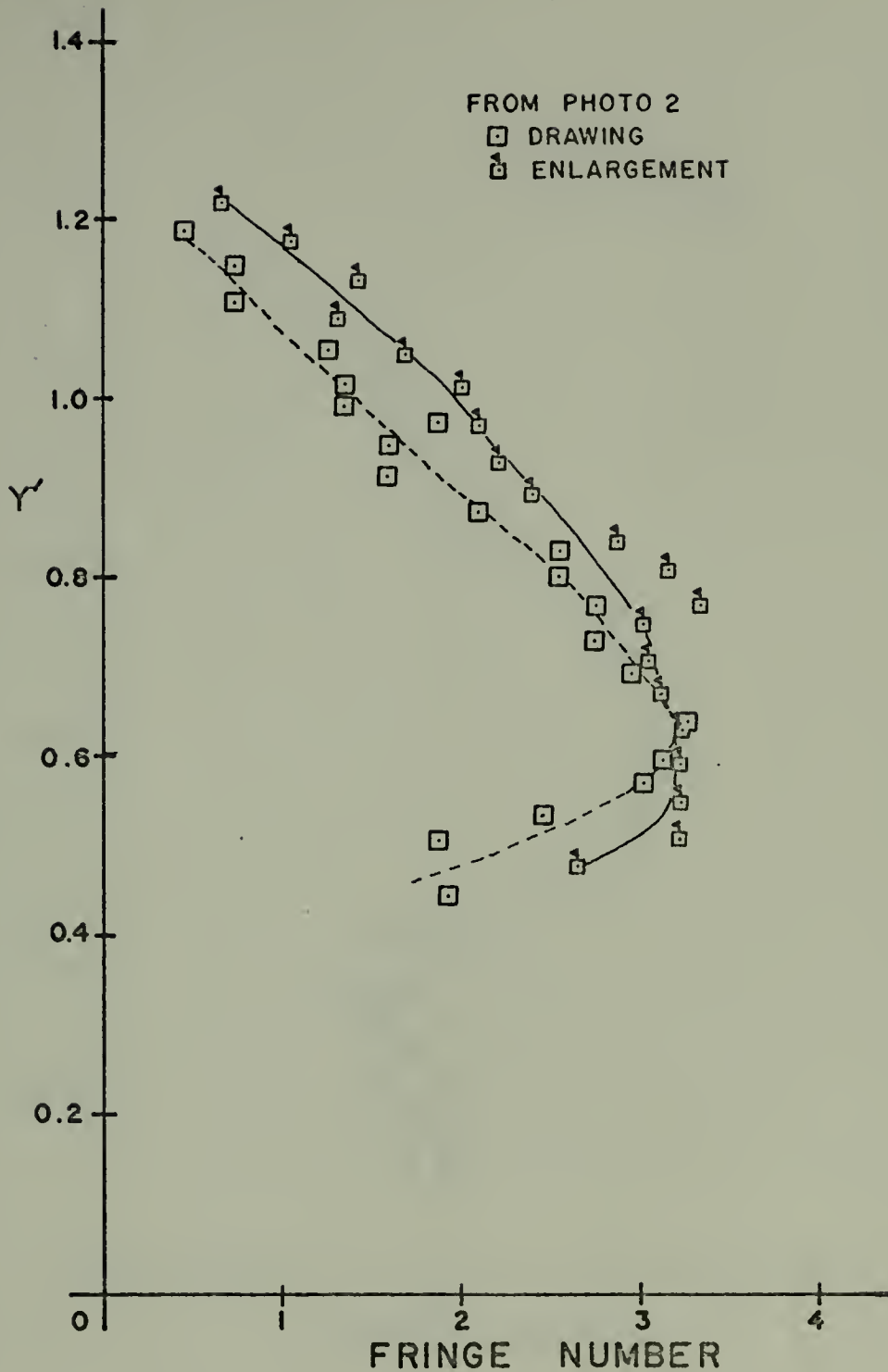


Figure 45. Comparison of Fringe Data Obtained from the Drawing and Photographic Enlargement of Interferogram Photograph 2 Aligned at $Y' = 0.847$

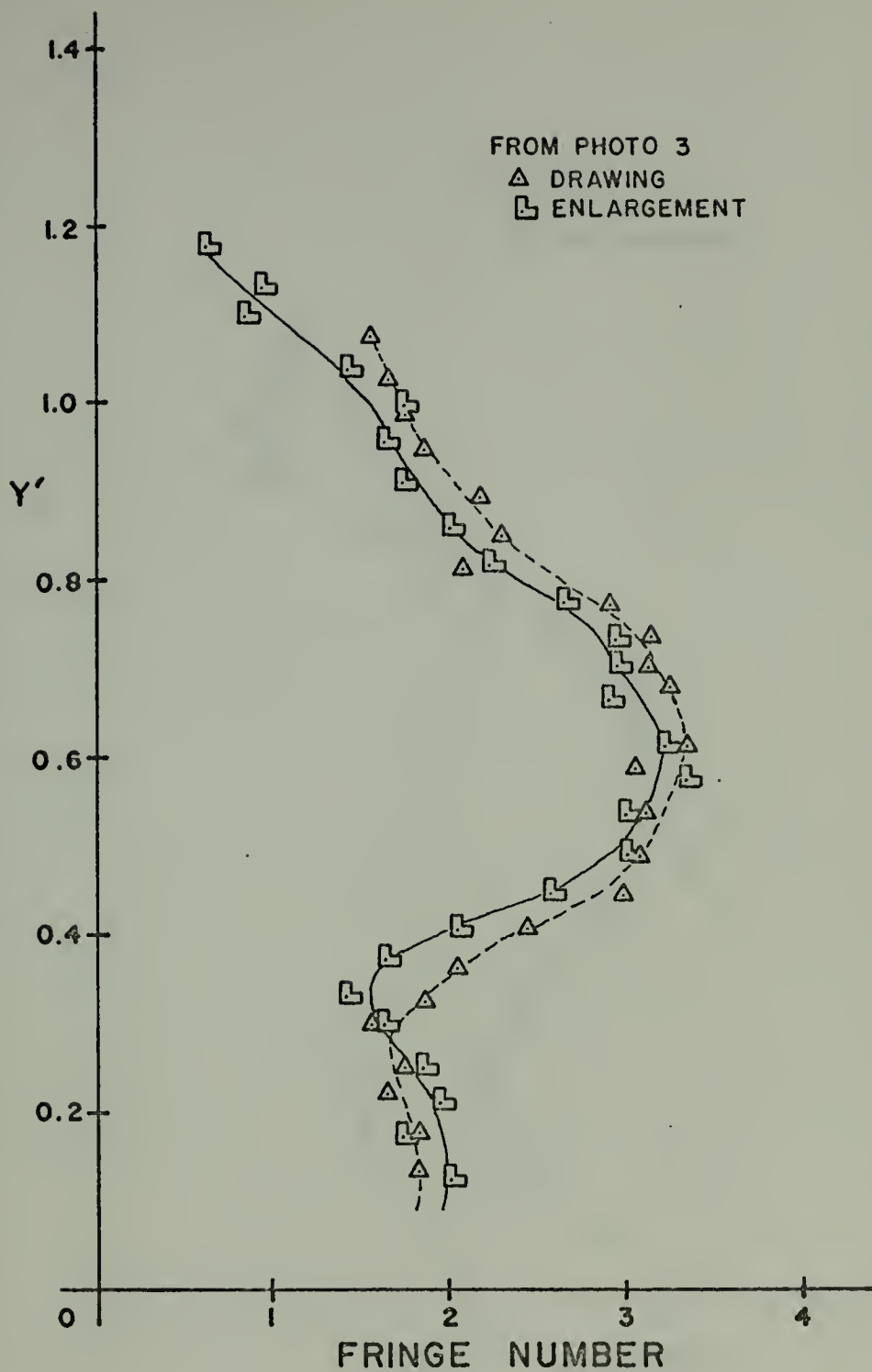


Figure 46. Comparison of Fringe Data Obtained from the Drawing and Photographic Enlargement of Interferogram Photograph 3 Aligned at $Y' = 0.451$

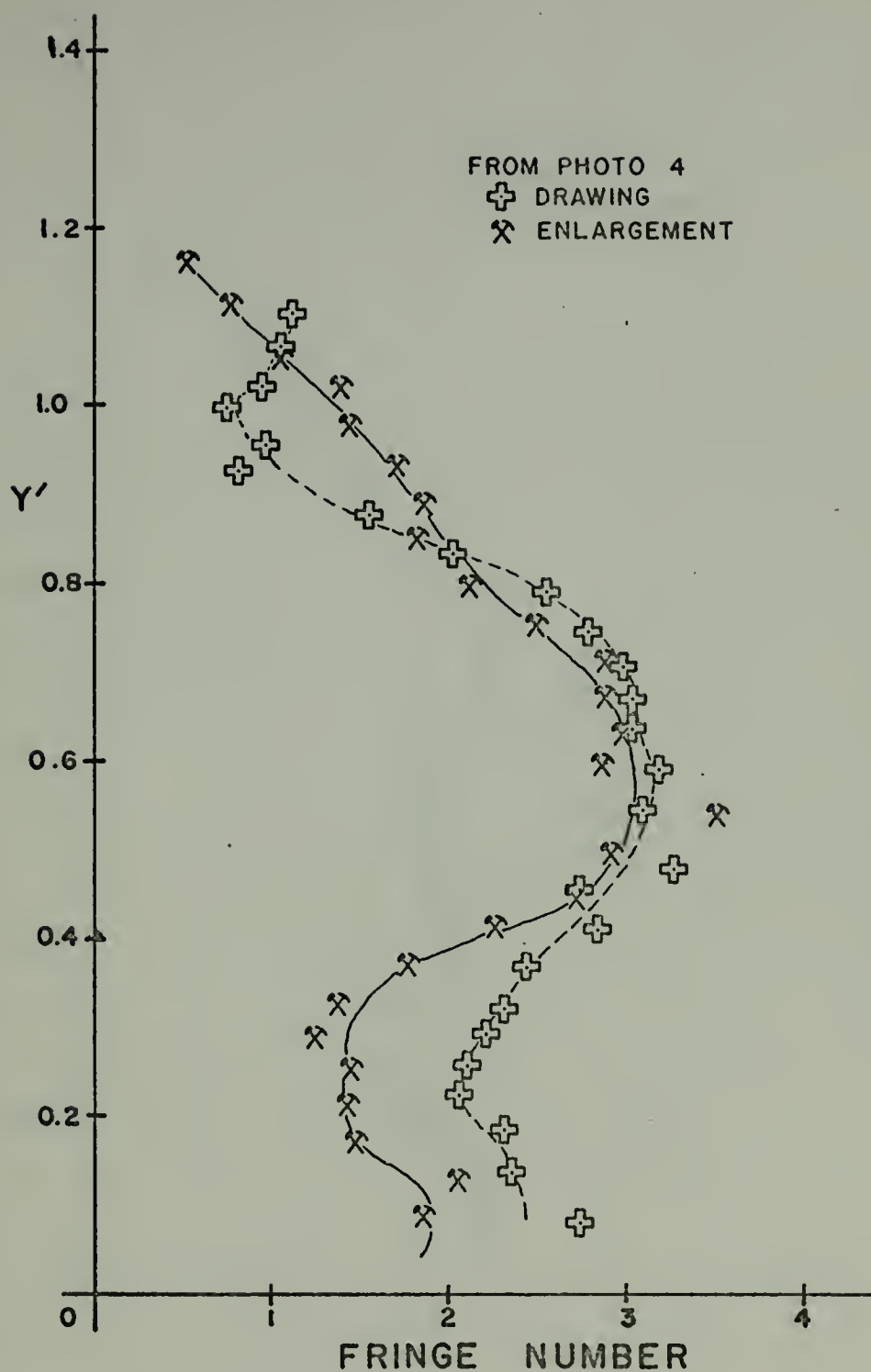


Figure 47. Comparison of Fringe Data Obtained from the Drawing and Photographic Enlargement of Interferogram Photograph 4 Aligned at $Y' = 0.055$

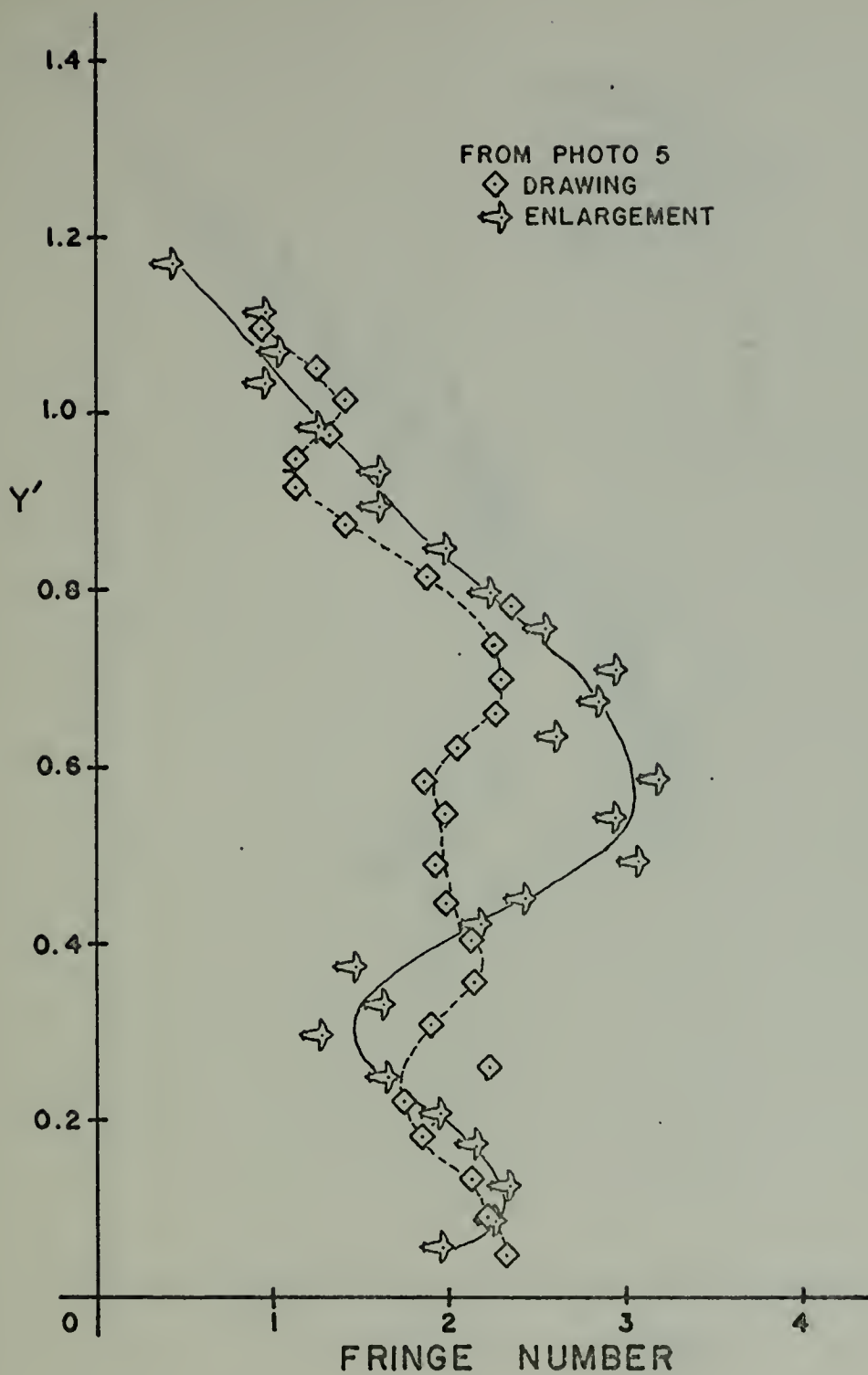


Figure 48. Comparison of Fringe Data Obtained from the Drawing and Photographic Enlargement of Interferogram Photograph 5 Aligned at $Y' = 0.055$

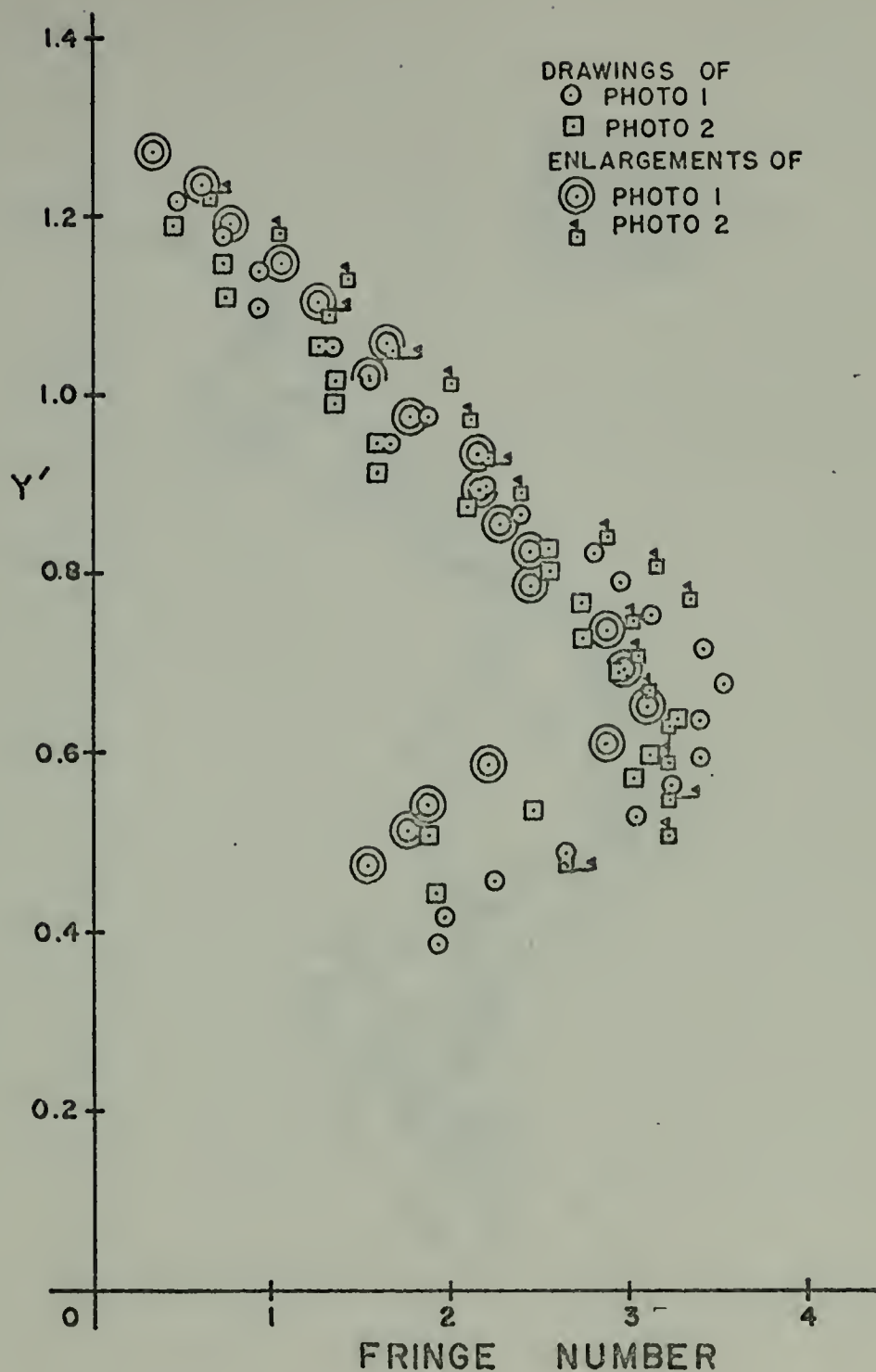


Figure 49. Comparison of Fringe Data Obtained from the Drawings and Photographic Enlargements of Interferogram Photographs 1 and 2 Aligned at $Y' = 0.847$

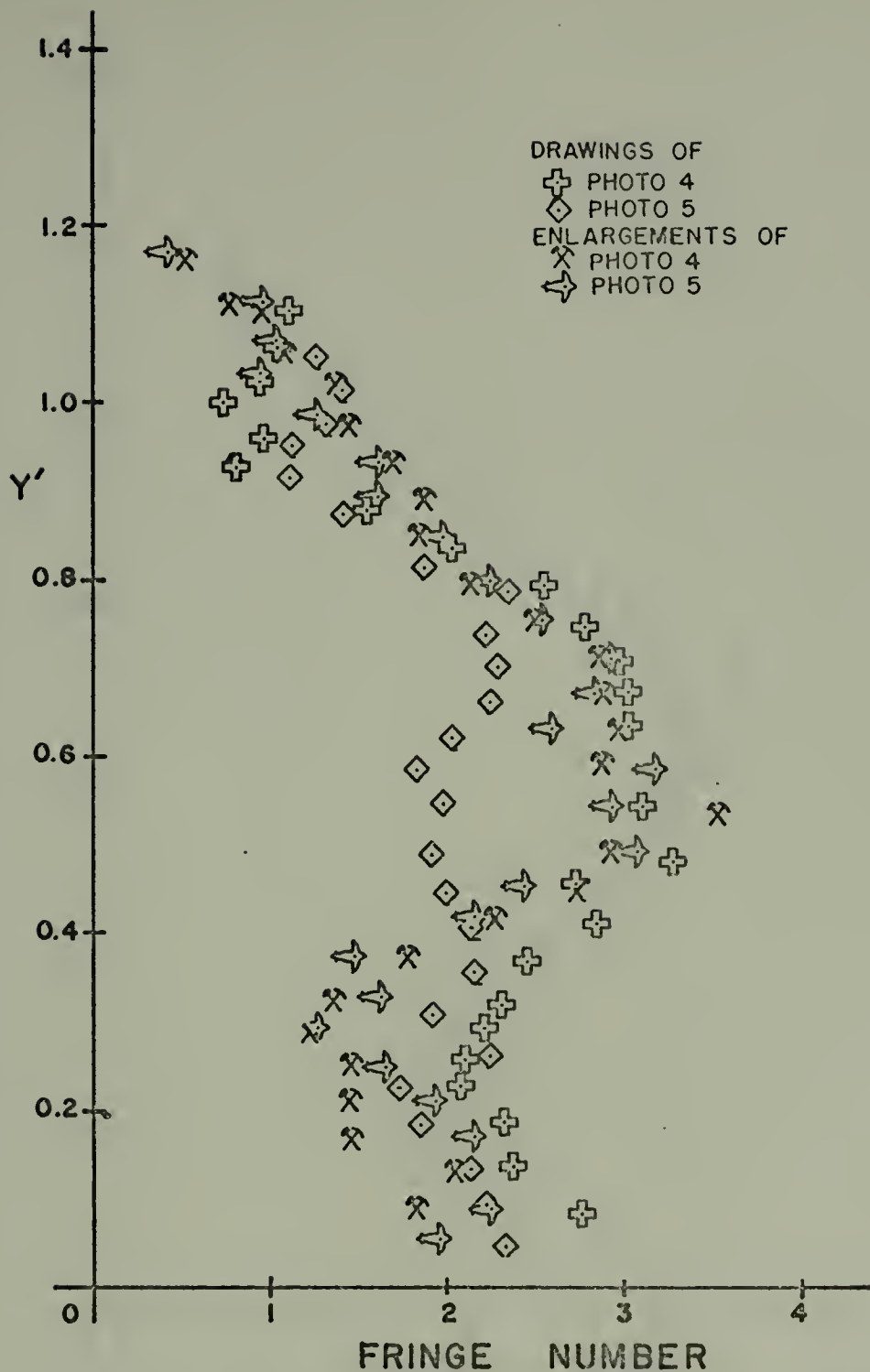


Figure 50. Comparison of Fringe Data Obtained from the Drawings and Photographic Enlargements of Interferogram Photographs 4 and 5 Aligned at $Y' = 0.055$

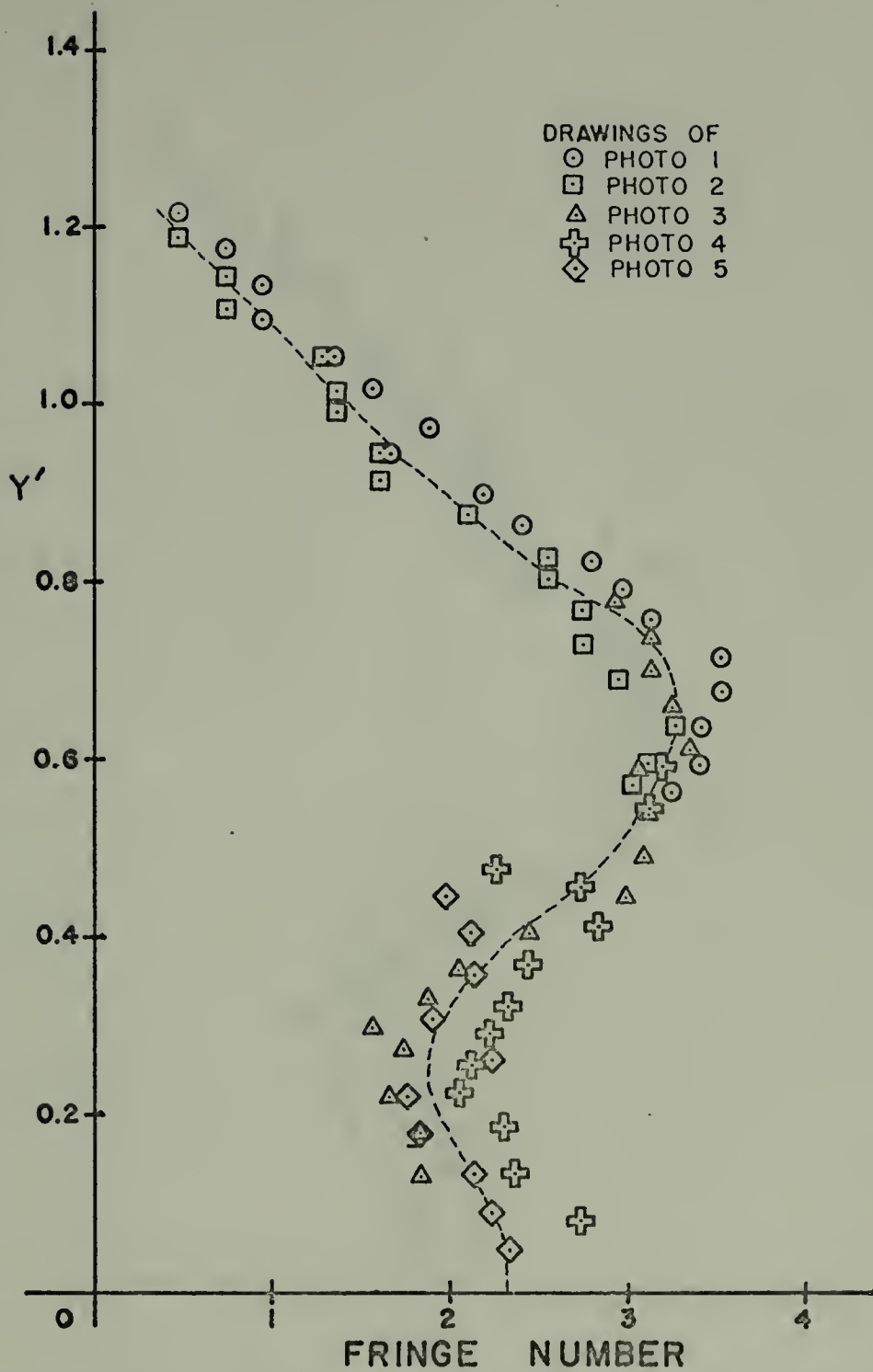


Figure 51. Fringe Number Across the Fin in the $Z = 0.387$ Plane for $\beta = 0^\circ$, Mach 2.84 as Determined from the Drawings of the Interferogram Photographs

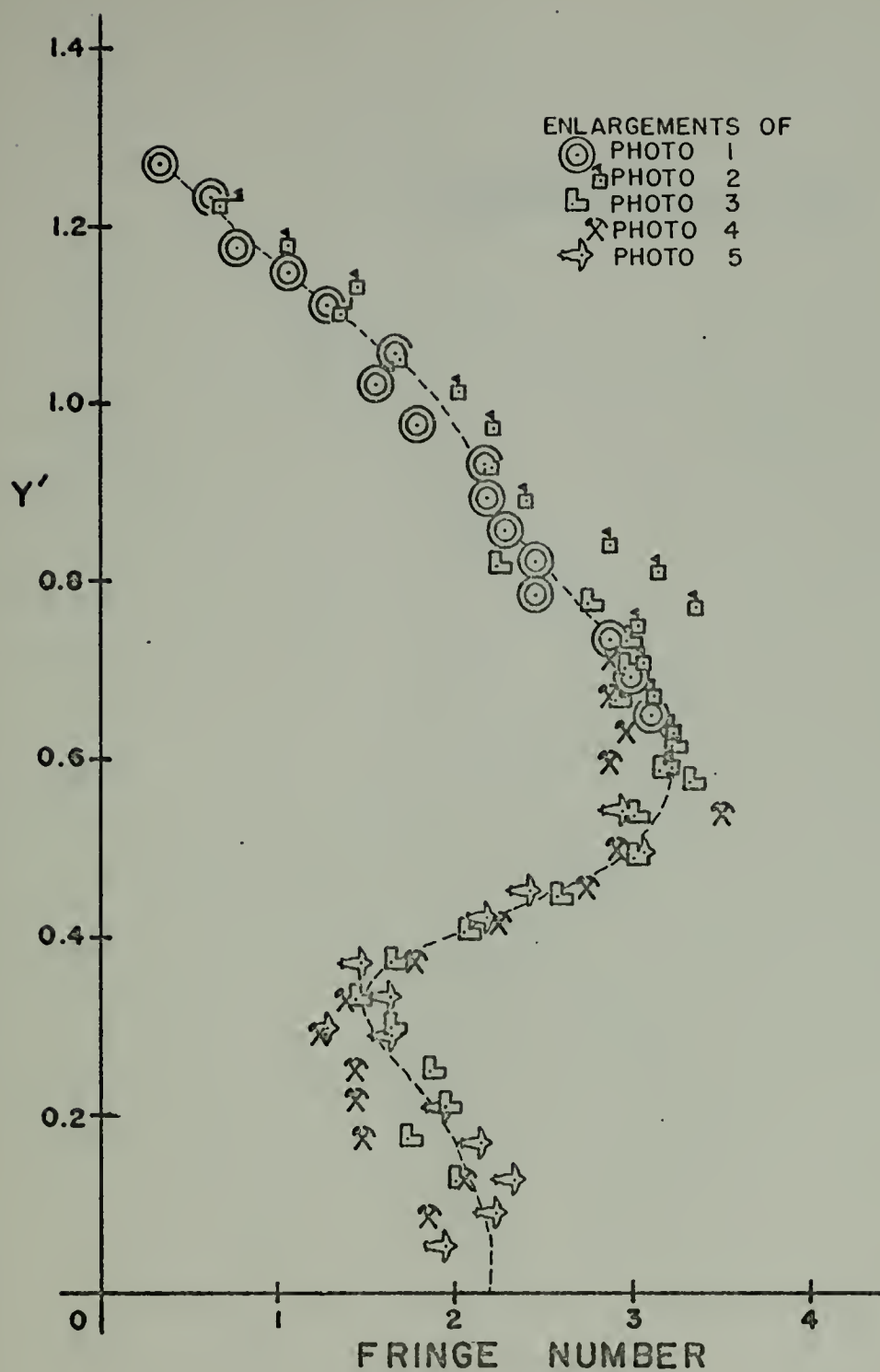


Figure 52. Fringe Number Across the Fin in the $Z = 0.387$ Plane for $\delta = 0^\circ$, Mach 2.84 as Determined from the Photographic Enlargements of the Interferogram Photographs

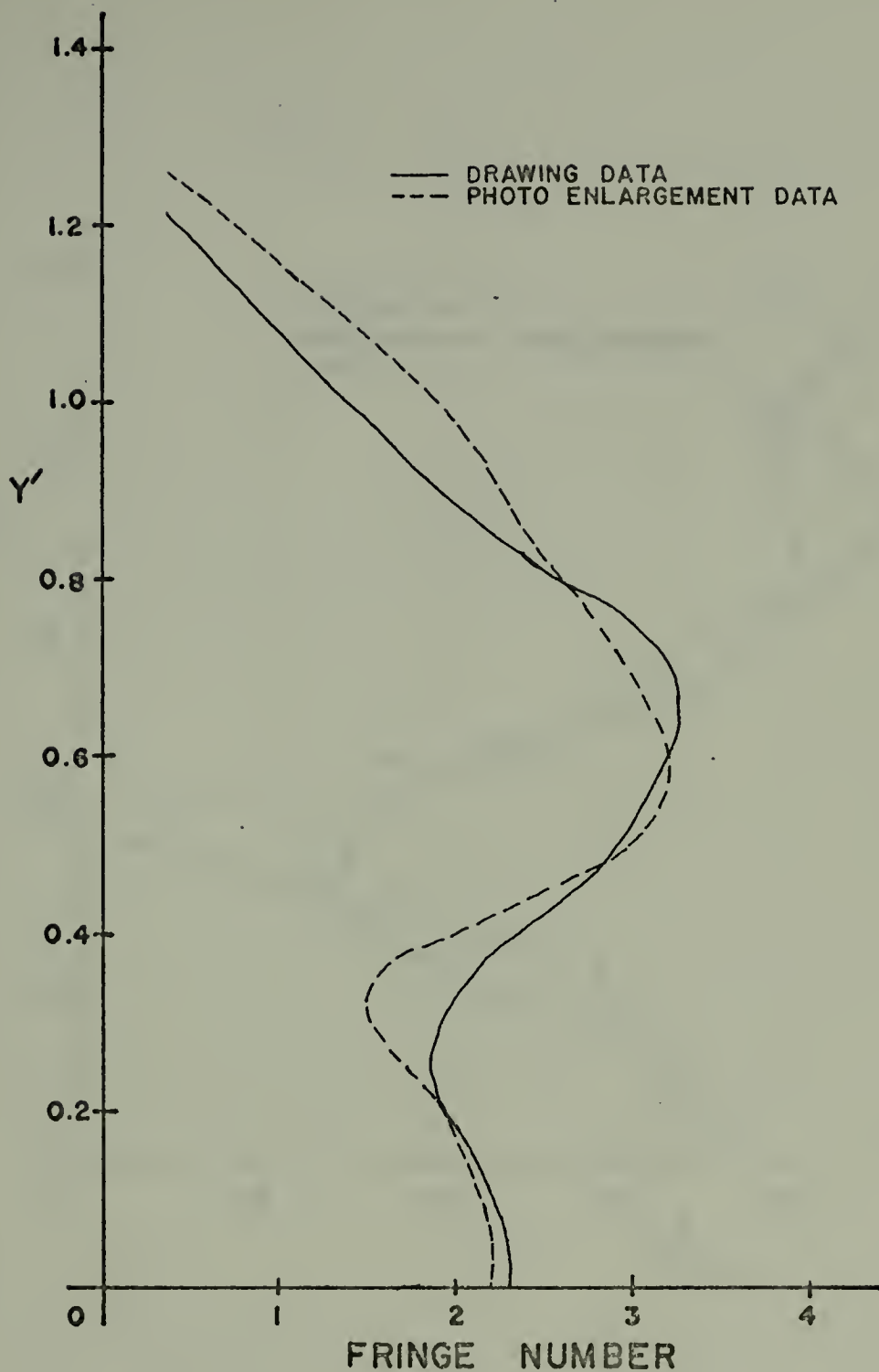


Figure 53. Comparison of the Fringe Numbers Across the Fin in the $Z = 0.387$ Plane for $\xi = 0^\circ$, Mach 2.84 as Determined from the Drawings and Photographic Enlargements of the Interferogram Photographs

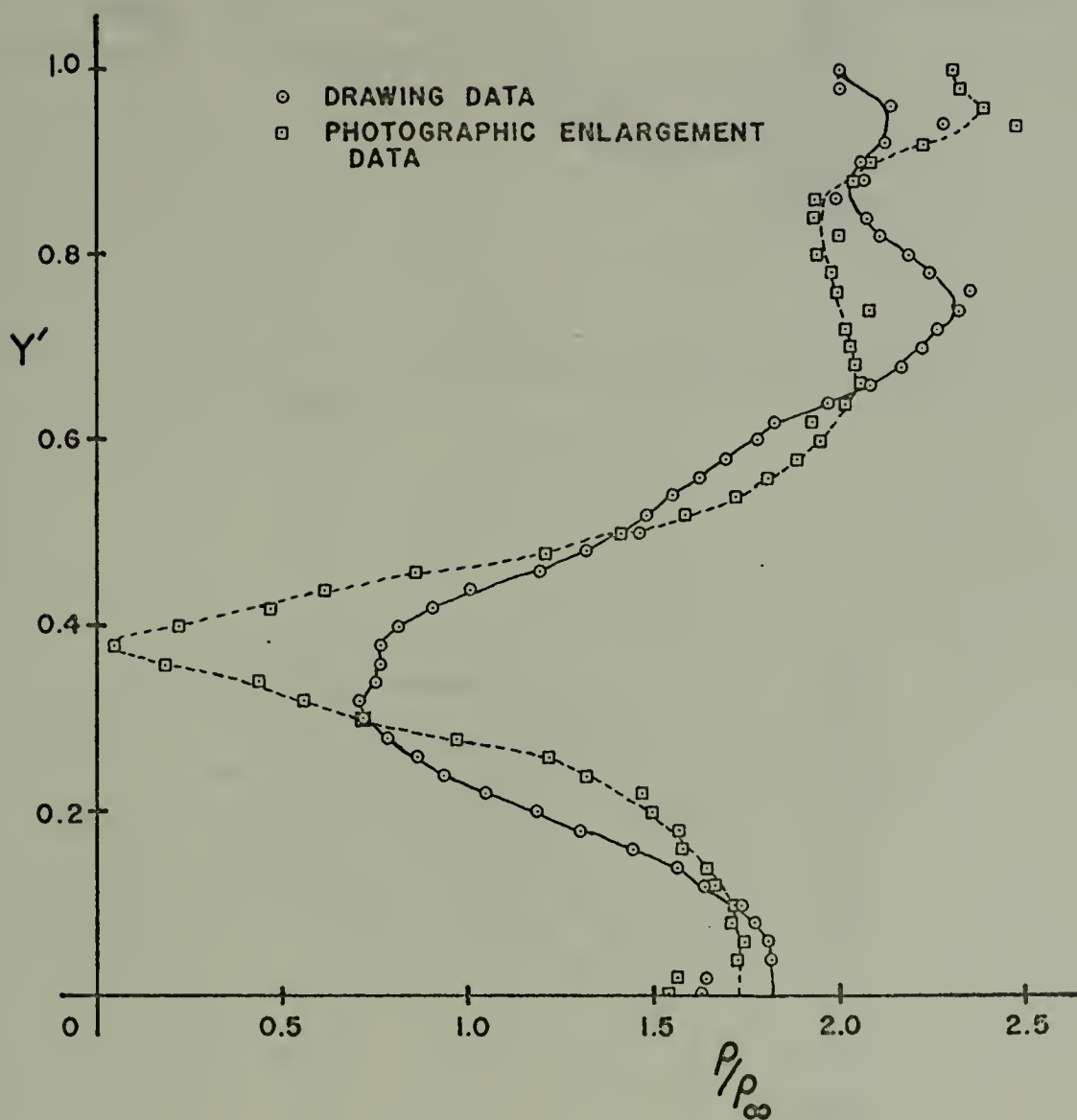


Figure 54. Comparison of the Density Distributions Calculated by HOLOVLR for an Axisymmetric Case

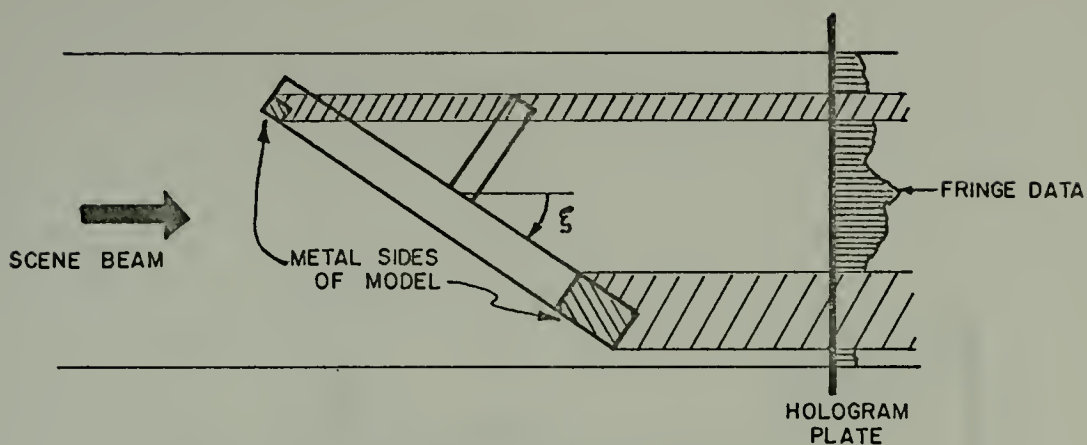


Figure 55. Schematic of the Model Center Section Rotated to Illustrate the Loss of Fringe Information Due to Model Shadows on the Hologram

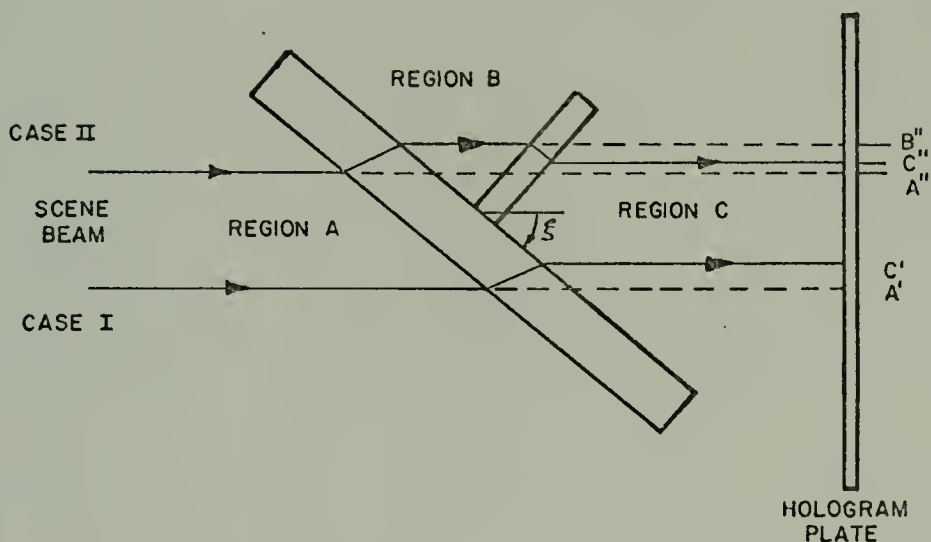


Figure 56. Schematic Illustrating the Problem of Different Fringe Information Being Superimposed on One Beam Caused by the Model Plastic

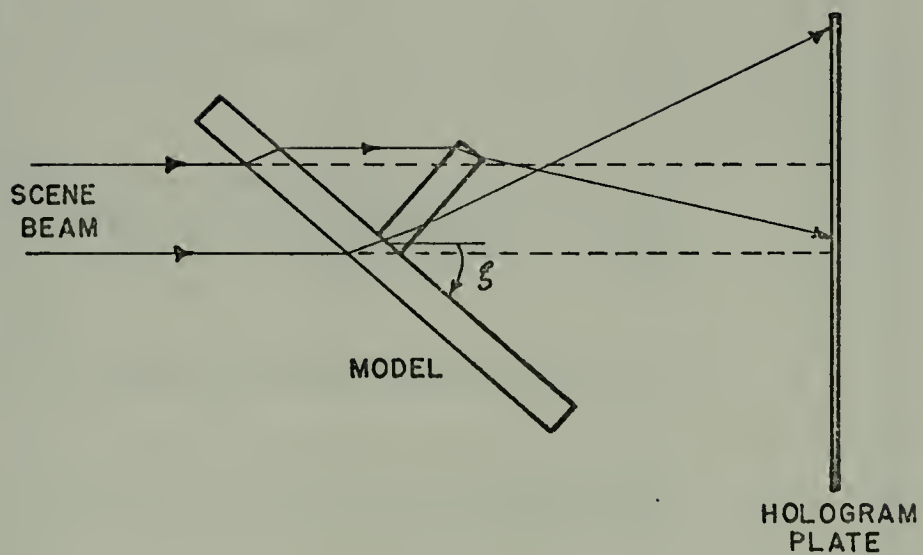


Figure 52. Schematic Illustrating the Scene Beam Refraction in the Fin Root and Tip Areas

Line No.	Distance Above Aligned Plane			Y' $\odot = \odot + .055$	Fringe Location (inches) \odot	Fringe Change $f = \odot - \odot$	Fringe Number $g = \frac{f}{h}$	Amount of 1.1 Fringe Correction Required	Corrected Values	
	Measured (inches)	Normalized \odot wing height	Corrected Distance from Tables						Y'	g
1	.190	.075	.071	.126	.360	.170	1.641	1.1	.081	2.74
2	.330	.131	.124	.179	.460	.130	1.255	1.1	.134	2.36
3	.465	.185	.176	.231	.590	.125	1.208	1.1	.186	2.31
4	.570	.226	.215	.270	.670	.100	.965	1.1	.225	2.07
5	.660	.262	.249	.304	.765	.105	1.013	1.1	.259	2.11
6	.745	.296	.281	.336	.860	.115	1.110	1.1	.291	2.21
7	.825	.327	.311	.366	.950	.125	1.208	1.1	.321	2.31
8	.950	.377	.358	.413	1.090	.140	1.352	1.1	.368	2.45
9	1.060	.421	.400	.455	1.240	.180	1.737	1.1	.410	2.84
10	1.180	.468	.445	.500	1.350	.170	1.641	1.1	.455	2.74
11	1.245	.494	.469	.524	1.500	.255	2.172	1.1	.479	3.27
12	1.350	.536	.509	.564	1.620	.270	2.607	.5	.543	3.11
13	1.430	.567	.539	.594	1.750	.320	3.090	.1	.590	3.19
14	1.533	.609	.579	.634	1.850	.315	3.041	0.	.634	3.04
15	1.625	.649	.617	.672	1.940	.315	3.041	0.	.672	3.04
16	1.720	.683	.649	.704	2.030	.310	2.994	0.	.704	2.99
17	1.830	.726	.690	.745	2.120	.290	2.800	0.	.745	2.80
18	1.955	.776	.737	.792	2.220	.265	2.560	0.	.792	2.56
19	2.080	.825	.783	.838	2.290	.210	2.028	0.	.838	2.03
20	2.180	.865	.821	.876	2.340	.160	1.545	0.	.876	1.55
21	2.315	.919	.872	.927	2.400	.085	.820	0.	.927	.82
22	2.400	.952	.904	.959	2.500	.100	.965	0.	.959	.97
23	2.500	.992	.942	.997	2.580	.080	.772	0.	.997	.77
24	2.570	1.020	.969	1.024	2.670	.100	.965	0.	1.024	.97
25	2.680	1.063	1.009	1.064	2.790	.110	1.062	0.	1.064	1.06
26	2.780	1.103	1.048	1.103	2.885	.115	1.110	0.	1.103	1.11

Wing height = 2.52 inches

Wing length = 2.92 inches

Average fringe interval = .1036 inches

Table I. Tabulation of Fringe Shift Data Taken From the Drawing of Photo 4

Line No.	Distance Above Aligned Plane				Y' ④ = ③ + .055	Fringe Location (inches) ⑤	Fringe Change f = ⑤ - ②	Fringe Number $g = \frac{f}{b}$
	Measured (inches) ①	Corrected to Free Stream (inches) ②	Normalized $\frac{②}{(\text{wing height})}$	Corrected Distance from Tables ③				
1	.190*	.076	.032	.030	.085	.270	.194	1.867
2	.290*	.176	.073	.069	.124	.390	.214	2.050
3	.410*	.296	.123	.117	.172	.450	.154	1.482
4	.525*	.411	.171	.162	.217	.560	.149	1.434
5	.615*	.501	.208	.198	.253	.650	.149	1.434
6	.710*	.596	.247	.235	.290	.725	.129	1.242
7	.800*	.686	.285	.271	.326	.830	.144	1.386
8	.910*	.796	.330	.314	.369	.980	.184	1.771
9	1.020*	.906	.376	.357	.412	1.140	.234	2.252
10	1.120*	1.006	.417	.396	.451	1.290	.284	2.738
11	1.230*	1.116	.463	.440	.495	1.420	.304	2.926
12	1.330*	1.216	.505	.480	.535	1.580	.364	3.509
13	1.370	1.370	.568	.540	.595	1.670	.300	2.887
14	1.460	1.460	.606	.576	.631	1.770	.310	2.984
15	1.560	1.560	.647	.615	.670	1.860	.300	2.887
16	1.660	1.660	.689	.655	.710	1.960	.300	2.887
17	1.760	1.760	.730	.694	.749	2.020	.260	2.502
18	1.880	1.880	.780	.741	.796	2.100	.220	2.117
19	2.000	2.000	.830	.788	.843	2.190	.190	1.829
20	2.110	2.110	.876	.832	.887	2.305	.195	1.877
21	2.220	2.220	.921	.875	.930	2.390	.170	1.704
22	2.330	2.330	.967	.919	.974	2.480	.150	1.444
23	2.445	2.445	1.015	.964	1.019	2.590	.145	1.396
24	2.570	2.570	1.066	1.013	1.068	2.680	.110	1.059
25	2.680	2.680	1.112	1.056	1.111	2.760	.080	.770
26	2.805	2.805	1.164	1.106	1.161	2.860	.055	.529

* Locations to be corrected to free stream conditions

Table II. Tabulation of Fringe Shift Data Taken From the Photographic Enlargement of Photo 4

APPENDIX A

REDUCTION OF AN INTERFEROGRAM TO OBTAIN FRINGE SHIFT DATA

The fringe shift reduction process was accomplished using two techniques. The first involved projecting the interferogram negative onto a sheet of white paper using a photo-enlarger. The light fringes offered the best contrast and were therefore traced out in Figures 30-34. In each drawing it was necessary to begin tracing the fringes above the fin and work towards the fin root since the transition across the fin tip determined the correct connection of the fringes across the fin leading edge shock. In order to determine the fringe change, one fringe line in the free stream region forward of the fin which appeared the straightest and paralleled the majority of other fringe lines was selected. A straight line, called the fringe reference line, was drawn over its centerline and extended to cross the y' axis. The remaining reference lines were then drawn parallel to the first and along the centerlines of the remaining free stream fringes. In reducing the drawings it was not realized until later that the free stream fringe patterns before and after the plate leading edge Prandtl-Meyer expansion differed considerably. This effect was taken into account later.

A ruler scaled to 0.01 inches was then placed along the y' axis and the distances of the fringes and reference lines above and below the aligned y' plane were then recorded in Table I for Photograph 4. The fin width and length were then measured and the average values were recorded. The average fringe interval was determined by measuring the distance between the first and last fringes used and dividing by the number of intervals. The fringe change was found by subtracting the fringe crossing

point. The fringe number was calculated by dividing the change by the average fringe interval. The reference line location was then normalized with respect to the measured fin height. Since the actual fin height was very close to one inch, the above number was considered to be the number of inches above or below the aligned plane. Thus the table computing the tunnel wall and grid refraction displacements in Appendix B could be entered to determine the actual reference line location with respect to the aligned plane of the drawing (see Figure 29). The locations were then converted to the y' axis system by adding the normalized location of the aligned plane. After realizing that not all the reference lines were referenced to the free stream density forward of the plate leading edge, the enlarged photographs (Figures 35-39) were checked against the drawings. It was found that the Prandtl-Meyer expansion caused a fringe number change of approximately 1.1. Consequently each reference line in the drawing was compared with the enlarged photograph and an appropriate percentage of the 1.1 fringe number was used as a correction (see Table I). The calculated fringe numbers had the correction fringe number added to them while the y' locations were corrected by

$$y'_{\text{corr}} = y'_{\text{orig}} - \frac{(1.1 \text{ Fringe no.}) \times (\text{Fringe Interval})}{(\text{Fin Height})} \quad (\text{A-1})$$

The second reduction technique was to use enlarged photographs made from the interferogram negatives to obtain the fringe change. The fringe lines were first traced over lightly with a pencil and then verified against the other photographs to ensure correct tracing. A datum fringe reference line was chosen as before and drawn. The remaining reference lines for the upper free stream fringe lines forward of the Prandtl-Meyer expansion were then drawn parallel to the datum. When it became impossible

to use fringe lines forward of the expansion, the reference lines were then drawn along the centerline of the fringes between the expansion and the fin. The same ruler was used to obtain the fringe crossing points, the reference crossing points, fin measurements, and the average fringe interval and they were recorded in Table 2. The reference line crossing points were then corrected to free stream conditions, using a 1.1 Fringe number correction for those referenced to the pattern between the expansion and fin leading edge. The fringe number and reference fin locations were calculated as before. This method was considered more accurate because the reference lines and fringe lines could easily be rechecked for accuracy and corrected in the event that a fringe line was traced incorrectly or a reference line was misaligned. The accuracy was directly proportional to the hologram resolution which was not true for the drawings since the reference lines are drawn parallel to hand-drawn fringe lines.

APPENDIX B

CALCULATION OF TUNNEL WALL AND GRID PLASTIC REFRACTION CORRECTION

In the interferogram photographs used to obtain the fringe change, every point off the alignment axis will be slightly distorted due to the plastic tunnel wall and grid. This effect is illustrated in Figure 19. From Snells Law of Refraction, the angles of incidence and refraction are related by

$$\sin \alpha = n \sin \beta \quad (B-1)$$

where n is the index of refraction between plastic and air. Then can be written

$$\beta = \sin^{-1} \left(\frac{\sin \alpha}{n} \right) \quad (B-2)$$

Since the tunnel wall and grid have the same index of refraction, they can be considered on material with thickness $t = ab$ in Figure 19. Then consider the height bd which can be written

$$bd = t \tan \alpha \quad (B-3)$$

The beam displacement, Δy , is then

$$\Delta Y = bd - bc = t \tan \alpha - t \tan \beta \quad (B-4)$$

but $\tan \alpha$ is

$$\tan \alpha = \frac{Y_{\text{observed}}}{L} \quad (B-5)$$

Combining Equation (B-2), (B-4), and (B-5) the beam displacement becomes

$$\Delta Y = t \left[\frac{Y_{\text{observed}}}{L} - \tan \left[\sin^{-1} \left(\frac{\sin \alpha}{n} \right) \right] \right] \quad (B-6)$$

The true location of the observed point is then

$$Y_{\text{true}} = Y_{\text{observed}} - \Delta Y \quad (B-7)$$

A FORTRAN computer program was written to generate a table giving the true locations versus the observed locations. In the program the constants and variables from the above equations were defined as

Y_{observed}	=	Y
Y_{true}	=	YTRUE
ΔY	=	DY
α	=	ALFA
L	=	L
n	=	N

Since the computer cannot calculate Equations (B-2) and (B-6) as written, they were constructed by parts using such letters as AA, AB, etc. The program and tables are included in the next few pages.


```

C      ****
C      **
C      ** THIS PROGRAM COMPUTES THE CORRECTION FOR THE
C      ** OFF AXIS TUNNEL WALL PARALLAX. THE FOLLOWING
C      ** INPUT PARAMETERS ARE REQUIRED:
C      ** L = DISTANCE FROM HOLOGRAM PLANE TO THE MODEL
C      ** CENTER LINE
C      ** N = INDEX OF REFRACTION FOR TUNNEL WALL
C      ** T = THICKNESS OF TUNNEL AND GRID PLEXIGLAS
C      ** Y = OBSERVED DISTANCE OF THE POINT IN THE
C      ** PHOTOGRAPH FROM THE ALIGNED POINT
C      ** YTRUE = TRUE DISTANCE FROM ALIGNED POINT TO
C      ** THE POINT ON THE MODEL PLANE
C      ** YMAX = MAXIMUM DISTANCE OF INTEREST FROM THE
C      ** ALIGNED POINT
C      ****
C
C      REAL*4 L,N
C
C      INPUT PARAMETERS
C
C      L=15.0
C      N=1.5
C      T=2.25
C      YMAX=2.5
C      PI=3.141593
C
C      OUTPUT FORMAT
C
C      WRITE(6,100)L,N,T
100  FORMAT('1',T25,'THE FOLLOWING TABLE IS TO ACCOUNT FOR'
1  ' THE PARALLAX'/T25,'ERROR IN VIEWING THE MODEL '
2  'THROUGH GLASS WALLS AT'/T25,'ANY OTHER POINT THAN '
3  'AT THE ALIGNMENT POINT. INPUT'/T25,'PARAMETERS ARE:'
4  '/T35,'(1) L = ',F6.3,' INCHES'/T35,'(2) N = ',F6.3,
5  ' INCHES'/T35,'(3) T = ',F6.3,' INCHES')
C      WRITE(6,110)
110  FORMAT(' ',T24,'OBSERVED',T40,'TRUE',T54,'ERROR',T70,
1  'RAY'/T24,'DISTANCE',T38,'DISTANCE',T69,'ANGLE'/T24,
2  '(INCHES)',T38,'(INCHES)',T53,'(INCHES)',T67,
3  '(DEGREES)'/)
C
C      CALCULATIONS
C
C      Y=0.0
10  DO 15 I=1,2000
C      AA=Y/L
C      AB=ATAN(AA)
C      ALFA=AB*180.0/PI
C      AC=SIN(AB)/N
C      BETA=ARSIN(AC)
C      AD=TAN(BETA)
C      DY=T*(AA-AD)
C      YTRUE=Y-DY
C
C      WRITE(6,200)Y,YTRUE,DY,ALFA
200  FORMAT(' ',T24,F7.4,T38,F7.4,T53,F8.6,T67,F8.4)
C      IF(MOD(I,10).EQ.0)WRITE(6,201)
201  FORMAT(' ')
C      IF(MOD(I,60).EQ.0)GO TO 11
C      GO TO 12
11  WRITE(6,202)
202  FORMAT('1')
C      WRITE(6,110)
12  Y=.002*FLOAT(I)
C      IF(Y.GE.YMAX)GO TO 20
15  CONTINUE
20  STOP
END

```


THE FOLLOWING TABLE IS TO ACCOUNT FOR THE PARALLAX ERROR IN VIEWING THE MODEL THROUGH GLASS WALLS AT ANY OTHER POINT THAN AT THE ALIGNMENT POINT. INPUT PARAMETERS ARE:

- (1) L = 15.000 INCHES
- (2) N = 1.500 INCHES
- (3) T = 2.250 INCHES

OBSERVED DISTANCE (INCHES)	TRUE DISTANCE (INCHES)	ERROR (INCHES)	RAY ANGLE (DEGREES)
0.0	0.0	0.0	0.0
0.0020	0.0019	0.000100	0.0076
0.0040	0.0038	0.000200	0.0153
0.0060	0.0057	0.000300	0.0229
0.0080	0.0076	0.000400	0.0306
0.0100	0.0095	0.000500	0.0382
0.0120	0.0114	0.000600	0.0458
0.0140	0.0133	0.000700	0.0535
0.0160	0.0152	0.000800	0.0611
0.0180	0.0171	0.000900	0.0688
0.0200	0.0190	0.001000	0.0764
0.0220	0.0209	0.001100	0.0840
0.0240	0.0228	0.001200	0.0917
0.0260	0.0247	0.001300	0.0993
0.0280	0.0266	0.001400	0.1070
0.0300	0.0285	0.001500	0.1146
0.0320	0.0304	0.001600	0.1222
0.0340	0.0323	0.001700	0.1299
0.0360	0.0342	0.001800	0.1375
0.0380	0.0361	0.001900	0.1451
0.0400	0.0380	0.002000	0.1528
0.0420	0.0399	0.002100	0.1604
0.0440	0.0418	0.002200	0.1681
0.0460	0.0437	0.002300	0.1757
0.0480	0.0456	0.002400	0.1833
0.0500	0.0475	0.002500	0.1910
0.0520	0.0494	0.002600	0.1986
0.0540	0.0513	0.002700	0.2063
0.0560	0.0532	0.002800	0.2139
0.0580	0.0551	0.002900	0.2215
0.0600	0.0570	0.003000	0.2292
0.0620	0.0589	0.003100	0.2368
0.0640	0.0608	0.003200	0.2445
0.0660	0.0627	0.003300	0.2521
0.0680	0.0646	0.003400	0.2597
0.0700	0.0665	0.003500	0.2674
0.0720	0.0684	0.003600	0.2750
0.0740	0.0703	0.003700	0.2827
0.0760	0.0722	0.003800	0.2903
0.0780	0.0741	0.003900	0.2979
0.0800	0.0760	0.004000	0.3056
0.0820	0.0779	0.004100	0.3132
0.0840	0.0798	0.004200	0.3209
0.0860	0.0817	0.004300	0.3285
0.0880	0.0836	0.004400	0.3361
0.0900	0.0855	0.004500	0.3438
0.0920	0.0874	0.004600	0.3514
0.0940	0.0893	0.004700	0.3590
0.0960	0.0912	0.004800	0.3667
0.0980	0.0931	0.004900	0.3743
0.1000	0.0950	0.005000	0.3820
0.1020	0.0969	0.005100	0.3896
0.1040	0.0988	0.005200	0.3972
0.1060	0.1007	0.005300	0.4049
0.1080	0.1026	0.005400	0.4125
0.1100	0.1045	0.005500	0.4202
0.1120	0.1064	0.005600	0.4278
0.1140	0.1083	0.005700	0.4354
0.1160	0.1102	0.005800	0.4431
0.1180	0.1121	0.005900	0.4507

OBSERVED DISTANCE (INCHES)	TRUE DISTANCE (INCHES)	ERROR (INCHES)	RAY ANGLE (DEGREES)
0.1200	0.1140	0.006000	0.4584
0.1220	0.1159	0.006100	0.4660
0.1240	0.1178	0.006200	0.4736
0.1260	0.1197	0.006300	0.4813
0.1280	0.1216	0.006400	0.4889
0.1300	0.1235	0.006500	0.4966
0.1320	0.1254	0.006600	0.5042
0.1340	0.1273	0.006700	0.5118
0.1360	0.1292	0.006800	0.5195
0.1380	0.1311	0.006900	0.5271
0.1400	0.1330	0.007000	0.5347
0.1420	0.1349	0.007100	0.5424
0.1440	0.1368	0.007200	0.5500
0.1460	0.1387	0.007300	0.5577
0.1480	0.1406	0.007400	0.5653
0.1500	0.1425	0.007500	0.5729
0.1520	0.1444	0.007600	0.5806
0.1540	0.1463	0.007700	0.5882
0.1560	0.1482	0.007800	0.5959
0.1580	0.1501	0.007901	0.6035
0.1600	0.1520	0.008001	0.6111
0.1620	0.1539	0.008101	0.6188
0.1640	0.1558	0.008201	0.6264
0.1660	0.1577	0.008301	0.6340
0.1680	0.1596	0.008401	0.6417
0.1700	0.1615	0.008501	0.6493
0.1720	0.1634	0.008601	0.6570
0.1740	0.1653	0.008701	0.6646
0.1760	0.1672	0.008801	0.6722
0.1780	0.1691	0.008901	0.6799
0.1800	0.1710	0.009001	0.6875
0.1820	0.1729	0.009101	0.6952
0.1840	0.1748	0.009201	0.7028
0.1860	0.1767	0.009301	0.7104
0.1880	0.1786	0.009401	0.7181
0.1900	0.1805	0.009501	0.7257
0.1920	0.1824	0.009601	0.7333
0.1940	0.1843	0.009701	0.7410
0.1960	0.1862	0.009801	0.7486
0.1980	0.1881	0.009901	0.7563
0.2000	0.1900	0.010001	0.7639
0.2020	0.1919	0.010101	0.7715
0.2040	0.1938	0.010201	0.7792
0.2060	0.1957	0.010301	0.7868
0.2080	0.1976	0.010401	0.7944
0.2100	0.1995	0.010501	0.8021
0.2120	0.2014	0.010601	0.8097
0.2140	0.2033	0.010701	0.8174
0.2160	0.2052	0.010801	0.8250
0.2180	0.2071	0.010901	0.8326
0.2200	0.2090	0.011001	0.8403
0.2220	0.2109	0.011101	0.8479
0.2240	0.2128	0.011201	0.8556
0.2260	0.2147	0.011301	0.8632
0.2280	0.2166	0.011401	0.8708
0.2300	0.2185	0.011502	0.8785
0.2320	0.2204	0.011602	0.8861
0.2340	0.2223	0.011702	0.8937
0.2360	0.2242	0.011802	0.9014
0.2380	0.2261	0.011902	0.9090

OBSERVED DISTANCE (INCHES)	TRUE DISTANCE (INCHES)	ERROR (INCHES)	RAY ANGLE (DEGREES)
0.2400	0.2280	0.012002	0.9167
0.2420	0.2299	0.012102	0.9243
0.2440	0.2318	0.012202	0.9319
0.2460	0.2337	0.012302	0.9396
0.2480	0.2356	0.012402	0.9472
0.2500	0.2375	0.012502	0.9548
0.2520	0.2394	0.012602	0.9625
0.2540	0.2413	0.012702	0.9701
0.2560	0.2432	0.012802	0.9778
0.2580	0.2451	0.012902	0.9854
0.2600	0.2470	0.013002	0.9930
0.2620	0.2489	0.013102	1.0007
0.2640	0.2508	0.013202	1.0083
0.2660	0.2527	0.013302	1.0159
0.2680	0.2546	0.013402	1.0236
0.2700	0.2565	0.013502	1.0312
0.2720	0.2584	0.013602	1.0388
0.2740	0.2603	0.013703	1.0465
0.2760	0.2622	0.013803	1.0541
0.2780	0.2641	0.013903	1.0618
0.2800	0.2660	0.014003	1.0694
0.2820	0.2679	0.014103	1.0770
0.2840	0.2698	0.014203	1.0847
0.2860	0.2717	0.014303	1.0923
0.2880	0.2736	0.014403	1.0999
0.2900	0.2755	0.014503	1.1076
0.2920	0.2774	0.014603	1.1152
0.2940	0.2793	0.014703	1.1229
0.2960	0.2812	0.014803	1.1305
0.2980	0.2831	0.014903	1.1381
0.3000	0.2850	0.015003	1.1458
0.3020	0.2869	0.015103	1.1534
0.3040	0.2888	0.015203	1.1610
0.3060	0.2907	0.015304	1.1687
0.3080	0.2926	0.015404	1.1763
0.3100	0.2945	0.015504	1.1839
0.3120	0.2964	0.015604	1.1916
0.3140	0.2983	0.015704	1.1992
0.3160	0.3002	0.015804	1.2069
0.3180	0.3021	0.015904	1.2145
0.3200	0.3040	0.016004	1.2221
0.3220	0.3059	0.016104	1.2298
0.3240	0.3078	0.016204	1.2374
0.3260	0.3097	0.016304	1.2450
0.3280	0.3116	0.016404	1.2527
0.3300	0.3135	0.016504	1.2603
0.3320	0.3154	0.016605	1.2679
0.3340	0.3173	0.016705	1.2756
0.3360	0.3192	0.016805	1.2832
0.3380	0.3211	0.016905	1.2908
0.3400	0.3230	0.017005	1.2985
0.3420	0.3249	0.017105	1.3061
0.3440	0.3268	0.017205	1.3138
0.3460	0.3287	0.017305	1.3214
0.3480	0.3306	0.017405	1.3290
0.3500	0.3325	0.017505	1.3367
0.3520	0.3344	0.017605	1.3443
0.3540	0.3363	0.017705	1.3519
0.3560	0.3382	0.017806	1.3596
0.3580	0.3401	0.017906	1.3672

OBSERVED DISTANCE (INCHES)	TRUE DISTANCE (INCHES)	ERROR (INCHES)	RAY ANGLE (DEGREES)
0.3600	0.3420	0.018006	1.3748
0.3620	0.3439	0.018106	1.3825
0.3640	0.3458	0.018206	1.3901
0.3660	0.3477	0.018306	1.3977
0.3680	0.3496	0.018406	1.4054
0.3700	0.3515	0.018506	1.4130
0.3720	0.3534	0.018606	1.4206
0.3740	0.3553	0.018706	1.4283
0.3760	0.3572	0.018807	1.4359
0.3780	0.3591	0.018907	1.4435
0.3800	0.3610	0.019007	1.4512
0.3820	0.3629	0.019107	1.4588
0.3840	0.3648	0.019207	1.4665
0.3860	0.3667	0.019307	1.4741
0.3880	0.3686	0.019407	1.4817
0.3900	0.3705	0.019507	1.4894
0.3920	0.3724	0.019607	1.4970
0.3940	0.3743	0.019708	1.5046
0.3960	0.3762	0.019808	1.5123
0.3980	0.3781	0.019908	1.5199
0.4000	0.3800	0.020008	1.5275
0.4020	0.3819	0.020108	1.5352
0.4040	0.3838	0.020208	1.5428
0.4060	0.3857	0.020308	1.5504
0.4080	0.3876	0.020408	1.5581
0.4100	0.3895	0.020509	1.5657
0.4120	0.3914	0.020609	1.5733
0.4140	0.3933	0.020709	1.5810
0.4160	0.3952	0.020809	1.5886
0.4180	0.3971	0.020909	1.5962
0.4200	0.3990	0.021009	1.6039
0.4220	0.4009	0.021109	1.6115
0.4240	0.4028	0.021209	1.6191
0.4260	0.4047	0.021310	1.6268
0.4280	0.4066	0.021410	1.6344
0.4300	0.4085	0.021510	1.6420
0.4320	0.4104	0.021610	1.6497
0.4340	0.4123	0.021710	1.6573
0.4360	0.4142	0.021810	1.6649
0.4380	0.4161	0.021910	1.6726
0.4400	0.4180	0.022011	1.6802
0.4420	0.4199	0.022111	1.6878
0.4440	0.4218	0.022211	1.6955
0.4460	0.4237	0.022311	1.7031
0.4480	0.4256	0.022411	1.7107
0.4500	0.4275	0.022511	1.7184
0.4520	0.4294	0.022611	1.7260
0.4540	0.4313	0.022712	1.7336
0.4560	0.4332	0.022812	1.7413
0.4580	0.4351	0.022912	1.7489
0.4600	0.4370	0.023012	1.7565
0.4620	0.4389	0.023112	1.7642
0.4640	0.4408	0.023212	1.7718
0.4660	0.4427	0.023312	1.7794
0.4680	0.4446	0.023413	1.7870
0.4700	0.4465	0.023513	1.7947
0.4720	0.4484	0.023613	1.8023
0.4740	0.4503	0.023713	1.8099
0.4760	0.4522	0.023813	1.8176
0.4780	0.4541	0.023913	1.8252

OBSERVED DISTANCE (INCHES)	TRUE DISTANCE (INCHES)	ERROR (INCHES)	RAY ANGLE (DEGREES)
0.4800	0.4560	0.024014	1.8328
0.4820	0.4579	0.024114	1.8405
0.4840	0.4598	0.024214	1.8481
0.4860	0.4617	0.024314	1.8557
0.4880	0.4636	0.024414	1.8634
0.4900	0.4655	0.024515	1.8710
0.4920	0.4674	0.024615	1.8786
0.4940	0.4693	0.024715	1.8863
0.4960	0.4712	0.024815	1.8939
0.4980	0.4731	0.024915	1.9015
0.5000	0.4750	0.025015	1.9092
0.5020	0.4769	0.025116	1.9168
0.5040	0.4788	0.025216	1.9244
0.5060	0.4807	0.025316	1.9320
0.5080	0.4826	0.025416	1.9397
0.5100	0.4845	0.025516	1.9473
0.5120	0.4864	0.025617	1.9549
0.5140	0.4883	0.025717	1.9626
0.5160	0.4902	0.025817	1.9702
0.5180	0.4921	0.025917	1.9778
0.5200	0.4940	0.026017	1.9855
0.5220	0.4959	0.026118	1.9931
0.5240	0.4978	0.026218	2.0007
0.5260	0.4997	0.026318	2.0083
0.5280	0.5016	0.026418	2.0160
0.5300	0.5035	0.026518	2.0236
0.5320	0.5054	0.026619	2.0312
0.5340	0.5073	0.026719	2.0389
0.5360	0.5092	0.026819	2.0465
0.5380	0.5111	0.026919	2.0541
0.5400	0.5130	0.027019	2.0618
0.5420	0.5149	0.027120	2.0694
0.5440	0.5168	0.027220	2.0770
0.5460	0.5187	0.027320	2.0846
0.5480	0.5206	0.027420	2.0923
0.5500	0.5225	0.027521	2.0999
0.5520	0.5244	0.027621	2.1075
0.5540	0.5263	0.027721	2.1152
0.5560	0.5282	0.027821	2.1228
0.5580	0.5301	0.027921	2.1304
0.5600	0.5320	0.028022	2.1380
0.5620	0.5339	0.028122	2.1457
0.5640	0.5358	0.028222	2.1533
0.5660	0.5377	0.028322	2.1609
0.5680	0.5396	0.028423	2.1686
0.5700	0.5415	0.028523	2.1762
0.5720	0.5434	0.028623	2.1838
0.5740	0.5453	0.028723	2.1914
0.5760	0.5472	0.028824	2.1991
0.5780	0.5491	0.028924	2.2067
0.5800	0.5510	0.029024	2.2143
0.5820	0.5529	0.029124	2.2220
0.5840	0.5548	0.029225	2.2296
0.5860	0.5567	0.029325	2.2372
0.5880	0.5586	0.029425	2.2448
0.5900	0.5605	0.029525	2.2525
0.5920	0.5624	0.029626	2.2601
0.5940	0.5643	0.029726	2.2677
0.5960	0.5662	0.029826	2.2754
0.5980	0.5681	0.029926	2.2830

OBSERVED DISTANCE (INCHES)	TRUE DISTANCE (INCHES)	ERROR (INCHES)	RAY ANGLE (DEGREES)
0.6000	0.5700	0.030027	2.2906
0.6020	0.5719	0.030127	2.2982
0.6040	0.5738	0.030227	2.3059
0.6060	0.5757	0.030327	2.3135
0.6080	0.5776	0.030428	2.3211
0.6100	0.5795	0.030528	2.3287
0.6120	0.5814	0.030628	2.3364
0.6140	0.5833	0.030729	2.3440
0.6160	0.5852	0.030829	2.3516
0.6180	0.5871	0.030929	2.3593
0.6200	0.5890	0.031029	2.3669
0.6220	0.5909	0.031130	2.3745
0.6240	0.5928	0.031230	2.3821
0.6260	0.5947	0.031330	2.3898
0.6280	0.5966	0.031431	2.3974
0.6300	0.5985	0.031531	2.4050
0.6320	0.6004	0.031631	2.4126
0.6340	0.6023	0.031731	2.4203
0.6360	0.6042	0.031832	2.4279
0.6380	0.6061	0.031932	2.4355
0.6400	0.6080	0.032032	2.4431
0.6420	0.6099	0.032133	2.4508
0.6440	0.6118	0.032233	2.4584
0.6460	0.6137	0.032333	2.4660
0.6480	0.6156	0.032434	2.4736
0.6500	0.6175	0.032534	2.4813
0.6520	0.6194	0.032634	2.4889
0.6540	0.6213	0.032735	2.4965
0.6560	0.6232	0.032835	2.5041
0.6580	0.6251	0.032935	2.5118
0.6600	0.6270	0.033035	2.5194
0.6620	0.6289	0.033136	2.5270
0.6640	0.6308	0.033236	2.5346
0.6660	0.6327	0.033336	2.5423
0.6680	0.6346	0.033437	2.5499
0.6700	0.6365	0.033537	2.5575
0.6720	0.6384	0.033637	2.5651
0.6740	0.6403	0.033738	2.5728
0.6760	0.6422	0.033838	2.5804
0.6780	0.6441	0.033938	2.5880
0.6800	0.6460	0.034039	2.5956
0.6820	0.6479	0.034139	2.6033
0.6840	0.6498	0.034239	2.6109
0.6860	0.6517	0.034340	2.6185
0.6880	0.6536	0.034440	2.6261
0.6900	0.6555	0.034541	2.6337
0.6920	0.6574	0.034641	2.6414
0.6940	0.6593	0.034741	2.6490
0.6960	0.6612	0.034842	2.6566
0.6980	0.6631	0.034942	2.6642
0.7000	0.6650	0.035042	2.6719
0.7020	0.6669	0.035143	2.6795
0.7040	0.6688	0.035243	2.6871
0.7060	0.6707	0.035343	2.6947
0.7080	0.6726	0.035444	2.7024
0.7100	0.6745	0.035544	2.7100
0.7120	0.6764	0.035645	2.7176
0.7140	0.6783	0.035745	2.7252
0.7160	0.6802	0.035845	2.7328
0.7180	0.6821	0.035946	2.7405

OBSERVED DISTANCE (INCHES)	TRUE DISTANCE (INCHES)	ERROR (INCHES)	RAY ANGLE (DEGREES)
0.7200	0.6840	0.036046	2.7481
0.7220	0.6859	0.036146	2.7557
0.7240	0.6878	0.036247	2.7633
0.7260	0.6897	0.036347	2.7710
0.7280	0.6916	0.036448	2.7786
0.7300	0.6935	0.036548	2.7862
0.7320	0.6954	0.036648	2.7938
0.7340	0.6973	0.036749	2.8014
0.7360	0.6992	0.036849	2.8091
0.7380	0.7011	0.036950	2.8167
0.7400	0.7029	0.037050	2.8243
0.7420	0.7048	0.037150	2.8319
0.7440	0.7067	0.037251	2.8395
0.7460	0.7086	0.037351	2.8472
0.7480	0.7105	0.037452	2.8548
0.7500	0.7124	0.037552	2.8624
0.7520	0.7143	0.037652	2.8700
0.7540	0.7162	0.037753	2.8776
0.7560	0.7181	0.037853	2.8853
0.7580	0.7200	0.037954	2.8929
0.7600	0.7219	0.038054	2.9005
0.7620	0.7238	0.038155	2.9081
0.7640	0.7257	0.038255	2.9157
0.7660	0.7276	0.038355	2.9234
0.7680	0.7295	0.038456	2.9310
0.7700	0.7314	0.038556	2.9386
0.7720	0.7333	0.038657	2.9462
0.7740	0.7352	0.038757	2.9538
0.7760	0.7371	0.038858	2.9615
0.7780	0.7390	0.038958	2.9691
0.7800	0.7409	0.039059	2.9767
0.7820	0.7428	0.039159	2.9843
0.7840	0.7447	0.039259	2.9919
0.7860	0.7466	0.039360	2.9996
0.7880	0.7485	0.039460	3.0072
0.7900	0.7504	0.039561	3.0148
0.7920	0.7523	0.039661	3.0224
0.7940	0.7542	0.039762	3.0300
0.7960	0.7561	0.039862	3.0376
0.7980	0.7580	0.039963	3.0453
0.8000	0.7599	0.040063	3.0529
0.8020	0.7618	0.040164	3.0605
0.8040	0.7637	0.040264	3.0681
0.8060	0.7656	0.040365	3.0757
0.8080	0.7675	0.040465	3.0834
0.8100	0.7694	0.040566	3.0910
0.8120	0.7713	0.040666	3.0986
0.8140	0.7732	0.040767	3.1062
0.8160	0.7751	0.040867	3.1138
0.8180	0.7770	0.040968	3.1214
0.8200	0.7789	0.041068	3.1291
0.8220	0.7808	0.041169	3.1367
0.8240	0.7827	0.041269	3.1443
0.8260	0.7846	0.041369	3.1519
0.8280	0.7865	0.041470	3.1595
0.8300	0.7884	0.041570	3.1671
0.8320	0.7903	0.041671	3.1748
0.8340	0.7922	0.041772	3.1824
0.8360	0.7941	0.041872	3.1900
0.8380	0.7960	0.041973	3.1976

OBSERVED DISTANCE (INCHES)	TRUE DISTANCE (INCHES)	ERROR (INCHES)	RAY ANGLE (DEGREES)
0.8400	0.7979	0.042073	3.2052
0.8420	0.7998	0.042174	3.2128
0.8440	0.8017	0.042274	3.2204
0.8460	0.8036	0.042375	3.2281
0.8480	0.8055	0.042475	3.2357
0.8500	0.8074	0.042576	3.2433
0.8520	0.8093	0.042676	3.2509
0.8540	0.8112	0.042777	3.2585
0.8560	0.8131	0.042877	3.2661
0.8580	0.8150	0.042978	3.2738
0.8600	0.8169	0.043078	3.2814
0.8620	0.8188	0.043179	3.2890
0.8640	0.8207	0.043280	3.2966
0.8660	0.8226	0.043380	3.3042
0.8680	0.8245	0.043481	3.3118
0.8700	0.8264	0.043581	3.3194
0.8720	0.8283	0.043682	3.3270
0.8740	0.8302	0.043782	3.3347
0.8760	0.8321	0.043883	3.3423
0.8780	0.8340	0.043983	3.3499
0.8800	0.8359	0.044084	3.3575
0.8820	0.8378	0.044185	3.3651
0.8840	0.8397	0.044285	3.3727
0.8860	0.8416	0.044386	3.3803
0.8880	0.8435	0.044486	3.3880
0.8900	0.8454	0.044587	3.3956
0.8920	0.8473	0.044688	3.4032
0.8940	0.8492	0.044788	3.4108
0.8960	0.8511	0.044889	3.4184
0.8980	0.8530	0.044989	3.4260
0.9000	0.8549	0.045090	3.4336
0.9020	0.8568	0.045190	3.4412
0.9040	0.8587	0.045291	3.4489
0.9060	0.8606	0.045392	3.4565
0.9080	0.8625	0.045492	3.4641
0.9100	0.8644	0.045593	3.4717
0.9120	0.8663	0.045693	3.4793
0.9140	0.8682	0.045794	3.4869
0.9160	0.8701	0.045895	3.4945
0.9180	0.8720	0.045995	3.5021
0.9200	0.8739	0.046096	3.5097
0.9220	0.8758	0.046197	3.5174
0.9240	0.8777	0.046297	3.5250
0.9260	0.8796	0.046398	3.5326
0.9280	0.8815	0.046499	3.5402
0.9300	0.8834	0.046599	3.5478
0.9320	0.8853	0.046700	3.5554
0.9340	0.8872	0.046800	3.5630
0.9360	0.8891	0.046901	3.5706
0.9380	0.8910	0.047002	3.5782
0.9400	0.8929	0.047102	3.5858
0.9420	0.8948	0.047203	3.5935
0.9440	0.8967	0.047304	3.6011
0.9460	0.8986	0.047404	3.6087
0.9480	0.9005	0.047505	3.6163
0.9500	0.9024	0.047606	3.6239
0.9520	0.9043	0.047706	3.6315
0.9540	0.9062	0.047807	3.6391
0.9560	0.9081	0.047908	3.6467
0.9580	0.9100	0.048009	3.6543

OBSERVED DISTANCE (INCHES)	TRUE DISTANCE (INCHES)	ERROR (INCHES)	RAY ANGLE (DEGREES)
0.9600	0.9119	0.048109	3.6619
0.9620	0.9138	0.048210	3.6695
0.9640	0.9157	0.048310	3.6771
0.9660	0.9176	0.048411	3.6848
0.9680	0.9195	0.048512	3.6924
0.9700	0.9214	0.048613	3.7000
0.9720	0.9233	0.048713	3.7076
0.9740	0.9252	0.048814	3.7152
0.9760	0.9271	0.048915	3.7228
0.9780	0.9290	0.049015	3.7304
0.9800	0.9309	0.049116	3.7380
0.9820	0.9328	0.049217	3.7456
0.9840	0.9347	0.049318	3.7532
0.9860	0.9366	0.049418	3.7608
0.9880	0.9385	0.049519	3.7684
0.9900	0.9404	0.049620	3.7760
0.9920	0.9423	0.049720	3.7836
0.9940	0.9442	0.049821	3.7913
0.9960	0.9461	0.049922	3.7989
0.9980	0.9480	0.050023	3.8065
1.0000	0.9499	0.050123	3.8141
1.0020	0.9518	0.050224	3.8217
1.0040	0.9537	0.050325	3.8293
1.0060	0.9556	0.050426	3.8369
1.0080	0.9575	0.050526	3.8445
1.0100	0.9594	0.050627	3.8521
1.0120	0.9613	0.050728	3.8597
1.0140	0.9632	0.050829	3.8673
1.0160	0.9651	0.050929	3.8749
1.0180	0.9670	0.051030	3.8825
1.0200	0.9689	0.051131	3.8901
1.0220	0.9708	0.051232	3.8977
1.0240	0.9727	0.051332	3.9053
1.0260	0.9746	0.051433	3.9129
1.0280	0.9765	0.051534	3.9205
1.0300	0.9784	0.051635	3.9281
1.0320	0.9803	0.051735	3.9357
1.0340	0.9822	0.051836	3.9433
1.0360	0.9841	0.051937	3.9509
1.0380	0.9860	0.052038	3.9586
1.0400	0.9879	0.052139	3.9662
1.0420	0.9898	0.052240	3.9738
1.0440	0.9917	0.052340	3.9814
1.0460	0.9936	0.052441	3.9890
1.0480	0.9955	0.052542	3.9966
1.0500	0.9974	0.052643	4.0042
1.0520	0.9993	0.052743	4.0118
1.0540	1.0012	0.052844	4.0194
1.0560	1.0031	0.052945	4.0270
1.0580	1.0050	0.053046	4.0346
1.0600	1.0069	0.053147	4.0422
1.0620	1.0088	0.053248	4.0498
1.0640	1.0107	0.053348	4.0574
1.0660	1.0125	0.053449	4.0650
1.0680	1.0144	0.053550	4.0726
1.0700	1.0163	0.053651	4.0802
1.0720	1.0182	0.053752	4.0878
1.0740	1.0201	0.053853	4.0954
1.0760	1.0220	0.053953	4.1030
1.0780	1.0239	0.054054	4.1106

OBSERVED DISTANCE (INCHES)	TRUE DISTANCE (INCHES)	ERROR (INCHES)	RAY ANGLE (DEGREES)
1.0800	1.0258	0.054155	4.1182
1.0820	1.0277	0.054256	4.1258
1.0840	1.0296	0.054357	4.1334
1.0860	1.0315	0.054458	4.1410
1.0880	1.0334	0.054559	4.1486
1.0900	1.0353	0.054660	4.1562
1.0920	1.0372	0.054760	4.1638
1.0940	1.0391	0.054861	4.1714
1.0960	1.0410	0.054962	4.1790
1.0980	1.0429	0.055063	4.1866
1.1000	1.0448	0.055164	4.1942
1.1020	1.0467	0.055265	4.2018
1.1040	1.0486	0.055366	4.2094
1.1060	1.0505	0.055467	4.2170
1.1080	1.0524	0.055568	4.2246
1.1100	1.0543	0.055668	4.2322
1.1120	1.0562	0.055769	4.2398
1.1140	1.0581	0.055870	4.2474
1.1160	1.0600	0.055971	4.2550
1.1180	1.0619	0.056072	4.2626
1.1200	1.0638	0.056173	4.2702
1.1220	1.0657	0.056274	4.2778
1.1240	1.0676	0.056375	4.2854
1.1260	1.0695	0.056476	4.2929
1.1280	1.0714	0.056577	4.3005
1.1300	1.0733	0.056678	4.3081
1.1320	1.0752	0.056779	4.3157
1.1340	1.0771	0.056880	4.3233
1.1360	1.0790	0.056981	4.3309
1.1380	1.0809	0.057082	4.3385
1.1400	1.0828	0.057183	4.3461
1.1420	1.0847	0.057284	4.3537
1.1440	1.0866	0.057385	4.3613
1.1460	1.0885	0.057486	4.3689
1.1480	1.0904	0.057586	4.3765
1.1500	1.0923	0.057687	4.3841
1.1520	1.0942	0.057788	4.3917
1.1540	1.0961	0.057889	4.3993
1.1560	1.0980	0.057990	4.4069
1.1580	1.0999	0.058091	4.4145
1.1600	1.1018	0.058192	4.4221
1.1620	1.1037	0.058293	4.4297
1.1640	1.1056	0.058394	4.4373
1.1660	1.1075	0.058495	4.4448
1.1680	1.1094	0.058596	4.4524
1.1700	1.1113	0.058697	4.4600
1.1720	1.1132	0.058798	4.4676
1.1740	1.1151	0.058899	4.4752
1.1760	1.1170	0.059000	4.4828
1.1780	1.1189	0.059101	4.4904
1.1800	1.1208	0.059202	4.4980
1.1820	1.1227	0.059303	4.5056
1.1840	1.1246	0.059404	4.5132
1.1860	1.1265	0.059506	4.5208
1.1880	1.1284	0.059607	4.5284
1.1900	1.1303	0.059708	4.5360
1.1920	1.1322	0.059809	4.5436
1.1940	1.1341	0.059910	4.5511
1.1960	1.1360	0.060011	4.5587
1.1980	1.1379	0.060112	4.5663

OBSERVED DISTANCE (INCHES)	TRUE DISTANCE (INCHES)	ERROR (INCHES)	RAY ANGLE (DEGREES)
1.2000	1.1398	0.060213	4.5739
1.2020	1.1417	0.060314	4.5815
1.2040	1.1436	0.060415	4.5891
1.2060	1.1455	0.060516	4.5967
1.2080	1.1474	0.060617	4.6043
1.2100	1.1493	0.060718	4.6119
1.2120	1.1512	0.060819	4.6195
1.2140	1.1531	0.060920	4.6270
1.2160	1.1550	0.061021	4.6346
1.2180	1.1569	0.061123	4.6422
1.2200	1.1588	0.061224	4.6498
1.2220	1.1607	0.061325	4.6574
1.2240	1.1626	0.061426	4.6650
1.2260	1.1645	0.061527	4.6726
1.2280	1.1664	0.061628	4.6802
1.2300	1.1683	0.061729	4.6878
1.2320	1.1702	0.061830	4.6954
1.2340	1.1721	0.061931	4.7029
1.2360	1.1740	0.062032	4.7105
1.2380	1.1759	0.062134	4.7181
1.2400	1.1778	0.062235	4.7257
1.2420	1.1797	0.062336	4.7333
1.2440	1.1816	0.062437	4.7409
1.2460	1.1835	0.062538	4.7485
1.2480	1.1854	0.062639	4.7560
1.2500	1.1873	0.062740	4.7636
1.2520	1.1892	0.062842	4.7712
1.2540	1.1911	0.062943	4.7788
1.2560	1.1930	0.063044	4.7864
1.2580	1.1949	0.063145	4.7940
1.2600	1.1968	0.063246	4.8016
1.2620	1.1987	0.063348	4.8092
1.2640	1.2006	0.063448	4.8167
1.2660	1.2024	0.063550	4.8243
1.2680	1.2043	0.063651	4.8319
1.2700	1.2062	0.063752	4.8395
1.2720	1.2081	0.063854	4.8471
1.2740	1.2100	0.063955	4.8547
1.2760	1.2119	0.064056	4.8622
1.2780	1.2138	0.064157	4.8698
1.2800	1.2157	0.064258	4.8774
1.2820	1.2176	0.064360	4.8850
1.2840	1.2195	0.064461	4.8926
1.2860	1.2214	0.064562	4.9002
1.2880	1.2233	0.064663	4.9078
1.2900	1.2252	0.064764	4.9153
1.2920	1.2271	0.064865	4.9229
1.2940	1.2290	0.064967	4.9305
1.2960	1.2309	0.065068	4.9381
1.2980	1.2328	0.065169	4.9457
1.3000	1.2347	0.065270	4.9533
1.3020	1.2366	0.065372	4.9608
1.3040	1.2385	0.065473	4.9684
1.3060	1.2404	0.065574	4.9760
1.3080	1.2423	0.065675	4.9836
1.3100	1.2442	0.065777	4.9912
1.3120	1.2461	0.065878	4.9987
1.3140	1.2480	0.065979	5.0063
1.3160	1.2499	0.066081	5.0139
1.3180	1.2518	0.066182	5.0215

OBSERVED DISTANCE (INCHES)	TRUE DISTANCE (INCHES)	ERROR (INCHES)	RAY ANGLE (DEGREES)
1.3200	1.2537	0.066283	5.0291
1.3220	1.2556	0.066384	5.0366
1.3240	1.2575	0.066486	5.0442
1.3260	1.2594	0.066587	5.0518
1.3280	1.2613	0.066688	5.0594
1.3300	1.2632	0.066789	5.0670
1.3320	1.2651	0.066891	5.0745
1.3340	1.2670	0.066992	5.0821
1.3360	1.2689	0.067093	5.0897
1.3380	1.2708	0.067195	5.0973
1.3400	1.2727	0.067296	5.1049
1.3420	1.2746	0.067398	5.1124
1.3440	1.2765	0.067499	5.1200
1.3460	1.2784	0.067600	5.1276
1.3480	1.2803	0.067701	5.1352
1.3500	1.2822	0.067803	5.1428
1.3520	1.2841	0.067904	5.1503
1.3540	1.2860	0.068005	5.1579
1.3560	1.2879	0.068107	5.1655
1.3580	1.2898	0.068208	5.1731
1.3600	1.2917	0.068309	5.1806
1.3620	1.2936	0.068411	5.1882
1.3640	1.2955	0.068512	5.1958
1.3660	1.2974	0.068614	5.2034
1.3680	1.2993	0.068715	5.2110
1.3700	1.3012	0.068816	5.2185
1.3720	1.3031	0.068918	5.2261
1.3740	1.3050	0.069019	5.2337
1.3760	1.3069	0.069121	5.2413
1.3780	1.3088	0.069222	5.2488
1.3800	1.3107	0.069323	5.2564
1.3820	1.3126	0.069425	5.2640
1.3840	1.3145	0.069526	5.2716
1.3860	1.3164	0.069628	5.2791
1.3880	1.3183	0.069729	5.2867
1.3900	1.3202	0.069830	5.2943
1.3920	1.3221	0.069932	5.3019
1.3940	1.3240	0.070033	5.3094
1.3960	1.3259	0.070135	5.3170
1.3980	1.3278	0.070236	5.3246
1.4000	1.3297	0.070338	5.3322
1.4020	1.3316	0.070439	5.3397
1.4040	1.3335	0.070540	5.3473
1.4060	1.3354	0.070642	5.3549
1.4080	1.3373	0.070743	5.3624
1.4100	1.3392	0.070845	5.3700
1.4120	1.3411	0.070946	5.3776
1.4140	1.3430	0.071048	5.3852
1.4160	1.3448	0.071149	5.3927
1.4180	1.3467	0.071251	5.4003
1.4200	1.3486	0.071352	5.4079
1.4220	1.3505	0.071454	5.4154
1.4240	1.3524	0.071555	5.4230
1.4260	1.3543	0.071657	5.4306
1.4280	1.3562	0.071758	5.4382
1.4300	1.3581	0.071860	5.4457
1.4320	1.3600	0.071961	5.4533
1.4340	1.3619	0.072063	5.4609
1.4360	1.3638	0.072164	5.4684
1.4380	1.3657	0.072266	5.4760

OBSERVED DISTANCE (INCHES)	TRUE DISTANCE (INCHES)	ERROR (INCHES)	RAY ANGLE (DEGREES)
1.4400	1.3676	0.072367	5.4836
1.4420	1.3695	0.072469	5.4912
1.4440	1.3714	0.072571	5.4987
1.4460	1.3733	0.072672	5.5063
1.4480	1.3752	0.072774	5.5139
1.4500	1.3771	0.072875	5.5214
1.4520	1.3790	0.072977	5.5290
1.4540	1.3809	0.073078	5.5366
1.4560	1.3828	0.073180	5.5441
1.4580	1.3847	0.073281	5.5517
1.4600	1.3866	0.073383	5.5593
1.4620	1.3885	0.073484	5.5668
1.4640	1.3904	0.073586	5.5744
1.4660	1.3923	0.073687	5.5820
1.4680	1.3942	0.073789	5.5895
1.4700	1.3961	0.073891	5.5971
1.4720	1.3980	0.073992	5.6047
1.4740	1.3999	0.074094	5.6122
1.4760	1.4018	0.074196	5.6198
1.4780	1.4037	0.074297	5.6274
1.4800	1.4056	0.074399	5.6349
1.4820	1.4075	0.074500	5.6425
1.4840	1.4094	0.074602	5.6501
1.4860	1.4113	0.074704	5.6576
1.4880	1.4132	0.074805	5.6652
1.4900	1.4151	0.074907	5.6728
1.4920	1.4170	0.075009	5.6803
1.4940	1.4189	0.075110	5.6879
1.4960	1.4208	0.075212	5.6955
1.4980	1.4227	0.075314	5.7030
1.5000	1.4246	0.075415	5.7106
1.5020	1.4265	0.075517	5.7182
1.5040	1.4284	0.075618	5.7257
1.5060	1.4303	0.075720	5.7333
1.5080	1.4322	0.075822	5.7408
1.5100	1.4341	0.075923	5.7484
1.5120	1.4360	0.076025	5.7560
1.5140	1.4379	0.076127	5.7635
1.5160	1.4398	0.076229	5.7711
1.5180	1.4417	0.076330	5.7787
1.5200	1.4436	0.076432	5.7862
1.5220	1.4455	0.076534	5.7938
1.5240	1.4474	0.076635	5.8013
1.5260	1.4493	0.076737	5.8089
1.5280	1.4512	0.076839	5.8165
1.5300	1.4531	0.076940	5.8240
1.5320	1.4550	0.077042	5.8316
1.5340	1.4569	0.077144	5.8391
1.5360	1.4588	0.077246	5.8467
1.5380	1.4607	0.077347	5.8543
1.5400	1.4625	0.077449	5.8618
1.5420	1.4644	0.077551	5.8694
1.5440	1.4663	0.077653	5.8769
1.5460	1.4682	0.077754	5.8845
1.5480	1.4701	0.077856	5.8921
1.5500	1.4720	0.077958	5.8996
1.5520	1.4739	0.078060	5.9072
1.5540	1.4758	0.078161	5.9147
1.5560	1.4777	0.078263	5.9223
1.5580	1.4796	0.078365	5.9299

OBSERVED DISTANCE (INCHES)	TRUE DISTANCE (INCHES)	ERROR (INCHES)	RAY ANGLE (DEGREES)
1.5600	1.4815	0.078467	5.9374
1.5620	1.4834	0.078568	5.9450
1.5640	1.4853	0.078670	5.9525
1.5660	1.4872	0.078772	5.9601
1.5680	1.4891	0.078874	5.9676
1.5700	1.4910	0.078976	5.9752
1.5720	1.4929	0.079078	5.9827
1.5740	1.4948	0.079179	5.9903
1.5760	1.4967	0.079281	5.9979
1.5780	1.4986	0.079383	6.0054
1.5800	1.5005	0.079485	6.0130
1.5820	1.5024	0.079587	6.0205
1.5840	1.5043	0.079689	6.0281
1.5860	1.5062	0.079790	6.0356
1.5880	1.5081	0.079892	6.0432
1.5900	1.5100	0.079994	6.0508
1.5920	1.5119	0.080096	6.0583
1.5940	1.5138	0.080198	6.0659
1.5960	1.5157	0.080300	6.0734
1.5980	1.5176	0.080402	6.0810
1.6000	1.5195	0.080503	6.0885
1.6020	1.5214	0.080605	6.0961
1.6040	1.5233	0.080707	6.1036
1.6060	1.5252	0.080809	6.1112
1.6080	1.5271	0.080911	6.1187
1.6100	1.5290	0.081013	6.1263
1.6120	1.5309	0.081115	6.1338
1.6140	1.5328	0.081217	6.1414
1.6160	1.5347	0.081319	6.1489
1.6180	1.5366	0.081421	6.1565
1.6200	1.5385	0.081523	6.1640
1.6220	1.5404	0.081624	6.1716
1.6240	1.5423	0.081726	6.1791
1.6260	1.5442	0.081828	6.1867
1.6280	1.5461	0.081930	6.1942
1.6300	1.5480	0.082032	6.2018
1.6320	1.5499	0.082134	6.2093
1.6340	1.5518	0.082236	6.2169
1.6360	1.5537	0.082338	6.2244
1.6380	1.5556	0.082440	6.2320
1.6400	1.5575	0.082542	6.2395
1.6420	1.5594	0.082644	6.2471
1.6440	1.5613	0.082746	6.2546
1.6460	1.5632	0.082848	6.2622
1.6480	1.5650	0.082950	6.2697
1.6500	1.5669	0.083052	6.2773
1.6520	1.5688	0.083154	6.2848
1.6540	1.5707	0.083256	6.2924
1.6560	1.5726	0.083358	6.2999
1.6580	1.5745	0.083460	6.3075
1.6600	1.5764	0.083562	6.3150
1.6620	1.5783	0.083664	6.3226
1.6640	1.5802	0.083766	6.3301
1.6660	1.5821	0.083868	6.3377
1.6680	1.5840	0.083970	6.3452
1.6700	1.5859	0.084072	6.3528
1.6720	1.5878	0.084174	6.3603
1.6740	1.5897	0.084276	6.3679
1.6760	1.5916	0.084378	6.3754
1.6780	1.5935	0.084480	6.3829

OBSERVED DISTANCE (INCHES)	TRUE DISTANCE (INCHES)	ERROR (INCHES)	RAY ANGLE (DEGREES)
1.6800	1.5954	0.084583	6.3905
1.6820	1.5973	0.084685	6.3980
1.6840	1.5992	0.084787	6.4056
1.6860	1.6011	0.084889	6.4131
1.6880	1.6030	0.084991	6.4207
1.6900	1.6049	0.085093	6.4282
1.6920	1.6068	0.085195	6.4358
1.6940	1.6087	0.085297	6.4433
1.6960	1.6106	0.085399	6.4508
1.6980	1.6125	0.085501	6.4584
1.7000	1.6144	0.085603	6.4659
1.7020	1.6163	0.085706	6.4735
1.7040	1.6182	0.085808	6.4810
1.7060	1.6201	0.085910	6.4886
1.7080	1.6220	0.086012	6.4961
1.7100	1.6239	0.086114	6.5036
1.7120	1.6258	0.086216	6.5112
1.7140	1.6277	0.086318	6.5187
1.7160	1.6296	0.086421	6.5263
1.7180	1.6315	0.086523	6.5338
1.7200	1.6334	0.086625	6.5413
1.7220	1.6353	0.086727	6.5489
1.7240	1.6372	0.086829	6.5564
1.7260	1.6391	0.086932	6.5640
1.7280	1.6410	0.087034	6.5715
1.7300	1.6429	0.087136	6.5790
1.7320	1.6448	0.087238	6.5866
1.7340	1.6467	0.087340	6.5941
1.7360	1.6486	0.087443	6.6017
1.7380	1.6505	0.087545	6.6092
1.7400	1.6524	0.087647	6.6167
1.7420	1.6543	0.087749	6.6243
1.7440	1.6561	0.087851	6.6318
1.7460	1.6580	0.087954	6.6393
1.7480	1.6599	0.088056	6.6469
1.7500	1.6618	0.088158	6.6544
1.7520	1.6637	0.088260	6.6620
1.7540	1.6656	0.088363	6.6695
1.7560	1.6675	0.088465	6.6770
1.7580	1.6694	0.088567	6.6846
1.7600	1.6713	0.088669	6.6921
1.7620	1.6732	0.088772	6.6996
1.7640	1.6751	0.088874	6.7072
1.7660	1.6770	0.088976	6.7147
1.7680	1.6789	0.089079	6.7222
1.7700	1.6808	0.089181	6.7298
1.7720	1.6827	0.089283	6.7373
1.7740	1.6846	0.089385	6.7448
1.7760	1.6865	0.089488	6.7524
1.7780	1.6884	0.089590	6.7599
1.7800	1.6903	0.089692	6.7674
1.7820	1.6922	0.089795	6.7750
1.7840	1.6941	0.089897	6.7825
1.7860	1.6960	0.089999	6.7900
1.7880	1.6979	0.090102	6.7976
1.7900	1.6998	0.090204	6.8051
1.7920	1.7017	0.090306	6.8126
1.7940	1.7036	0.090409	6.8202
1.7960	1.7055	0.090511	6.8277
1.7980	1.7074	0.090613	6.8352

OBSERVED DISTANCE (INCHES)	TRUE DISTANCE (INCHES)	ERROR (INCHES)	RAY ANGLE (DEGREES)
1.8000	1.7093	0.090716	6.8428
1.8020	1.7112	0.090818	6.8503
1.8040	1.7131	0.090921	6.8578
1.8060	1.7150	0.091023	6.8654
1.8080	1.7169	0.091125	6.8729
1.8100	1.7188	0.091228	6.8804
1.8120	1.7207	0.091330	6.8879
1.8140	1.7226	0.091433	6.8955
1.8160	1.7245	0.091535	6.9030
1.8180	1.7264	0.091637	6.9105
1.8200	1.7283	0.091740	6.9181
1.8220	1.7302	0.091842	6.9256
1.8240	1.7321	0.091945	6.9331
1.8260	1.7340	0.092047	6.9406
1.8280	1.7358	0.092150	6.9482
1.8300	1.7377	0.092252	6.9557
1.8320	1.7396	0.092355	6.9632
1.8340	1.7415	0.092457	6.9708
1.8360	1.7434	0.092559	6.9783
1.8380	1.7453	0.092662	6.9858
1.8400	1.7472	0.092764	6.9933
1.8420	1.7491	0.092867	7.0009
1.8440	1.7510	0.092969	7.0084
1.8460	1.7529	0.093072	7.0159
1.8480	1.7548	0.093174	7.0234
1.8500	1.7567	0.093277	7.0310
1.8520	1.7586	0.093379	7.0385
1.8540	1.7605	0.093482	7.0460
1.8560	1.7624	0.093584	7.0535
1.8580	1.7643	0.093687	7.0611
1.8600	1.7662	0.093790	7.0686
1.8620	1.7681	0.093892	7.0761
1.8640	1.7700	0.093995	7.0836
1.8660	1.7719	0.094097	7.0912
1.8680	1.7738	0.094200	7.0987
1.8700	1.7757	0.094302	7.1062
1.8720	1.7776	0.094405	7.1137
1.8740	1.7795	0.094507	7.1213
1.8760	1.7814	0.094610	7.1288
1.8780	1.7833	0.094713	7.1363
1.8800	1.7852	0.094815	7.1438
1.8820	1.7871	0.094918	7.1513
1.8840	1.7890	0.095020	7.1589
1.8860	1.7909	0.095123	7.1664
1.8880	1.7928	0.095226	7.1739
1.8900	1.7947	0.095328	7.1814
1.8920	1.7966	0.095431	7.1889
1.8940	1.7985	0.095533	7.1965
1.8960	1.8004	0.095636	7.2040
1.8980	1.8023	0.095739	7.2115
1.9000	1.8042	0.095841	7.2190
1.9020	1.8061	0.095944	7.2265
1.9040	1.8080	0.096047	7.2340
1.9060	1.8098	0.096149	7.2416
1.9080	1.8117	0.096252	7.2491
1.9100	1.8136	0.096355	7.2566
1.9120	1.8155	0.096457	7.2641
1.9140	1.8174	0.096560	7.2716
1.9160	1.8193	0.096663	7.2792
1.9180	1.8212	0.096765	7.2867

OBSERVED DISTANCE (INCHES)	TRUE DISTANCE (INCHES)	ERROR (INCHES)	RAY ANGLE (DEGREES)
1.9200	1.8231	0.096868	7.2942
1.9220	1.8250	0.096971	7.3017
1.9240	1.8269	0.097073	7.3092
1.9260	1.8288	0.097176	7.3167
1.9280	1.8307	0.097279	7.3242
1.9300	1.8326	0.097382	7.3318
1.9320	1.8345	0.097484	7.3393
1.9340	1.8364	0.097587	7.3468
1.9360	1.8383	0.097690	7.3543
1.9380	1.8402	0.097793	7.3618
1.9400	1.8421	0.097895	7.3693
1.9420	1.8440	0.097998	7.3769
1.9440	1.8459	0.098101	7.3844
1.9460	1.8478	0.098204	7.3919
1.9480	1.8497	0.098306	7.3994
1.9500	1.8516	0.098409	7.4069
1.9520	1.8535	0.098512	7.4144
1.9540	1.8554	0.098615	7.4219
1.9560	1.8573	0.098718	7.4294
1.9580	1.8592	0.098820	7.4370
1.9600	1.8611	0.098923	7.4445
1.9620	1.8630	0.099026	7.4520
1.9640	1.8649	0.099129	7.4595
1.9660	1.8668	0.099232	7.4670
1.9680	1.8687	0.099335	7.4745
1.9700	1.8706	0.099437	7.4820
1.9720	1.8725	0.099540	7.4895
1.9740	1.8744	0.099643	7.4970
1.9760	1.8763	0.099746	7.5045
1.9780	1.8782	0.099849	7.5121
1.9800	1.8800	0.099952	7.5196
1.9820	1.8819	0.100054	7.5271
1.9840	1.8838	0.100157	7.5346
1.9860	1.8857	0.100260	7.5421
1.9880	1.8876	0.100363	7.5496
1.9900	1.8895	0.100466	7.5571
1.9920	1.8914	0.100569	7.5646
1.9940	1.8933	0.100672	7.5721
1.9960	1.8952	0.100775	7.5796
1.9980	1.8971	0.100878	7.5871
2.0000	1.8990	0.100981	7.5946
2.0020	1.9009	0.101084	7.6021
2.0040	1.9028	0.101186	7.6096
2.0060	1.9047	0.101289	7.6172
2.0080	1.9066	0.101392	7.6247
2.0100	1.9085	0.101495	7.6322
2.0120	1.9104	0.101598	7.6397
2.0140	1.9123	0.101701	7.6472
2.0160	1.9142	0.101804	7.6547
2.0180	1.9161	0.101907	7.6622
2.0200	1.9180	0.102010	7.6697
2.0220	1.9199	0.102113	7.6772
2.0240	1.9218	0.102216	7.6847
2.0260	1.9237	0.102319	7.6922
2.0280	1.9256	0.102422	7.6997
2.0300	1.9275	0.102525	7.7072
2.0320	1.9294	0.102628	7.7147
2.0340	1.9313	0.102731	7.7222
2.0360	1.9332	0.102834	7.7297
2.0380	1.9351	0.102937	7.7372

OBSERVED DISTANCE (INCHES)	TRUE DISTANCE (INCHES)	ERROR (INCHES)	RAY ANGLE (DEGREES)
2.0400	1.9370	0.103040	7.7447
2.0420	1.9389	0.103143	7.7522
2.0440	1.9408	0.103246	7.7597
2.0460	1.9426	0.103349	7.7672
2.0480	1.9445	0.103453	7.7747
2.0500	1.9464	0.103556	7.7822
2.0520	1.9483	0.103659	7.7897
2.0540	1.9502	0.103762	7.7972
2.0560	1.9521	0.103865	7.8047
2.0580	1.9540	0.103968	7.8122
2.0600	1.9559	0.104071	7.8197
2.0620	1.9578	0.104174	7.8272
2.0640	1.9597	0.104277	7.8347
2.0660	1.9616	0.104380	7.8422
2.0680	1.9635	0.104483	7.8497
2.0700	1.9654	0.104587	7.8572
2.0720	1.9673	0.104690	7.8647
2.0740	1.9692	0.104793	7.8722
2.0760	1.9711	0.104896	7.8797
2.0780	1.9730	0.104999	7.8872
2.0800	1.9749	0.105102	7.8947
2.0820	1.9768	0.105205	7.9022
2.0840	1.9787	0.105309	7.9097
2.0860	1.9806	0.105412	7.9172
2.0880	1.9825	0.105515	7.9246
2.0900	1.9844	0.105618	7.9321
2.0920	1.9863	0.105721	7.9396
2.0940	1.9882	0.105825	7.9471
2.0960	1.9901	0.105928	7.9546
2.0980	1.9920	0.106031	7.9621
2.1000	1.9939	0.106134	7.9696
2.1020	1.9958	0.106238	7.9771
2.1040	1.9977	0.106341	7.9846
2.1060	1.9996	0.106444	7.9921
2.1080	2.0015	0.106547	7.9996
2.1100	2.0033	0.106650	8.0071
2.1120	2.0052	0.106754	8.0146
2.1140	2.0071	0.106857	8.0220
2.1160	2.0090	0.106960	8.0295
2.1180	2.0109	0.107064	8.0370
2.1200	2.0128	0.107167	8.0445
2.1220	2.0147	0.107270	8.0520
2.1240	2.0166	0.107374	8.0595
2.1260	2.0185	0.107477	8.0670
2.1280	2.0204	0.107580	8.0745
2.1300	2.0223	0.107683	8.0820
2.1320	2.0242	0.107787	8.0894
2.1340	2.0261	0.107890	8.0969
2.1360	2.0280	0.107993	8.1044
2.1380	2.0299	0.108097	8.1119
2.1400	2.0318	0.108200	8.1194
2.1420	2.0337	0.108303	8.1269
2.1440	2.0356	0.108407	8.1344
2.1460	2.0375	0.108510	8.1419
2.1480	2.0394	0.108613	8.1493
2.1500	2.0413	0.108717	8.1568
2.1520	2.0432	0.108820	8.1643
2.1540	2.0451	0.108924	8.1718
2.1560	2.0470	0.109027	8.1793
2.1580	2.0489	0.109131	8.1868

OBSERVED DISTANCE (INCHES)	TRUE DISTANCE (INCHES)	ERROR (INCHES)	RAY ANGLE (DEGREES)
2.1600	2.0508	0.109234	8.1943
2.1620	2.0527	0.109337	8.2017
2.1640	2.0546	0.109441	8.2092
2.1660	2.0565	0.109544	8.2167
2.1680	2.0584	0.109647	8.2242
2.1700	2.0602	0.109751	8.2317
2.1720	2.0621	0.109854	8.2392
2.1740	2.0640	0.109958	8.2466
2.1760	2.0659	0.110061	8.2541
2.1780	2.0678	0.110165	8.2616
2.1800	2.0697	0.110268	8.2691
2.1820	2.0716	0.110372	8.2766
2.1840	2.0735	0.110475	8.2840
2.1860	2.0754	0.110579	8.2915
2.1880	2.0773	0.110682	8.2990
2.1900	2.0792	0.110786	8.3065
2.1920	2.0811	0.110889	8.3140
2.1940	2.0830	0.110993	8.3214
2.1960	2.0849	0.111096	8.3289
2.1980	2.0868	0.111200	8.3364
2.2000	2.0887	0.111303	8.3439
2.2020	2.0906	0.111407	8.3514
2.2040	2.0925	0.111510	8.3588
2.2060	2.0944	0.111614	8.3663
2.2080	2.0963	0.111717	8.3738
2.2100	2.0982	0.111821	8.3813
2.2120	2.1001	0.111924	8.3887
2.2140	2.1020	0.112028	8.3962
2.2160	2.1039	0.112131	8.4037
2.2180	2.1058	0.112235	8.4112
2.2200	2.1077	0.112339	8.4187
2.2220	2.1096	0.112442	8.4261
2.2240	2.1115	0.112546	8.4336
2.2260	2.1133	0.112650	8.4411
2.2280	2.1152	0.112753	8.4486
2.2300	2.1171	0.112857	8.4560
2.2320	2.1190	0.112960	8.4635
2.2340	2.1209	0.113064	8.4710
2.2360	2.1228	0.113168	8.4784
2.2380	2.1247	0.113271	8.4859
2.2400	2.1266	0.113375	8.4934
2.2420	2.1285	0.113479	8.5009
2.2440	2.1304	0.113582	8.5083
2.2460	2.1323	0.113686	8.5158
2.2480	2.1342	0.113790	8.5233
2.2500	2.1361	0.113893	8.5308
2.2520	2.1380	0.113997	8.5382
2.2540	2.1399	0.114101	8.5457
2.2560	2.1418	0.114205	8.5532
2.2580	2.1437	0.114308	8.5606
2.2600	2.1456	0.114412	8.5681
2.2620	2.1475	0.114516	8.5756
2.2640	2.1494	0.114620	8.5830
2.2660	2.1513	0.114723	8.5905
2.2680	2.1532	0.114827	8.5980
2.2700	2.1551	0.114931	8.6055
2.2720	2.1570	0.115034	8.6129
2.2740	2.1589	0.115138	8.6204
2.2760	2.1608	0.115242	8.6279
2.2780	2.1627	0.115346	8.6353

OBSERVED DISTANCE (INCHES)	TRUE DISTANCE (INCHES)	ERROR (INCHES)	RAY ANGLE (DEGREES)
2.2800	2.1645	0.115450	8.6428
2.2820	2.1664	0.115553	8.6503
2.2840	2.1683	0.115657	8.6577
2.2860	2.1702	0.115761	8.6652
2.2880	2.1721	0.115865	8.6727
2.2900	2.1740	0.115969	8.6801
2.2920	2.1759	0.116072	8.6876
2.2940	2.1778	0.116176	8.6951
2.2960	2.1797	0.116280	8.7025
2.2980	2.1816	0.116384	8.7100
2.3000	2.1835	0.116488	8.7174
2.3020	2.1854	0.116592	8.7249
2.3040	2.1873	0.116695	8.7324
2.3060	2.1892	0.116799	8.7398
2.3080	2.1911	0.116903	8.7473
2.3100	2.1930	0.117007	8.7548
2.3120	2.1949	0.117111	8.7622
2.3140	2.1968	0.117215	8.7697
2.3160	2.1987	0.117319	8.7772
2.3180	2.2006	0.117423	8.7846
2.3200	2.2025	0.117527	8.7921
2.3220	2.2044	0.117631	8.7995
2.3240	2.2063	0.117735	8.8070
2.3260	2.2082	0.117839	8.8145
2.3280	2.2101	0.117942	8.8219
2.3300	2.2120	0.118046	8.8294
2.3320	2.2138	0.118150	8.8368
2.3340	2.2157	0.118254	8.8443
2.3360	2.2176	0.118358	8.8518
2.3380	2.2195	0.118462	8.8592
2.3400	2.2214	0.118566	8.8667
2.3420	2.2233	0.118670	8.8741
2.3440	2.2252	0.118774	8.8816
2.3460	2.2271	0.118878	8.8890
2.3480	2.2290	0.118982	8.8965
2.3500	2.2309	0.119086	8.9040
2.3520	2.2328	0.119190	8.9114
2.3540	2.2347	0.119294	8.9189
2.3560	2.2366	0.119398	8.9263
2.3580	2.2385	0.119502	8.9338
2.3600	2.2404	0.119606	8.9412
2.3620	2.2423	0.119711	8.9487
2.3640	2.2442	0.119815	8.9561
2.3660	2.2461	0.119919	8.9636
2.3680	2.2480	0.120023	8.9711
2.3700	2.2499	0.120127	8.9785
2.3720	2.2518	0.120231	8.9860
2.3740	2.2537	0.120335	8.9934
2.3760	2.2556	0.120439	9.0009
2.3780	2.2575	0.120543	9.0083
2.3800	2.2594	0.120647	9.0158
2.3820	2.2612	0.120751	9.0232
2.3840	2.2631	0.120856	9.0307
2.3860	2.2650	0.120960	9.0381
2.3880	2.2669	0.121064	9.0456
2.3900	2.2688	0.121168	9.0530
2.3920	2.2707	0.121272	9.0605
2.3940	2.2726	0.121376	9.0679
2.3960	2.2745	0.121480	9.0754
2.3980	2.2764	0.121585	9.0828

OBSERVED DISTANCE (INCHES)	TRUE DISTANCE (INCHES)	ERROR (INCHES)	RAY ANGLE (DEGREES)
2.4000	2.2783	0.121689	9.0903
2.4020	2.2802	0.121793	9.0977
2.4040	2.2821	0.121897	9.1052
2.4060	2.2840	0.122001	9.1126
2.4080	2.2859	0.122106	9.1201
2.4100	2.2878	0.122210	9.1275
2.4120	2.2897	0.122314	9.1350
2.4140	2.2916	0.122418	9.1424
2.4160	2.2935	0.122523	9.1498
2.4180	2.2954	0.122627	9.1573
2.4200	2.2973	0.122731	9.1647
2.4220	2.2992	0.122835	9.1722
2.4240	2.3011	0.122940	9.1796
2.4260	2.3030	0.123044	9.1871
2.4280	2.3049	0.123148	9.1945
2.4300	2.3067	0.123253	9.2020
2.4320	2.3086	0.123357	9.2094
2.4340	2.3105	0.123461	9.2168
2.4360	2.3124	0.123565	9.2243
2.4380	2.3143	0.123670	9.2317
2.4400	2.3162	0.123774	9.2392
2.4420	2.3181	0.123879	9.2466
2.4440	2.3200	0.123983	9.2541
2.4460	2.3219	0.124087	9.2615
2.4480	2.3238	0.124191	9.2689
2.4500	2.3257	0.124296	9.2764
2.4520	2.3276	0.124400	9.2838
2.4540	2.3295	0.124505	9.2913
2.4560	2.3314	0.124609	9.2987
2.4580	2.3333	0.124713	9.3061
2.4600	2.3352	0.124818	9.3136
2.4620	2.3371	0.124922	9.3210
2.4640	2.3390	0.125027	9.3285
2.4660	2.3409	0.125131	9.3359
2.4680	2.3428	0.125235	9.3433
2.4700	2.3447	0.125340	9.3508
2.4720	2.3466	0.125444	9.3582
2.4740	2.3484	0.125549	9.3657
2.4760	2.3503	0.125653	9.3731
2.4780	2.3522	0.125758	9.3805
2.4800	2.3541	0.125862	9.3880
2.4820	2.3560	0.125967	9.3954
2.4840	2.3579	0.126071	9.4028
2.4860	2.3598	0.126176	9.4103
2.4880	2.3617	0.126280	9.4177
2.4900	2.3636	0.126385	9.4251
2.4920	2.3655	0.126489	9.4326
2.4940	2.3674	0.126594	9.4400
2.4960	2.3693	0.126698	9.4474
2.4980	2.3712	0.126803	9.4549
2.5000	2.3731	0.126907	9.4623

APPENDIX C

APPLICATION OF COMPUTER PROGRAM "HOLOFER"

The computer program is an adptation of the inversion first proposed by C. D. Maldonado [9, 10, 11] and is designed to invert fringe numbers across a field to the density field. It can be operated in three different modes as described below:

(a) Mode 1

Mode 1 is utilized as a self-test of the computer program. It can either generate its own input density field using Subroutine FUNCT or read in a density field through Subroutine FREAD. The program then generates the fringe array and inverts the array back to the original density field. This mode was utilized in the present investigation to determine the value of the scale factor, α , required to obtain the correct density across the fin.

(b) Mode 2

This mode reads in irregularly spaced fringe data and generates the fringe array at regular intervals across the field using Subroutine SHEET. By specifying NCODE = 1, the fringe array can be generated by one of the functions in Subroutine FUNCT. Mode 2 was not utilized.

(c) Mode 3

Mode 3 reads in the fringe data at regularly spaced intervals and inverts the array to density data across the field. The Subroutine GARRAY calls Subroutine READ to read in the fringe data. The first two cards preceeding the fringe data provide the program with the fringe field size, location, and symmetry.

The following parameters were used in considering the symmetric field case:

<u>PARAMETER</u>	<u>INPUT</u>
NOF	Run Number
IMAX	201
JMAX	1
ISYM	101
JSYM	1
IMS	2
JMS	100
Z	0.387
XO	0.0
YO	0.0
PHISYM	0.0

References [3] and [12] contain further details and applications of the computer program. A print-out of the program is included in the next few pages of this appendix.


```

NPTS=AR(15)
NLINS=AR(16)
SD=AR(18)
PHIZ=AR(19)
DELPHI=AR(20)
YPZERO=AR(21)
YPRNG=AR(22)
XPZERO=AR(23)
XPRNG=AR(24)
NGF=AR(25)
NAF=AR(26)
IPT=AR(27)
KPT=AR(28)
LPT=AR(29)
BND=AR(30)
A=AR(31)
B=AR(32)
C=AR(33)
D=AR(34)
E=AR(35)
P=AR(36)
S=AR(37)
T=AR(38)
U=AR(39)
V=AR(40)
W=AR(41)
Q=AR(42)
WRITE(6,90)
WRITE(6,98)
WRITE(6,91)
WRITE(6,92)
WRITE(6,93)
WRITE(6,94)
WRITE(6,95)
WRITE(6,96)
WRITE(6,97)
WRITE(6,98)
FORMAT(//5X,/,*,IMAX,0)
1, MEXTRA *,/3X,6F10.0)
1, FORMAT(/5X,/,*,ALPHA,3,F10.3,2F10.3,*,SIZE,*,EPS,*,RHO-INF,*,LAMBDA,*,SET00340
1, BETA *,/3X,*,MODE,*,F10.3)
1, FORMAT(/5X,/,*,2X,5F10.0,*,DELPHI,*,YPZERO,*,YPRANGE,*,XPZERO,*,SET
1, STD.DEV *,/5X,/,*,PHIZERO,*,F10.3)
1, FORMAT(/5X,/,*,4X,6F10.3)
1, XPRANGE *,/5X,/,*,1ST FUN,*,ADD FUN,*,GARRAY,*,GRAPH,*,LIN PRT,*,SET00400
1, MAP BND *,/2X,6F10.0)

```

```

CAL00480
CAL00490
CAL00500
CAL00510
CAL00520
CAL00530
CAL00540
CAL00550
CAL00560
CAL00570
CAL00580
CAL00590
CAL00600
CAL00610
CAL00620
CAL00630
CAL00640
CAL00650
CAL00660
CAL00670
CAL00680
CAL00690
CAL00700
CAL00710
CAL00720
CAL00730
CAL00740

```



```

96  FORMAT (/5X,'* A * B * C * D * E *',SET00420
97  1,  FORMAT (/5X,'* /4X,6F10.3) * T * U * V * W *',SET00440
98  1,  FORMAT (/3X,'* /4X,6F10.3) *
      FORMAT (/3X,75A1)
      IF (DGN.GE.4) WRITE (6,89) (AR(I),I=1,42)
      NNN=2
      IF (MODE.LT.0) NNN=1
      IF (MODE.GT.5) NNN=3
      IF (MODE.GT.5) MODE=MODE-10
      NGP=0
      IF (KLIMIT.LT.KEXTRA) KEXTRA=KLIMIT
      IF (MLIMIT.LT.MEXTRA) MEXTRA=MLIMIT
      IF (IPT.LT.0) NGP=IPT
      IF (IPT.LT.0) IPT=-IPT
      ISYM=2.1-(FLOAT(JSYM)/2.-FLOAT(JSYM/2))*2
      IF (JSYM.EQ.0) ISYM=1
      IF (JSYM.GT.JMAX) ISYM=2
      IF (ISYM.EQ.1) JMAX=((JMAX+1)/2)*2
      RJMX=JMAX
      MSYM=JSYM
      IF ((MSYM.EQ.0).OR.(MSYM.GT.JMAX)) MSYM=1
      FCU=ISYM*JSYM*JMAX
      IF ((JSYM.GT.JMAX).OR.(JSYM.EQ.0)) FCU=JMAX
      QSYM=FCU/RJMX
      IMS=(IMAX+ISYM-1)/ISYM
      JMS=JMAX
      IF (ISYM.EQ.1) JMS=(JMAX/2+1)/2
      IF (JSYM.EQ.0) JMS=JMAX/2
      MODE=ABS(AR(13))
      XQ=0.
      YO=0.
      ZD=0.
      PHISYM=0.
      HS=SIZE/2.
      RHOS=1.286
      BOX=RHOFINF*BETA/RHOS/RLAMDA
      RPTS=NPTS
      XPR=0.
      IF (NPTS.GT.1) XPR=XPRNG/(RPTS-1.)/2.
      XPM=-XPR
      PIE=3.141592653589793
      MONE=1
      WRITE (6,58) IMAX,JMAX,IMS,JMS,ISYM,JSYM,MSYM,QSYM,FCU, /
      FORMAT (3X,' I MAX, J MAX, I MS, J MS, I SYM, J SYM, M SYM, Q SYM, F CU', /
      715,2F7.3/)
      1  NTWO=2
      IX=IMAX+JMAX

```



```

15
NF=IN1
IF ((MODE.EQ.1.) .AND. (NOF.EQ.8) .AND. (DGN.GE.1.)) WRITE (6,69)
IF ((MODE.EQ.1.) .AND. (NOF.EQ.8)) CALL FREAD (NO,RO,NF,ZD)
Z=ZD
IF (DGN.GE.1.) WRITE (6,68)
CALL GARRAY (G,GA,NOF,DGN,MONE,XO,YO,PHISYM)
LM=1
IF ((LPT.EQ.0) .AND. (BND.EQ.0)) LM=0
IF IMX=IMAX+1
JMX=JMAX+1
IJMX=IMAX*JMAX
NBD=1
IF (JSYM.EQ.0) NBD=2
KBD=KLIMIT*NBD
DO 15 IJ=1, IJMX
GA(IJ)=0
IF (NAF.EQ.0) GO TO 16
NF=IN2
IF ((NAF.EQ.8) .AND. (DGN.GE.1.)) WRITE (6,69)
IF (NAF.EQ.8) CALL FREAD (NA,RA,NF,ZD)
MST=MODE
MODE=1
IF (DGN.GE.1.) WRITE (6,68)
IF (NAF.NE.0) CALL GARRAY (GA,G,NAF,DGN,NTWO,XO,YO,PHISYM)
MODE=MST
DO 6 IJ=1, IJMX
G(IJ)=G(IJ)+GA(IJ)
RLINS=NLINS
IF (NAF.EQ.8) WRITE (6,88) NA,(RA(L),L=1,NA)
IF (NOF.EQ.8) WRITE (6,87) NO,(RO(I),I=1,NO)
IF (LM.EQ.0) GO TO 14
RB(1)=-1.
DO 1 I=2,7
RB(I)=RB(I-1)+.5
TPIE=2.*PIE
MPIE=-PIE
DYP=0.
DXP=0.
IF (NLINS.GT.1) DYP=YPRNG/(RLINS-1.)
IF (NPPTS.GT.1) DXP=XPRNG/(RPTS-1.)
IF ((DGN.GE.1.) .AND. (NNN.EQ.2)) WRITE (6,64)
IF (NNN.EQ.2) CALL BDGEN (G,H,SCF,DGN,NBD,BDA,KBD)
DO 5 J=1,NLINS
IF (DGN.GE.1.) WRITE (6,67) J
RJMJ=J-1
PHI=PHI+DELPHI*RJM
YP(J)=YPZERO+DYP*RJM
PSI=(PHI+90.)*PIE/180.

```

```

CAL01180
CAL01190
CAL01200
CAL01210
CAL01220
CAL01230
CAL01240
CAL01250
CAL01260
CAL01270
CAL01280
CAL01290
CAL01300
CAL01310
CAL01320
CAL01330
CAL01340
CAL01350
CAL01360
CAL01370
CAL01380
CAL01390
CAL01400
CAL01410
CAL01420
CAL01430
CAL01440
CAL01450
CAL01460
CAL01470
CAL01480
CAL01490
CAL01500
CAL01510
CAL01520
CAL01530
CAL01540
CAL01550
CAL01560
CAL01570
CAL01580
CAL01590
CAL01600
CAL01610
CAL01620
CAL01630
CAL01640
CAL01650

```


CAL01660
CAL01670
CAL01680
CAL01690
CAL01700
CAL01710
CAL01720
CAL01730
CAL01740
CAL01750
CAL01760
CAL01770
CAL01780
CAL01790
CAL01800
CAL01810
CAL01820
CAL01830
CAL01840
CAL01850
CAL01860
CAL01870
CAL01880
CAL01890
CAL01900
CAL01910
CAL01920
CAL01930
CAL01940
CAL01950
CAL01960
CAL01970
CAL01980
CAL01990
CAL02000
CAL02010
CAL02020
CAL02030
CAL02040
CAL02050
CAL02060
CAL02070
CAL02080
CAL02090
CAL02100
CAL02110
CAL02120
CAL02130

```

TAU=PSI-PHISYM
IF (LPT.EQ.0) GO TO 9
IF (LPT.LE.1) WRITE (6,78) (ST,I=1,124)
IF (LPT.GT.1) WRITE (6,74) (ST,I=1,95)
IF ((CMS.EQ.1).AND.(LPT.GT.1)) READ (5,79) ZZ
WRITE (6,86)
WRITE (6,85) Z,PHI,YP(J)
WRITE (6,76)
IF (MODE.EQ.1) WRITE (6,83) (RB(I),I=1,7)
IF (MODE.GT.1) WRITE (6,80) (RB(I),I=1,7)
WRITE (6,81) (DH,I=1,54),(PL,I=1,13)
IC=0
DO 3 I=1,NPTS
  RIM=I-1
  THEO(I,J)=0.
  CA(I,J)=0.
  FA(I,J)=0.
  ERR(I)=0.
  CALC(I,J)=0.
  RHU(I)=0.
  XP(I)=XPZERO+DXP*RIM
  XPI=ABS(XP(I))
  IF (XPI.LT.1.E-10) XP(I)=0.
  RS=SQR(XP(I)**2+YP(J)**2)/HS
  IF (RS.GT.1.) GO TO 13
  THT=ATANM(YP(J),XP(I))
  IF (XPI.EQ.0.) THT=0.
  SIG=TAU-PIE/2.+THT
  IF (SIG.GT.PIE) SIG=SIG-TPIE
  IF (SIG.LT.MPIE) SIG=SIG+TPIE
  SIGI=SIG
  XS=RS*COS(SIG)
  IF (DGN.GE.1.) WRITE (6,44) SIG
  FORMAT ('SIG=',E10.3)
  YS=RS*SIN(SIG)
  IF (DGN.GE.5) WRITE (6,57) PHI,DELPHI,PSI,TAU,THT,SIG,SIGI,XS,YS
  IF (DGN.GE.5) ANGLES='10E10.3)
  RI=I
  F=0.
  IF (DGN.GE.2.) WRITE (6,66) I
  CALL FUNCT (XS,YS,FA(I,J),NAF,DGN,NTWO)
  IF (MODE.EQ.1) CALL FUNCT (XS,YS,F,NOF,DGN,MONE)
  THEO(I,J)=F
  IF (NNN.GE.2) REWIND 3
  IF (NNN.GE.2) CALL FIELD (RS,SIGI,SOLN,NBD,BDA,DGN,KBD)
  IF (NNN.EQ.1) CALL FIELD2 (RS,SIGI,SOLN,G,H,SCF,DGN)
  CA(I)=SOLN/BOX/HS
  CALC(I,J)=CA(I)-FA(I,J)

```



```

13  RHO(I)=RHOINF*(CALC(I,J)+1.)
    ERR(I)=CA(I)
    IF (MODE.EQ.1) ERR(I)=(CALC(I,J)-THEO(I,J))
    IF (MODE.GT.1) THEO(I,J)=FA(I,J)
    IF (LPT.EQ.0) GO TO 3
    LC=0
    TL(I)=BL
    TTL=0
    IF ((XP(I).GT.XPM).AND.(XP(I).LT.XPR)) TTL=1.
    IF (IC.EQ.5) IC=0
    IF (IC.EQ.0) TL(I)=PL
    DO 2 L=2,62
    TL(L)=BL
    IF ((I.EQ.1).OR.(TTL.EQ.1).OR.(I.EQ.NPTS)) TL(L)=PL
    IF (LC.EQ.10) LC=0
    IF ((IC.EQ.0).AND.(LC.EQ.0)) TL(L)=PL
    LC=LC+1
    TL(2)=PL
    TL(22)=PL
    TL(62)=PL
    IC=IC+1
    RLW=(CA(I)+1.)*20.+2.5
    LW=RLW
    IF (LW.GT.62) LW=62
    IF (LW.LT.2) LW=2
    TL(LW)=SC
    RLY=(FA(I,J)+1.)*20.+2.5
    LY=RLY
    IF (LY.GT.62) LY=62
    IF (LY.LT.2) LY=2
    IF (NAF.NE.0) TL(LY)=ST
    RLX=(THEO(I,J)+1.)*20.+2.5
    LX=RLX
    IF (LX.GT.62) LX=62
    IF (LX.LT.2) LX=2
    IF (MODE.EQ.1) TL(LX)=OH
    RLZ=(CALC(I,J)+1.)*20.+2.5
    LZ=RLZ
    IF (LZ.GT.62) LZ=62
    IF (LZ.LT.2) LZ=2
    TL(LZ)=EX
    WRITE (6,82) MOUT,KOUT,INDEX,THEO(I,J),ERR(I),CALC(I,J),RHO(I),
1 XPR(I),TL(L),L=1,62)
    IF ((NPTS.LE.20).AND.(I.NE.NPTS)) WRITE (6,79)
    CONTINUE
    IF (LPT.NE.0) WRITE (6,81) (DH,I=1,54),(PL,I=1,13)
    IMAX=0.
    TMIN=0.
2
3

```

```

CAL02140
CAL02150
CAL02160
CAL02170
CAL02180
CAL02190
CAL02200
CAL02210

CAL02260
CAL02270
CAL02280
CAL02290
CAL02300
CAL02310
CAL02320
CAL02330
CAL02340
CAL02350
CAL02360
CAL02370
CAL02380
CAL02390
CAL02400
CAL02410
CAL02420
CAL02430
CAL02440
CAL02450
CAL02460
CAL02470
CAL02480
CAL02490
CAL02500
CAL02510
CAL02520
CAL02530
CAL02540
CAL02550
CAL02560
CAL02570
CAL02580
CAL02590
CAL02600
CAL02610

```



```

IE=0
BE=0.
DO 4 I=1,NPTS
  TH=THEO(I,J) TMAX=TH
  IF (TH.GT.TMAX) TMIN=TH
  IF (TH.LT.TMIN) TMIN=TH
  ER=ABS(CALC(I,J)-TH)
  IF (ER.LE.BE) GO TO 4
BE=ER
IE=I
CONTINUE -TMIN
TMM=TMXINFE*(CALC(IE,J)-THEO(IE,J))*100./TMM
EB=RHOINFE*(CALC(IE,J)-THEO(IE,J)) WRITE (6,75) EB,XP(IE),BE
IF (TMM.NE.O.) BE=(CALC(IE,J)-THEO(IE,J)) WRITE (6,75) EB,XP(IE),BE
IF ((MODE.EQ.1).AND.(LPT.NE.O)) WRITE (6,75) EB,XP(IE),BE
IF (DELPHI.NE.O.) YP(J)=PHI
CONTINUE
IF (BND.EQ.O.) GO TO 14
IF (LPT.EQ.O.) WRITE (6,78) (ST,I=1,124)
IF (LPT.GT.1) WRITE (6,74) (ST,I=1,95)
IF ((CMS.EQ.1).AND.(LPT.GT.1)) READ (5,79) ZZ
IF (DGN.GE.1) WRITE (6,63)
CALL MAP(NPTS,NLINS,CALC,NOF,Z,BND)
IF (NAF.EQ.O.) GO TO 10
NAO=10*NOF+NAF
IF ((DGN.GE.1).AND.(NGP.EQ.-3)) WRITE (6,62)
IF (NGP.EQ.-3) CALL GPUNCH (Z,XO,YO,PHISYM,NAO,IMAX,JMAX,G)
DO 7 IJ=1,IJMX
  G(IJ)=G(IJ)-GA(IJ)
  IF (IPT.LE.O) GO TO 11
  IF ((IPT.EQ.1).OR.(IPT.EQ.3)) WRITE (6,78) (ST,I=1,124)
  IF ((IPT.EQ.2).OR.(IPT.GE.4)) WRITE (6,74) (ST,I=1,95)
  IF ((CMS.EQ.1).AND.(IPT.EQ.2).OR.(IPT.GE.4)) READ (5,79) ZZ
  CALL GPRINT (G,MONE)
  IF (NGP.EQ.-1) CALL GPUNCH (Z,XO,YO,PHISYM,NOF,IMAX,JMAX,G)
  IF (IPT.EQ.3) WRITE (6,78) (ST,I=1,124)
  IF (IPT.GE.4) WRITE (6,74) (ST,I=1,95)
  IF ((CMS.EQ.1).AND.(IPT.GE.4)) READ (5,79) ZZ
  IF (IPT.GE.3) CALL GPRINT (GA,NTWO)
  IF (KPT.LE.O) GO TO 12
  IF ((KPT.EQ.1).OR.(KPT.EQ.3)) WRITE (6,78) (ST,I=1,124)
  IF ((KPT.EQ.2).OR.(KPT.GE.4)) WRITE (6,74) (ST,I=1,95)
  IF ((CMS.EQ.1).AND.(KPT.EQ.2).OR.(KPT.GE.4)) READ (5,79) ZZ
  IF (DGN.GE.1) WRITE (6,61)
  CALL GPLOTT (G,GA,JMS)
  WRITE (6,78) (EX,I=1,124)
  AGAIN=ST

```

CAL02620
 CAL02630
 CAL02640
 CAL02650
 CAL02660
 CAL02670
 CAL02680
 CAL02690
 CAL02700
 CAL02710
 CAL02720
 CAL02730
 CAL02740
 CAL02750
 CAL02760
 CAL02770
 CAL02780
 CAL02790
 CAL02800
 CAL02810
 CAL02820
 CAL02830
 CAL02840
 CAL02850
 CAL02860
 CAL02870
 CAL02880
 CAL02890
 CAL02900
 CAL02910
 CAL02920
 CAL02930
 CAL02940
 CAL02950
 CAL02960
 CAL02970
 CAL02980
 CAL02990
 CAL03000
 CAL03010
 CAL03020
 CAL03030
 CAL03040
 CAL03050
 CAL03060
 CAL03070
 CAL03080
 CAL03090


```

C          SUBROUTINE BDGEN (G,H,SCF,DGN,NBD,BDA,KBD)
C          BDGEN EVALUATES THE B AND D COEFFICIENTS FOR ALL M AND K, AND WRITES
C          THE ARRAY LINEARLY ON DISK.
C
COMMON IMAX,JMAX,IIMX,JJMX,IJMX,ALPHA,SIZE,EPS,MODE,BOX,SD,IX,Z
COMMON /TAB/ INDEX,KEXTRA,MEXTRA,KLIMIT,MLIMIT,KOUT,MOUT
COMMON /SYM/ ISYM,JSYM,MSYM,FCU,IMS,JMS,QSYM
DIMENSION G(IJMX),H(IIMX,5),SCF(JJMX,6),BDA(KBD)
INITIALIZE THE VALUES:
INDEX=0
KL2=NBD*KLIMIT
REWIND 3
JJMX6=JJMX*6
IIMX2=(IIMX+1)/2
PIE=3.141592653589793
RIMAX=IMAX
KLMP=KLIMIT+1
DX=2./RIMAX
RJMAX=JMAX
DXI=2.*PIE/FCU
INITIALIZE THE MODIFIED HERMITE POLYNOMIAL ARRAY:  VECTORS:
(1)=H1, (2)=H2, (3)=ALPHA*X(I), (4)=HM+2 STORED, (5)=HM+1 STORED
DO 1 I=1,IIMX2
RII=IIMX-I+1
IIM=IIMX-RII+1
H(II,3)=ALPHA*(RII*DX-DX-1.)
H(II,3)=-H(II,3)
H(II,1)=2.*H(II,3)
H(II,2)=(H(II,3)*H(II,1)-1.)/3.
H(II,1)=-H(II,1)
H(II,2)=H(II,2)
H(II,5)=H(II,2)
H(II,4)=H(II,2)
H(II,5)=H(II,2)
H(II,4)=H(II,1)
H(II,4)=H(II,1)
SIGN=1.
INITIATE THE SIN/COS ARRAY:
DO 2 J=1,JJMX
RJM=J-1
SCF(J,1)=0.
SCF(J,2)=1.
SCF(J,3)=SIN(RJM*DXI-PIE/2.)
SCF(J,4)=COS(RJM*DXI-PIE/2.)
SCF(J,5)=0.
SCF(J,6)=0.
MS=0
C          COMMENCE THE M LOOP:

```



```

DO 7 MP=1,MLIMIT
M=MP-1
RM=M
SIGN=-SIGN
IF (DGN.LE.-4) WRITE (6,88) SCF(1,1),SCF(2,1),SCF(1,2),SCF(2,2)
TEST FOR SYMMETRY SKIPS:
IF (MS.EQ.MSYM) MS=0
TOTAL=0.
MS=MS+1
IF (MS.NE.1) GO TO 6
C COMMENCE THE K LOOP:
DO 5 KP=1,KLIMIT
K=KP-1
PK=KP
RK=K
INDEX=INDEX+1
C CALL THE B & D COEFFICIENTS AND WRITE THEM ON DISK:
CALL BD (M,K,G,H,SCF,B,D,JJMX6)
IF (DGN.LE.3.) WRITE (6,89) M,K,B,D
IF (DGN.LE.-2) WRITE (6,89) M,K,B,D
IF (DGN.LE.-4) WRITE (6,88) H(1,1),H(1,2),H(1,4),H(1,5)
KK=K*NBD+1
K2=KP*NBD
BDA(K2)=D
BDA(KK)=B
C GENERATE THE NEXT ORDER OF THE SET OF HERMITE POLYNOMIALS FOR NEW K:
ORDER=M+2*KP+1
HA=SQRT(PK*(PK+RM))/ORDER
HB=2.*SQRT((PK+1.)*(RM+PK+1.))/(ORDER+2.)
DO 5 I=1,IIMX2
IIM=IIMX-I+1
H(I,1)=2.*(H(I,3)*H(I,2)-HA*H(I,1))
H(I,1)=SIGN*H(I,1)
H(I,2)=HB*(H(I,3)*H(I,1)-ORDER*H(I,2))
C ADVANCE THE SIN/COS ARRAY FOR THE NEXT M:
DO 3 J=1,JJMX
IF (DGN.LE.-5) WRITE (6,87) (SCF(J,NT),NT=1,6)
IF (FORMAT(1) SIN/COS MXI:'8E10.3)
TEMP=SCF(J,1)
SCF(J,1)=SCF(J,4)+SCF(J,2)*SCF(J,3)
SCF(J,2)=SCF(J,2)*SCF(J,3)-TEMP*SCF(J,3)
DO 4 J=1,JJMAX
SCF(J,5)=SCF(J+1,1)-SCF(J,1)
SCF(J,6)=SCF(J+1,2)-SCF(J,2)
WRITE (3) (BDA(I),I=1,KBD)
IF (DGN.LE.-3) WRITE (6,88) (BDA(I),I=1,10)
IF (JSYM.GT.JMAX) RETURN
RM=RM+1

```



```

C      REGENERATE THE HERMITE ARRAY FOR NEW M, K=0:
DO 7 II=1,IIMX2
  IIM=IIMX-II+1
  H(II,2)=H(II,5)*(RM+1.)
  H(II,1)=H(II,5)*(RM+2.)
  H(IIM,1)=-SIGN*H(II,1)
  H(II,2)=2.*SQRTRM+1)*H(II,3)*H(II,1)-(RM+1.)*H(II,2))
  H(II,2)=H(II,2))/(RM+2.))/(RM+3.)
  H(II,4)=H(II,1)
  H(II,5)=H(II,2)
  H(II,5)=H(II,2)
  FORMAT ('M=',I4,'', K=',I4,'', B=',E10.4,'', D=',E10.4)
89  FORMAT (2X,10E10.3)
88  RETURN
C000002
C

```

```

SUBROUTINE FIELD (RS,SIG,SOLN,NBD,BDA,DGN,KBD)
C
C      FIELD EVALUATES THE VALUE OF THE FIELD FUNCTION AT A PARTICULAR
C      POINT DESIGNATED IN CYLINDRICAL COORDINATES, BY USING THE INVERSION
C      EQUATION OF MALDONADO, ET.AL. FIELD USES THE ARRAY OF B & D
C      COEFFICIENTS GENERATED IN SUBROUTINE BDGEN.
C
COMMON IMAX,JMAX,IIMX,JJMX,IJMX,ALPHA,SIZE,EPS,MODE,BOX,SD,IX,Z
COMMON /TAB/ INDEX,KEXTRA,MEXTRA,KLIMIT,MLIMIT,KOUT,MOUT
COMMON /SYM/ ISYM,JSYM,MSYM,FCU,IMS,JMS,QSYM
DIMENSION BDA(KBD),STK(52),STM(52)
C      INITIALIZE THE VALUES:
INDEX=0
ITIMER=0
KOUT=0
MOUT=0
MMAX=0
KMAX=0
TOTAL=0.
JJMX6=JJMX*6
REWIND 3
AR=ALPHA*RS
ARG=AR**2
EXPON=EXP(-ARG)
PIE=3.141592653589793
APP=ALPHA/PIE/PIE
M=0
RM=M
RIMAX=IMAX
DX=2./RIMAX
C
SUB01140
SUB01150
SUB01160
SUB01170
SUB01180
SUB01190
SUB01200
SUB01210
SUB01220
SUB01230
SUB01240
SUB01250
SUB01260
SUB01270
SUB01280
SUB01290
SUB01300
SUB01310
SUB01320
SUB01330
SUB01340
SUB01350
SUB01360
SUB01370
SUB01380
SUB01390
SUB01400
SUB01410
SUB01420
SUB01430
SUB00980
SUB00990
SUB01000
SUB01010
SUB01020
SUB01030
SUB01040
SUB01050
SUB01060
SUB01070
SUB01080
SUB01090
SUB01100
SUB01110
SUB01120
SUB01130

```



```

16 RJMAX=JMAX
   SIGN=1.
   STK(1)=0.
   STM(1)=0.
   SMS=0.
   CMS=1.
   SMI=1.
   CMI=1.
   MEP=1.
   DO 16 MB=1,MEP
     STM(MB)=0.
     FM=1.
     MS=0
2   C  COMMENCE THE M LOOP:
     SIGN=-SIGN
     K=0
     RK=K
     RM=M
     ARM=1.
     IF (M.NE.0) ARM=AR**M
     KTIMER=0
     KEPM=KEXTRA+1
     DO 15 KB=1,KEP
       STK(KB)=0.
       SIGNK=-1.
15  C  COMPUTE THE K=0 & K=1 ORDERS OF LAGUERRE POLYNOMIAL FOR GIVEN M:
       PM=0.
       P=SQRT(1./FM)
       PP=(RM+1.-ARG)*SQRT(1./FM/(RM+1.))
       C  TEST FOR SYMMETRY SKIPS:
       IF (MS.EQ.MSYM) MS=0
       MS=MS+1
       C  IF (MS.NE.1) GO TO 7 COEFFICIENTS FOR GIVEN M:
       READ A LINE OF 8 & D
       READ (3) (BDA(I),I=1,KBD)
       IF (DGN.LE.-6) WRITE (6,88) (BDA(I),I=1,10)
       C  COMMENCE THE K LOOP:
       INDEX=INDEX+1
       SIGNK=-SIGNK
       C  COMPUTE THE M,K SUMMATION TERM:
       KK=K*NBD+1
       B=BDA(KK)
       D=0.
       IF (NBD.EQ.2) D=BDA(KK+1)
       BRAKET=B
       IF (RM.EQ.0.) GO TO 4
       BRAKET=B+CMS+D*SMS
       ADD=SIGNK*BRAKET*P*ARM
4

```

SUB01440
 SUB01450
 SUB01460
 SUB01470
 SUB01480
 SUB01490
 SUB01500
 SUB01510
 SUB01520
 SUB01530
 SUB01540
 SUB01550
 SUB01560
 SUB01570
 SUB01580
 SUB01590
 SUB01600
 SUB01610
 SUB01620
 SUB01630
 SUB01640
 SUB01650
 SUB01660
 SUB01670
 SUB01680
 SUB01690
 SUB01700
 SUB01710
 SUB01720
 SUB01730
 SUB01740
 SUB01750
 SUB01760
 SUB01770
 SUB01780
 SUB01790
 SUB01800
 SUB01810
 SUB01820
 SUB01830
 SUB01840
 SUB01850
 SUB01860
 SUB01870
 SUB01880
 SUB01890
 SUB01900
 SUB01910


```

TOTAL=TOTAL+ADD
IF (DGN.GT.-5) GO TO 5
STOT=TOTAL*EXPON#APP/BOX/SIZE
WRITE (6,89) M,K,STOT,ADD,BRAKET,P,ARM,B,CMS,D,SMS
ESTABLISH CHECK AS THE RELATIVE SIZE OF THE M,K TERM OF THE SERIES:
5 CHECK=ABS(ADD)
IF (TOTAL.GT.EPS) CHECK=ABS(ADD/TOTAL)
C ADVANCE THE K INDEX:
K=K+1
RK=K
DO 10 KA=1,KEXTRA
KB=KEXTRA-KA+1
STK(KB+1)=STK(KB)
STK(2)=TOTAL
ORDER=M+2*K+1
C GENERATE THE NEXT ORDER OF LAGUERRE POLYNOMIAL FOR NEW K:
PM=PP
P=PP
PP=P*(ORDER-ARG)-PM*SQRT(RK*(RM+RK))
PP=PP/SQRT((RK+1.)*(RM+RK+1.))
C SET K TIMER TO PROVIDE EXTRA K TERMS AFTER CHECK < EPS:
KTIMER=KTIMER+1
IF (K.GE.KLIMIT) GO TO 6
IF (CHECK.GE.EPS) KTIMER=0
IF (KTIMER.LE.KEXTRA) GO TO 3
GO TO 7
6 KOUT=KOUT+1
IF (KEXTRA.EQ.0) GO TO 7
TOTAL=0.
DO 11 KA=1,KEXTRA
TOTAL=TOTAL+STK(KA+1)
RKX=KEXTRA
TOTAL=TOTAL/RKX
C END OF K LOOP: ADVANCE M:
M=M+1
RM=M
STP=SMS
SMS=SMS*CMI+CMS*SMI
SMS=SMS*CMI-STP*SMI
CMS=CMS*CMI-KMAX
IF (K.GT.KMAX) KMAX=K
FM=FM*RM
DO 12 MA=1,MEXTRA
MB=MEXTRA-MA+1
STM(MB+1)=STM(MB)
STM(2)=TOTAL
C SET M TIMER FOR EXTRA M TERMS:
MTIMER=MTIMER+1
IF (JSYM.GT.JMAX) GO TO 9

```

SUB01920
SUB01930
SUB01940
SUB01950
SUB01960
SUB01970
SUB01980
SUB01990
SUB02000
SUB02010
SUB02020
SUB02030
SUB02040
SUB02050
SUB02060
SUB02070
SUB02080
SUB02090
SUB02100
SUB02110
SUB02120
SUB02130
SUB02140
SUB02150
SUB02160
SUB02170
SUB02180
SUB02190
SUB02200
SUB02210
SUB02220
SUB02230
SUB02240
SUB02250
SUB02260
SUB02270
SUB02280
SUB02290
SUB02300
SUB02310
SUB02320
SUB02330
SUB02340
SUB02350
SUB02360
SUB02370
SUB02380
SUB02390


```

13 IF (K.GT.KEXTRA) MTIMER=0
   IF (M.GE.MLIMIT) GO TO 13
   IF (MTIMER.LE.MEXTRA) GO TO 2
   IF (MEXTRA.EQ.0) GO TO 9
   TOTAL=0.
   DO 14 MA=1,MEXTRA
   TOTAL=TOTAL+STM(MA+1)
14 RMX=MEXTRA
   TOTAL=TOTAL/RMX
   END OF M LOOP: COMPUTE OUTPUT SOLN.
9 MOUT=M-1
  IF (KOUT.EQ.0) KOUT=KMAX-1
  SOLN=TOTAL*EXPON*APP/2.
89 FORMAT (' M=',I4,' K=',I4,' SUBTOTAL=',9E10.3)
88 RETURN
   END
C000003
C

```

```

C
C SUBROUTINE BD (M,K,G,H,SCF,B,D,JJMX6)
C
C BD EVALUATES THE FIRST (B) AND SECOND (D) COEFFICIENTS IN THE
C INVERSION EQUATION. FOR A PARTICULAR SET OF INDEXES M & K.
C BD MAKES USE OF THE HERMITE POLYNOMIAL ARRAY GENERATED BY
C SUBROUTINE FIELD AS M & K ADVANCE.
C

```

```

COMMON IMAX,JMAX,IIMX,JJMX,IJMX,ALPHA,SIZE,EPS,MODE,BOX,SD,IX,Z
COMMON /SYM/ ISYM,JSYM,MSYM,FCU,IMS,JMS,QSYM
DIMENSION G(IJMX),SCF(JJMX6),H(IIMX)
PIE=3.141592653589793
B=0.
D=0.
RM=M
RK=K
RJMAXX=JMAX
JJMX4=4*JJMX
DXI=2.*PIE/FCU
FORMAT(1X,I10,/)
200 IF (JSYM.LE.0) GO TO 4
   IF (M.NE.0) GO TO 2
   S=DXI
   DO 1 J=1,JMAX
   DO 1 I=1,IMAX
   II=I+1
   IJ=IMAX*(J-1)+I

```



```

1      DH=H(I I)-H(I)
      B=B+G(I J)*S*DH
      B=B*QSYM/2.
      RETURN
2      DO 3 J=1,JMAX
      JS=J+J J M X 4
      S=SCF(JS)/RM
      DO 3 I=1,I MAX
      II=I+1
      IX=I MAX*(J-1)+I
      IJ=I MAX*(J-1)+I
      DH=H(I I)-H(I)
      B=B+G(I J)*S*DH
      B=B*QSYM
      RETURN
3      IF (M.NE.O) GO TO 6
      S=DX I
      DO 5 J=1,JMAX
      DO 5 I=1,I MAX
      II=I+1
      IX=I MAX*(J-1)+I
      IJ=I MAX*(J-1)+I
      DH=H(I I)-H(I)
      B=B+G(I J)*S*DH
      B=B/2.
      RETURN
4      DO 7 J=1,JMAX
      JS=J+J J M X 4
      J2=JS+J J M X
      S=SCF(JS)/RM
      C=SCF(J2)/RM
      DO 7 I=1,I MAX
      II=I+1
      IX=I MAX*(J-1)+I
      IJ=I MAX*(J-1)+I
      DH=H(I I)-H(I)
      B=B+G(I J)*S*DH
      FORMAT (' BD:',4I5,10F6.2)
      D=D-G(I J)*C*DH
      RETURN
5      END
6      C000004

```

SUBROUTINE FIELD2 (RS,SIG,SOLN,G,H,SCF,DGN)

```

C      FIELD2 COMPUTES THE SAME INVERSION AS SUBROUTINE FIELD, EXCEPT THAT
C      THE COEFFICIENTS B AND D ARE COMPUTED INDIVIDUALLY AS USED BY
C      CALLING BD. DISK STORAGE IS NOT REQUIRED, BUT COMPUTING TIME IS
C      MUCH GREATER. FIELD2 IS UTILIZED BY SPECIFYING A NEGATIVE MODE ON

```

SUB02850
SUB02860
SUB02870
SUB02880
SUB02890
SUB02900
SUB02910
SUB02920
SUB02930
SUB02940
SUB02950
SUB02960
SUB02970
SUB02980
SUB02990
SUB03000
SUB03010
SUB03020
SUB03030
SUB03040
SUB03050
SUB03060
SUB03070
SUB03080
SUB03090
SUB03100
SUB03110
SUB03120
SUB03130
SUB03140

SUB03160
SUB03170
SUB03180
SUB03190
SUB03200
SUB03210
SUB03220
SUB03230
SUB03240

SUB03250
SUB03260
SUB03270
SUB03280
SUB03290
SUB03300


```

C THE INPUT PARAMETER. VALUE OF THE FIELD FUNCTION AT A PARTICULAR
C FIELD EVALUATES THE VALUE OF THE FIELD FUNCTION AT A PARTICULAR
C POINT DESIGNATED IN CYLINDRICAL COORDINATES, BY USING THE INVERSION
C EQUATION OF MALDONADO, ET AL. FIELD CALLS SUBROUTINES BD & GARRAY.
C
COMMON IMAX,JMAX,IIMX,JJMX,IJMX,ALPHA,SIZE,EPS,MODE,BOX,SD,IX,Z
COMMON /TAB/ INDEX,KEXTRA,MEXTRA,KLIMIT,MLIMIT,KOUT,MOUT
COMMON /SYM/ ISYM,JSYM,MSYM,FCU,IMS,JMS,QSYM
DIMENSION G(IJMX),H(IIMX,5),SCF(IJMX,6)
C INITIALIZE THE VALUES:
INDEX=0
MTIMER=0
KOUT=0
MOUT=0
MMAX=0
KMAX=0
TOTAL=0.
JJMX6=JJMX*6
IIMX2=(IIMX+1)/2
AR=ALPHA*RS
EXPON=EXP(-ARG)
PIE=3.141592653589793
APP=ALPHA/PIE/PIE
M=0
RM=M
RIMAX=IMAX
DX=2./RIMAX
RJMAX=JMAX
DXI=2.*PIE/FCU
C INITIALIZE THE MODIFIED HERMITE POLYNOMIAL ARRAY: VECTORS:
C (1)=H1, (2)=H2, (3)=ALPHA*X(I), (4)=HM+2 STORED, (5)=HM+1 STORED
DO 1 I=1,IIMX2
RII=II
IIM=IIMX-II+1
H(II,3)=ALPHA*(RII*DX-DX-1.)
H(IIM,3)=-H(II,3)
H(II,1)=2.*H(II,3)
H(II,2)=(H(II,3)*H(II,1)-1.)/3.
H(IIM,1)=-H(II,1)
H(IIM,2)=H(II,2)
H(IIM,5)=H(II,2)
H(IIM,4)=H(II,1)
H(IIM,4)=H(IIM,1)
SIGN=1.
FM=1.
C INITIALIZE THE SIN/COS ARRAY:

```



```

DO 11 J=1,JJMX
  RJM=J-1
  SCF(J,1)=0.
  SCF(J,2)=1.
  SCF(J,3)=SIN(RJM*DXI-PIE)
  SCF(J,4)=COS(RJM*DXI-PIE)
  SCF(J,5)=0.
  SCF(J,6)=0.
  MS=0
  COMMENCE THE M LOOP:
  SIGN=-SIGN
  K=0
  RK=K
  ARM=1.
  IF (M.NE.0) ARM=AR**M
  KTIMER=0
  SIGNK=-1.
  COMPUTE THE K=0 & K=1 ORDERS OF LAGUERRE POLYNOMIAL FOR GIVEN M:
  PM=0.
  P=SQRT(1./FM)
  PP=(RM+1.-ARG)*SQRT(1./FM/(RM+1.))
  ADVANCE THE SIN/COS ARRAY FOR NEW M:
  DO 12 J=1,JJMX
    SCF(J,1)=SCF(J,1)*SCF(J,4)+SCF(J,2)*SCF(J,3)
    SCF(J,2)=SCF(J,2)*SCF(J,4)-SCF(J,1)*SCF(J,3)
    DO 13 J=1,JMAX
      SCF(J,5)=SCF(J+1,1)-SCF(J,1)
      SCF(J,6)=SCF(J+1,2)-SCF(J,2)
    TEST FOR SYMMETRY SKIPS:
    IF (MS.EQ.MSYM) MS=0
    TOTAL=0.
    MS=MS+1
    IF (MS.NE.1) GO TO 7
    RMS=RM**SIGN
    RMS=COS(RMS)
    SMS=SIN(RMS)
    COMMENCE THE K LOOP:
    INDEX=INDEX+1
    SIGNK=-SIGNK
    CALL THE B & D COEFFICIENTS AND COMPUTE THE M,K SUMMATION TERM:
    CALL BD (M,K,G,H,SCF,B,D,JJMX6)
    IF (DGN.LE.-2.) WRITE (6,89) M,K,B,D
    BRACKET=B
    IF (RM.EQ.0.) GO TO 4
    BRACKET=B*CMS+D*SMS
    ADD=SIGNK*BRACKET*P*ARM
    TOTAL=TOTAL+ADD
  ESTABLISH CHECK AS THE RELATIVE SIZE OF THE M,K TERM OF THE SERIES:

```

SUB03790
 SUB03800
 SUB03810
 SUB03820
 SUB03830
 SUB03840
 SUB03850
 SUB03860
 SUB03870
 SUB03880
 SUB03890
 SUB03900
 SUB03910
 SUB03920
 SUB03930
 SUB03940
 SUB03950
 SUB03960
 SUB03970
 SUB03980
 SUB03990
 SUB04000
 SUB04010
 SUB04020
 SUB04030
 SUB04040
 SUB04050
 SUB04060
 SUB04070
 SUB04080
 SUB04090
 SUB04100
 SUB04110
 SUB04120
 SUB04130
 SUB04140
 SUB04150
 SUB04160
 SUB04170
 SUB04180
 SUB04190
 SUB04200
 SUB04210
 SUB04220
 SUB04230
 SUB04240
 SUB04250


```

C      CHECK=ABS(ADD)
C      IF (TOTAL.GT.EPS) CHECK=ABS(ADD/TOTAL)
C      ADVANCE THE K INDEX:
C      K=K+1
C      RK=K
C      ORDER=M+2*K+1
C      GENERATE THE NEXT ORDER OF LAGUERRE POLYNOMIAL FOR NEW K:
C      PM=P
C      P=PP
C      PP=PP*(ORDER-ARG)-PM*SQRT(RK*(RM+RK))
C      PP=PP/SQRT((RK+1.)*(RM+RK+1.))
C      GENERATE THE NEXT ORDER OF THE SET OF HERMITE POLYNOMIALS FOR NEW K:
C      HA=SQRT(RK*(RK+RM))/ORDER
C      HB=2.*SQRT((RK+1.)*(RM+RK+1.))/(ORDER+1.)/(ORDER+2.)
C      DO 5 I I=1, IIMX2
C      IIM=IIMX-I I+1
C      H(I I,1)=2.*(H(I I,3)*H(I I,2)-HA*H(I I,1))
C      H(I I,1)=SIGN*H(I I,1)
C      H(I I,2)=HB*(H(I I,3)*H(I I,1)-ORDER*H(I I,2))
5 C      SET K TIMER TO PROVIDE EXTRA K TERMS AFTER CHECK < EPS:
C      KTIMER=KTIMER+1
C      IF (K.GE.KLIMIT) GO TO 6
C      IF (MTIMER.LE.MEXTRA) GO TO 2
C      IF (CHECK.GE.EPS) KTIMER=0
C      IF (KTIMER.LE.KEXTRA) GO TO 3
C      GO TO 7
C      END OF K LOOP: ADVANCE M AND COMPUTE NEW TOTAL:
6 KOUT=KOUT+1
7 M=M+1
C      IF (K.GT.KMAX) KMAX=K
C      RM=M
C      FM=FM*RM
C      REGENERATE THE HERMITE ARRAY FOR NEW M, K=0:
C      DO 8 I I=1, IIMX2
C      IIM=IIMX-I I+1
C      H(I I,2)=H(I I,4)*SQRT(RM)/(RM+1.)
C      H(I I,1)=H(I I,5)*((RM+2.))
C      H(I I,M,1)=-SIGN*H(I I,1)
C      H(I I,2)=2.*SQRT(RM+1.)*(H(I I,3)*H(I I,1)-(RM+1.)*H(I I,2))
C      H(I I,2)=H(I I,2)/(RM+2.)/(RM+3.)
C      H(I I,4)=H(I I,1)
C      H(I I,5)=H(I I,2)
C      SET M TIMER FOR EXTRA M TERMS:
C      IF (MS.EQ.1) MTIMER=MTIMER+1
C      IF (JSYM.GT.JMAX) GO TO 9
C      IF (K.GT.KEXTRA) MTIMER=0
C      IF (M.GE.MLIMIT) GO TO 9
C      END OF M LOOP: COMPUTE OUTPUT SOLN.

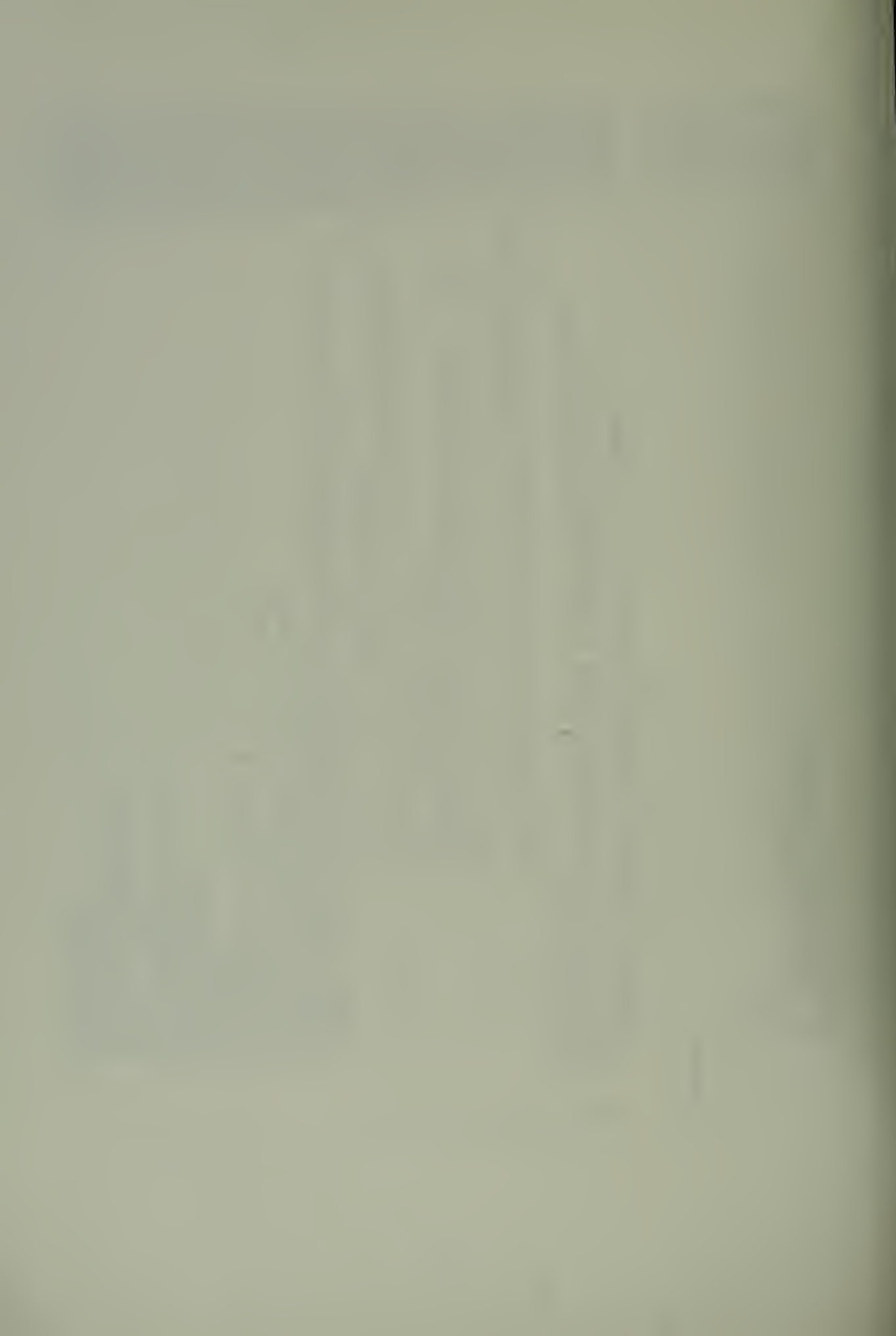
```



```

9      MOUT=M-1
      IF (KOUT.EQ.0) KOUT=KMAX-1
      SOLN=TOTAL#EXPON#APP/2.
89     FORMAT ('M=',I4,'', B='E10.4','', D='E10.4')
      RETURN
      END
C000005
C
SUBROUTINE GARRAY (G,GA,NOF,DGN,NUMB,XO,YO,PHISYM)
C
C   GARRAY FILLS THE DATA ARRAY OVER AN ORTHOGONAL AREA WITH
C   THE REGULAR DATA OBTAINED BY THE METHOD CORRESPONDING TO THE
C   PARTICULAR MODE:
C
C   MODE 1 - DATA OBTAINED BY SAMPLING A KNOWN FUNCTION SUPPLIED
C             IN SUBROUTINE FUNCT AND SAMPLED IN SUBROUTINE GOLP.
C
C   MODE 2 - DATA OBTAINED BY GENERATING A REGULAR ARRAY FROM
C             IRREGULAR EXPERIMENTAL INPUT DATA READ IN. CALLS
C             SUBROUTINE SHEET. (EXPERIMENTAL DATA MAY
C             BE SIMULATED, SEE 'SHEET')
C
C   MODE 3 - UTILIZES RAW DATA TAKEN AT THE PROPER INTERVAL,
C             OR PREVIOUSLY GENERATED, AND READ DIRECTLY INTO THE
C             GARRAY. CALLS SUBROUTINE READ.
C
COMMON IMAX,JMAX,IIMX,JJMX,IJMX,ALPHA,SIZE,EPS,MODE,BOX,SD,IX,Z
COMMON /SYM/ ISYM,JSYM,MSYM,FCU,IMS,JMS,QSYM
COMMON /IO/ CMS,INI,IN2,IN4
DIMENSION G(IMAX,JMAX),GA(IMAX,JMAX)
PIE=3.141592653589793
HS=SIZE/2.
IF (MODE.GT.3) MODE=1
RIMX=IMAX
RJMX=JMAX
DELR=SIZE/RIMX
DELXI=2.*PIE/FCU
IF (MODE.GT.1) GO TO 2
DO 1 J=1,JMS
RJ=J
XI=(RJ-.5)*DELXI-PIE
J2=J+2*(JMS-J)
J3=J+JMAX/2
J4=J2+JMAX/2

```



SUB00390
SUB00400
SUB00410
SUB00420
SUB00430
SUB00440
SUB00450
SUB00460
SUB00470
SUB00480
SUB00490
SUB00500
SUB00510
SUB00520
SUB00530
SUB00540
SUB00550
SUB00560
SUB00570
SUB00580
SUB00590
SUB00600
SUB00610
SUB00620

```

DO 1 I=1,IMS
RI=I
II=I MAX+1-I
R=(RI-.5)*DELR-HS
CALL GOLF (R,XI,GIJ,NOF,DGN,NUMB)
G(I,J)=GIJ
IF (ISYM.EQ.2) G(II,J)=GIJ
IF (ISYM.EQ.2) GO TO 1
G(II,J3)=GIJ
IF (JSYM.EQ.0) GO TO 1
G(I,J2)=GIJ
G(II,J4)=GIJ
CONTINUE
GO TO 4
1 IF (MODE.GT.2) GO TO 3
2 CALL SHEET (G,GA,XO,YO,PHISYM,NOF)
GO TO 4
3 CALL READ (Z,XO,YO,PHISYM,NOF,IMAX,JMAX,G)
4 IF (DGN.GE.2) WRITE (6,39)
39 RETURN
FORMAT (' GARRAY RETURNS ')
END
C000006
C

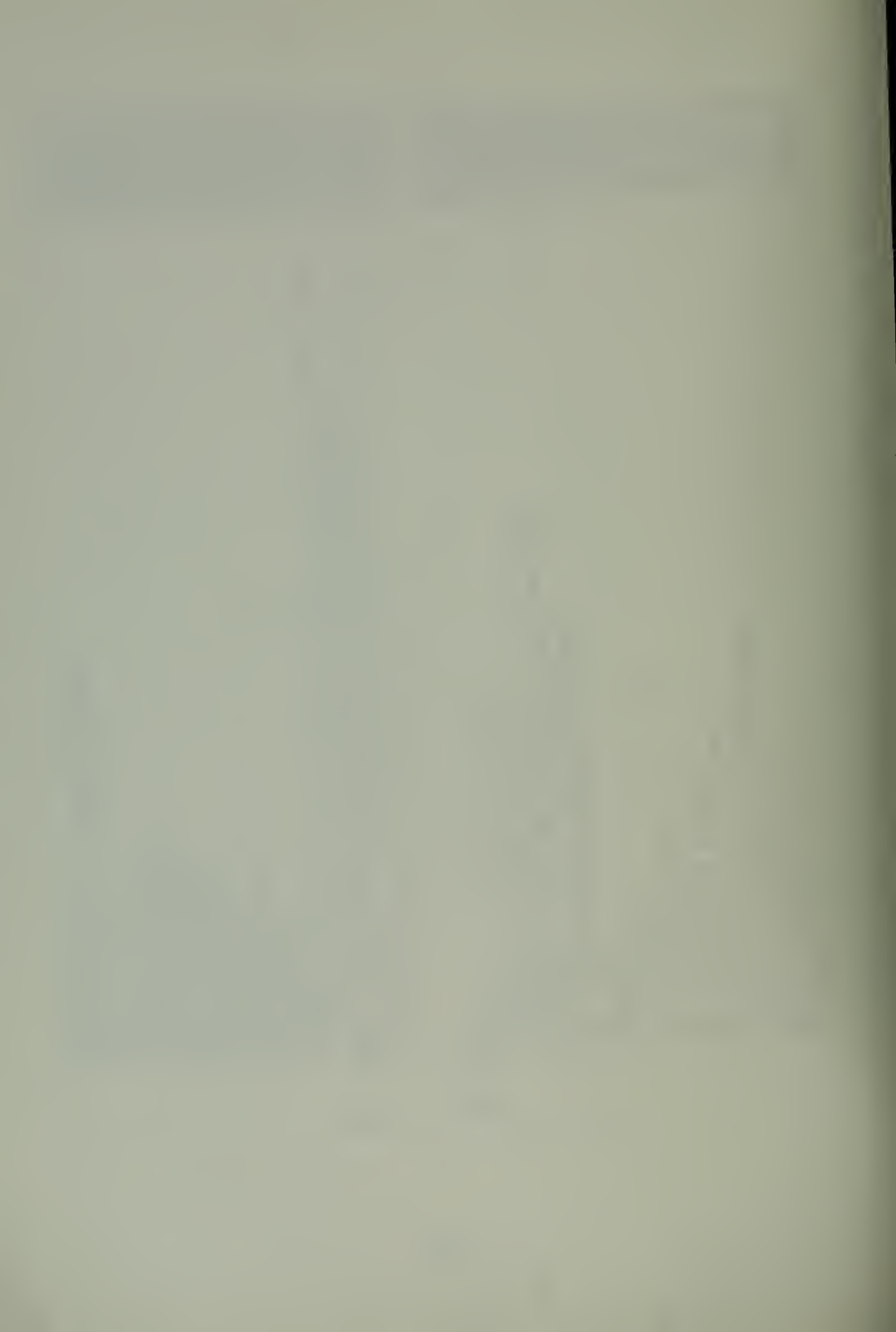
```

SUB00630
SUB00640
SUB00650
SUB00660
SUB00670
SUB00680
SUB00690
SUB00700
SUB00710
SUB00720
SUB00730
SUB00740
SUB00750
SUB00760
SUB00770
SUB00780
SUB00790
SUB00800
SUB00810
SUB00820
SUB00830
SUB00840

```

SUBROUTINE GOLF (R,XI,GIJ,NOF,DGN,NUMB)
C
C GOLF COMPUTES THE FUNCTION G(R,XI) FOR A PARTICULAR LINE OF SIGHT
C FROM A KNOWN FUNCTION CONTAINED IN SUBROUTINE FUNCT.
C
COMMON IMAX,JMAX,IIMX,JJMX,IJMX,ALPHA,SIZE,EPS,MODE,BOX,SD,IX,Z
ZERO=0.
LMAX=IMAX*3
RLMAX=LMAX
DELXP=SIZE/RLMAX
SXI=SIN(XI)
CXI=COS(XI)
DELYS=DELXP*CXI
DELYS=DELXP*SXI
XP=DELXP*.5-SIZE/2.
XS=XP*CXI-R*SXI
YS=XP*SXI+R*CXI
GIJ=0.
DO 1 L=1,LMAX
RL=L
CALL FUNCT (XS,YS,F,NOF,DGN,NUMB)
GIJ=GIJ+F

```




```

1  XS=XS+DELYS
   YS=YS+DELYS
   IF (GIJ.NE.0.) GIJ=GIJ*DELP*BOX
   IF ((SD.EQ.0.) .OR. (NUMB.EQ.1)) GO TO 2
   IF (DGN.GE.3) WRITE (6,28) IX
   CALL GAUSS (IX,SD,ZERO,RV)
   GIJ=GIJ+RV
2  IF (DGN.GE.3) WRITE (6,29) R,XI,GIJ
   RETURN
29  FORMAT (1 R=1,F8.3,1 XI=1,F8.3,1, GIJ=1,F8.3)
28  FORMAT (1 GAUSS, IX=1,I8)
   END
C000007
C

C SUBROUTINE FUNCT (XS,YS,F,NOF,DGN,NUMB)
C
CP67USERID 1095BOXJ
C
C FUNCT EVALUATES AS INPUT FUNCTION AT POSITION (X,Y) IN THE TEST
C SECTION COORDINATE SYSTEM. NOF IDENTIFIES THE EQUATION USED.
C
COMMON IMAX,JMAX,IIMX,JJMX,IJMX,ALPHA,SIZE,EPS,MODE,BOX,SD,IX,Z
COMMON /EQPARA/ A,B,C,D,E,P,Q,S,T,U,V,W,RO,RA,NO,NA,N1,N2
DIMENSION RO(101),RA(101)
AA=A
BB=B
CC=C
DD=D
EE=E
PP=P
IF (NUMB.LE.1) GO TO 50
AA=S
BB=T
CC=U
DD=V
EE=W
PP=Q
PIE=3.141592653589793
HS=SIZE/2.
R=SQRT(XS**2+YS**2)/HS
F=0.
IF (R.GT.1.) GO TO 11
IF (NOF.LE.0) GO TO 11
C 1. AXISYMMETRIC GAUSSIAN:
SUB000850
SUB000860
SUB000870
SUB000880
SUB000890
SUB000900
SUB000910
SUB000920
SUB000930
SUB000940
SUB000950
SUB000960
SUB000970
SUB000980

SUB000990
SUB01000

SUB01020
SUB01030
SUB01040
SUB01050
SUB01060
SUB01070
SUB01080
SUB01090
SUB01100
SUB01110
SUB01120
SUB01130
SUB01140
SUB01150
SUB01160
SUB01170
SUB01180
SUB01190
SUB01200
SUB01210
SUB01220
SUB01230
SUB01240
SUB01250
SUB01260
SUB01270
SUB01280

```



```

1      IF (NOF.GT.1) GO TO 2
      F=AA*EXP(-1.*(R*HS/BB)**2)
      GO TO 11
C
C
2      ADJUSTABLE RECTANGULAR STEP FUNCTION:
      IF (NOF.GT.2) GO TO 3
      F=PP
      IF ((ABS(XS-DD).LE.BB).AND.(ABS(YS-EE).LE.CC)) F=AA
      GO TO 11
C
C
3      DISPLACABLE ELLIPTICAL GAUSSIAN:
      IF (NOF.GT.3) GO TO 4
      F=AA*EXP(-1.*(XS-DD)/BB)**2+((YS-EE)/CC)**2)
      GO TO 11
C
C
4      CONSTANT:
      IF (NOF.GT.4) GO TO 5
      F=AA
      GO TO 11
C
C
5      ADJUSTABLE AND DISPLACABLE ELLIPTIC RAMP FUNCTION:
      IF (NOF.GT.5) GO TO 6
      RBC=SQRT(((XS-DD)/BB)**2+((YS-EE)/CC)**2)
      F=0.
      IF (RBC.LT.1.) F=AA*((1.-RBC)**PP)
      GO TO 11
C
C
6      DISPLACABLE ELLIPTIC STEP FUNCTION:
      IF (NOF.GT.6) GO TO 7
      RBC=SQRT(((XS-DD)/BB)**2+((YS-EE)/CC)**2)
      F=0.
      IF (RBC.LT.1.) F=AA
      GO TO 11
C
C
7      CIRCULAR COSINE-SQUARED FUNCTION OF BB MAXIMA:
      IF (NOF.GT.7) GO TO 8
      F=AA*COS((2.*BB-1.)*PIE/R/2.))**2
      GO TO 11
C
C
8      NUMERICAL FUNCTION: REQUIRES AN INPUT ARRAY READ IN BY
      SUBROUTINE FREAD: N FOLLOWED BY N POINT VALUES. (101 MAX)
      A CONSTANT VALUE AA IS ADDED TO THE FUNCTION.
      IF (NOF.GT.8) GO TO 9
      IF (NUMB.LE.1) N=NO
      IF (NUMB.GT.1) N=NA
      NM=N-1
      NMM=N-2
      RN=N

```


SUB03130
 SUB03140
 SUB03150
 SUB03160
 SUB03170
 SUB03180
 SUB03190
 SUB03200
 SUB03210
 SUB03220
 SUB03230
 SUB03240
 SUB03250
 SUB03260
 SUB03270
 SUB03280
 SUB03290
 SUB03300
 SUB03310
 SUB03320
 SUB03330
 SUB03340
 SUB03350
 SUB03360
 SUB03370
 SUB03380
 SUB03390
 SUB03400
 SUB03410
 SUB03420
 SUB03430
 SUB03440
 SUB03450
 SUB03460
 SUB03470
 SUB03480
 SUB03490
 SUB03500
 SUB03510
 SUB03520
 SUB03530
 SUB03540
 SUB03550
 SUB03560
 SUB03570
 SUB03580
 SUB03590
 SUB03600

```

RRH=100GO.
XH=RRH*COS(XIH)
YH=RRH*SIN(XIH)
IF (LPR.EQ.1) GO TO 7
YTX=-RR(IMT)*SIN(XI(IMT))-YO
YTN=-RR(IMT)*SIN(XI(IMT))-YO
XTX=RR(IMT)*COS(XI(IMT))-XO
XTN=RR(IMT)*COS(XI(IMT))-XO
UA=TAN(XI(IMT))
UC=TAN(XI(IMT))
UB=YTX-UA*XTX
UD=YTN-UC*XTN
UH=(UD-UB)/(UA-UC)
YH=XH*UA+UB
RRH=SQRT((XH-XO)**2+(YH-YO)**2)
XIH=ATANM((YH-YO),(XH-XO))
CONTINUE
7 C  FILL THE ANGLE AND RADIUS FOR ANY CODE 3 OR 4 LINES:
DO 9 I=1,IM
IF(XY(I).NE.3.) GO TO 8
BAS=SQRT(RRH**2-RR(I)**2)
XI(I)=XIH-ATANM(RR(I),BAS)
GO TO 9
8 XI(I)= ATANM((YH-YD(I)),(XH-XD(I)))
RR(I)=RRH*SIN(XI(I)-XIH)
9 CONTINUE
C  ANGLES AND RADII ARE NOW FILLED FOR ALL POINTS IN THIS LINE.
C  VACATE THE SET OF VECTORS TO BE USED AS TEMPORARY STORAGE:
DO 10 I=1,IM
XD(I)=0.
YD(I)=0.
XG(I)=0.
YG(I)=RR(I)
XY(I)=D(I,J)
RR(I)=0.
D(I,J)=0.
XI(I)=C.
10 C  CONVERT THE LINE TO REGULAR RADII USING INTERPOLATION:
RR(1)=R+DR
CALL SPLINE(YG,XY,IM,RR(1),D(1,J))
DO 11 I=2,IMAX
RI=I
RR(I)=R+DR*RI
CALL SPLINR(YG,XY,IM,RR(I),D(I,J))
11 C  GENERATE THE VECTOR OF ANGLES FOR THIS COLUMN AND STORE IN G ARRAY:
DO 12 I=1,IMAX
BAS=SQRT(RRH**2-RR(I)**2)
G(I,J)=XIH-ATANM(RR(I),BAS)

```



```

12      YG(I)=0.
C      D(I,J)=XY(I)
C      XY(I)=0.
C      COLUMNS ARE NOW ALL REGULARLY FILLED.
C      NEXT, INTERPOLATE EACH ROW REGULARLY OVER THE ANGLES.
C      DO 23 I=1,IMAX
C      EXPAND THE DATA TO 2 SETS TO ESTABLISH SMOOTH INTERPOLATION.
      JM3=3*JM
      II=IMAX+1-I
      IF (JSYM.NE.0) GO TO 14
      DO 13 J=1,JMS
      J2=J+JMS
      J3=J2+JMS
      XD(J2)=D(I,J)
      XD(J3)=D(I,J)
      XG(J)=G(I,J)-TPIE-PHISYM
      XG(J2)=G(I,J)-PIE-PHISYM
      XG(J3)=G(I,J)-PHISYM
      GO TO 16
13      DO 15 J=1,JMS
14      J1=JMS+1-J
      J2=JMS+J
      J3=JM3+1-J
      XD(J1)=D(I,J)
      XD(J2)=D(I,J)
      XD(J3)=D(I,J)
      XG(J1)=G(I,J)-2.*(G(I,J)-PHISYM)-PIE-PHISYM
      XG(J2)=G(I,J)-PIE-PHISYM
      XG(J3)=G(I,J)+2.*(DAN+PHISYM-G(I,J))-PIE-PHISYM
      CONTINUE
      JM2=2*JMS
      JP=JMS/2
      DO 17 J=1,JM2
      XD(J)=XD(J+JP)
      XG(J)=XG(J+JP)
      JJS=JM2+1
      DO 18 J=JJS,JM3
      XD(J)=0.
      XG(J)=0.
15      FIND THE SMALLEST ANGLE
16      XY(1)=1.
      SA=XG(1)
      DO 19 J=1,JM2
      IF (XG(J).GE.SA) GO TO 19
      SA=XG(J)
      XY(1)=J
      CONTINUE
17
18
19

```



```

C      FIND THA MAX ANGLE IN THE ROW:
      XY(JM2)=JM2
      SB=XG(JM2)
      DO 20 J=1,JM2
      IF (XG(J).LE.SB) GO TO 20
      SB=XG(J)
      XY(JM2)=J
      CONTINUE
      DETERMINE THE ORDER OF INCREASING ANGLE IN THE ROW
      SB=XG(JM2)
      J=2
      JSA=XY(JJ-1)
      SA=XG(JJ-1)
      JTS=0
      DO 22 J=1,JM2
      IF (XG(J).LE.SA) GO TO 22
      IF (XG(J).GT.SB) GO TO 22
      SB=XG(J)
      XY(JJ)=J
      JTS=1
      CONTINUE
      IF (JTS.EQ.0) JM2=JJ
      JJ=JJ+1
      IF (JJ.LE.JM2) GO TO 21
      DO 23 J=1,JM2
      JX=XY(J)
      YD(J)=XD(JX)
      INTERPOLATE:
      DXI=2.*PIE/FCU
      XI(J)=DXI/2.-PIE-PHISYM
      CALL SPLINE (XG,YD,JM2,XI(J),G(I,J))
      DO 24 J=2,JMS
      XI(J)=XI(J-1)+DXI
      CALL SPLIN (XG,YD,JM2,XI(J),G(I,J))
      DO 25 J=1,JMS
      XIJ=XI(J)
      XU=XMX
      IF ((XIJ.GE.0.).AND.(XIJ.LT.PIE)) XU=XMN
      YU=YMN
      IF ((XIJ.GE.MPIT).AND.(XIJ.LT.PIT)) YU=YMX
      XL=XMN
      IF ((XIJ.GE.0.).AND.(XIJ.LT.PIE)) XL=XMX
      YL=YMX
      IF ((XIJ.GE.MPIT).AND.(XIJ.LT.PIT)) YL=YMN
      XIJ=SI(XIJ)
      CXIJ=COS(XIJ)
      RMN=(XO-XL)*SXIJ-(YO-YL)*CXIJ
      RMX=(XO-XU)*SXIJ-(YO-YU)*CXIJ

```

SUB04090
SUB04100
SUB04110
SUB04120
SUB04130
SUB04140
SUB04150
SUB04160
SUB04170
SUB04180
SUB04190
SUB04200
SUB04210
SUB04220
SUB04230
SUB04240
SUB04250
SUB04260
SUB04270
SUB04280
SUB04290
SUB04300
SUB04310
SUB04320
SUB04330
SUB04340
SUB04350
SUB04360
SUB04370
SUB04380
SUB04390
SUB04400
SUB04410
SUB04420
SUB04430
SUB04440
SUB04450
SUB04460
SUB04470
SUB04480
SUB04490
SUB04500
SUB04510
SUB04520
SUB04530
SUB04540
SUB04550
SUB04560


```

25 DO 25 I=1,IMAX
   IF (RR(I).LT.RMN) G(I,J)=0.
   IF (RR(I).GT.RMX) G(I,J)=0.
C CONTINUE
25 EXPAND SYMMETRY SECTOR INTO AN ORTHOGONAL INTERVAL.
C IF (ISYM.EQ.2) GO TO 27
DO 26 J=1,JMS
J2=JMAX/2+1-J
J3=JMAX/2+J
J4=JMAX+1-J
DO 26 I=1,IMAX
II=IMAX+1-I
G(I,J2)=G(I,J)
G(II,J3)=G(I,J)
G(II,J4)=G(I,J)
26 RETURN
C FOR EVEN SYMMETRY, AVERAGE THE GARRY COLUMNS.
27 IMS=(2*IMAX+1)/2
DO 28 J=1,JMAX
DO 28 I=1,IMS
II=IMAX+1-I
GST=(G(I,J)+G(II,J))/2.
G(I,J)=GST
G(II,J)=GST
28 RETURN (5I5)
59 FORMAT (10F7.3)
58
C000010
C
C FUNCTION ATANM(Y,X)
C COMPUTES THE ARCTAN OF Y/X BETWEEN -PI AND +PI.
C
PIE=3.141592653589793
PI2=PIE/2.
ATANM=SIGN(PI2,Y)
IF(X.NE.0.) ATANM=ATAN(Y/X)
IF(X.EQ.0.) RETURN
IF(Y.GE.0.) ATANM=PIE+ATANM
IF(Y.LT.0.) ATANM=-PIE+ATANM
RETURN
END
C000011
C
SUB04570
SUB04580
SUB04590
SUB04600
SUB04610
SUB04620
SUB04630
SUB04640
SUB04650
SUB04660
SUB04670
SUB04680
SUB04690
SUB04700
SUB04710
SUB04720
SUB04730
SUB04740
SUB04750
SUB04760
SUB04780
SUB04790
SUB04800
SUB04810
SUB04820
SUB04830
SUB04840
SUB04850
SUB04860
SUB04870
SUB04880
SUB04890
SUB04900
SUB04910
SUB04920
SUB04930
SUB04940
SUB04950
SUB04960
SUB04970
SUB04980
SUB04990
SUB05000
SUB05010

```



```

SUBROUTINE SIM (XD,YD,XG,YG,D,R,XI,XY,XO,YO,PS,XM,XN,YN,I,IM,
1DG,NF)
SIM SIMULATES THE FRINGE NUMBER DATA ONE WOULD OBTAIN FROM THE
HOLOGRAPHIC INTERFEROGRAM PROCESS FOR A KNOWN FUNCTION AS
CONTAINED IN SUBROUTINE FUNCT. THE GRID BOX DIMENSIONS MUST
EXCEED THE INVERSION CIRCLE SIZE, AND APERTURE POINTS SPECIFIED
MUST FALL BETWEEN XI=-40 DEGREES, AND XI=+130 DEGREES.
SUB050200
SUB050230
SUB05030
SUB05030
SUB05040
SUB05050
SUB05050
SUB05060
SUB05070
SUB05080
SUB05090
SUB05100
SUB05110
SUB05120
SUB05130
SUB05140
SUB05150
SUB05160
SUB05170
SUB05180
SUB05190
SUB05200
SUB05210
SUB05220
SUB05230
SUB05240
SUB05250
SUB05260
SUB05270
SUB05280
SUB05290
SUB05300
SUB05310
SUB05320
SUB05330
SUB05340
SUB05350
SUB05360
SUB05370
SUB05380
SUB00010
SUB00020

COMMON IMAX,JMAX,IIMX,IJMX,ALF,SIZ,EPS,MOD,BOX,SD,IX,Z
COMMON /IO/ CMS,IN1,IN2,IN4
READ (IN1,29) XH,YH
ZER=0.
RIM=IM
RI=I
DX=(XM-XN)/(RIM-1.)
DY=(YM-YN)/(RIM-1.)
X1=XM-(RIM-1.)*DX
Y1=YM-(RIM-1.)*DY
XI1=ATANM (YH-Y1,XH-X1)-PS
RRH=SQRT((XH-XO)**2+(YH-YO)**2)
XIO=ATANM(YH-YO,XH-XO)-PS
R1=RRH*SIN(XI1-XIO)
IF ((I.GT.1).AND.(I.LT.IM)) GO TO 1
IF (ABS(R1).LT.SIZ/2.) R1=SIGN(SIZ/2.,R1)
XY=3.
GO TO 2
1 CALL GOLF (R,XI,D,NR,ZER,ZER)
XD=XN
YD=YN
IF (XH.NE.X1) YD=Y1-(X1-XN)*(YH-Y1)/(XH-X1)
IF (YS.GE.YN) GO TO 2
YD=YN
IF (YH.NE.Y1) XD=X1-(Y1-YN)*(XH-X1)/(YH-Y1)
RETURN
FORMAT (10F7.3)
END

C000012
C

SUBROUTINE FREAD (NO,RO,NF,ZZ)
FREAD READS THE NUMERIC ARRAY WHICH IS USED FOR EQUATION 8 OF
SUBROUTINE FUNCT. FIRST CARD IS NUMBER OF POINTS (N.GE.1),
FOLLOWED BY ONE POINT PER CARD.
C
C
C DIMENSION RO(101)
SUB000030
SUB000040
SUB000050
SUB000060
SUB000070
SUB000080
SUB000090

```



```

SUB000100
      READ (NF,89) NO,ZZ
      WRITE(6,90) NO,ZZ
      DO 10 I=1,NO
      READ(NF,88) RO(I)
      WRITE(6,88) RO(I)
      CONTINUE
      10 FORMAT(15,F9.3)
      88 FORMAT(F8.5)
      90 FORMAT(1X,15,F9.3)
      RETURN
      END
C0000013
C
      SUBROUTINE GPRINT (G,NUMB)
C
C      GPRINT PRINTS THE DATA ARRAY 'G' WHICH WAS INPUT TO
C      THE PROGRAM IN SUBROUTINE GARRY.
C
      COMMON IMAX,JMAX,IIMX,JJMX,IJMX,ALPHA,SIZE,EPS,MODE,BOX,SD,IX,Z
      DIMENSION G(IJMX)
      DIMENSION X(15)
      DATA HYP,VERT/1H-,1H1/
      IF (NUMB.EQ.1) WRITE (6,99) MODE,Z
      IF (NUMB.EQ.2) WRITE (6,92) Z
      JM2=JMAX/2
      RIJMX=IJMX/2
      RIMAX=IMAX
      RJMAX=JMAX
      DX=SIZE/RIJMX
      DXI=360./RJMAX
      INTRVL SETS THE NUMBER OF TERMS PRINTED PER LINE. IF IT IS ALTERED,
      ONE MUST ALSO REDIMENSION X AND ALTER FORMATS 98, 97, AND 95.
      INTRVL=15
      IB=1
      IT=IB+INTRVL-1
      IF (IT.GT.IMAX) IT=IMAX
      IBT=IT-IB+1
      WRITE (6,98) (II,II=IB,IT)
      DO 2 I=1,IBT
      RI=IB-1+I
      X(I)=-SIZE/2.+(RI-.5)*DX
      LM=7*IBT+1
      WRITE (6,97) (X(I),I=1,IBT)
      WRITE (6,96) (HYP,L=1,LM),VERT
      JMH=JM2+1
      DO 3 J=JMH,JMAX
      RJ=J

```



```

COMMON /IO/ CMS, IN1, IN2, IN4
DIMENSION G(IMAX, JMAX)
READ (IN1, 39) NOF, IMAX, JMAX, ISYM, JSYM, IMS, JMS
READ (IN1, 40) Z, XO, YO, PHISYM
DO 10 J=1, JMS
  READ (IN1, 38) (G(I, J), I=1, IMS)
  WRITE (6, 37) NOF, Z, XO, YO, PHISYM, IMAX, JMAX, JSYM
  RJMX=JMAX
  MSYM=JSYM
  IF ((MSYM.EQ.0).OR.(MSYM.GT.JMAX)) MSYM=1
  FCU=ISYM*JSYM*JMAX
  IF (JSYM.GT.JMAX) FCU=JMAX
  QSYM=FCU/RJMX
  DO 4 J=1, JMS
    IF (ISYM.EQ.1) GO TO 2
    DO 1 I=1, IMS
      II=IMAX+1-II
      G(II, J)=G(I, J)
    GO TO 4
  J2=JMAX/2+1-J
  J3=JMAX/2+J
  J4=JMAX+1-J
  DO 3 I=1, IMAX
    II=IMAX+1-II
    G(I, J2)=G(II, J)
    G(II, J3)=G(I, J)
    G(II, J4)=G(I, J)
  CONTINUE
  FORMAT(10I5)
  FORMAT(4F7.3)
  FORMAT(10F7.3)
  MODE 3 READS GARRAY DIRECTLY: NOF='I4',
1, ' , XO='F7.3', PHISYM='F7.3',
2, ' , JMAX='I4', JSYM='I4//';
  RETURN
END
C000016
C

SUBROUTINE MAP (IM, JM, A, N, Z, BAND)
C
C MAP CALLS SUBROUTINE MIMPII AND PLOTS A CONTOUR MAP OF THE ARRAY
C
  DIMENSION A(IM, JM), T(24)
  DATA BL/1H/
  DO 1 I=1, 24
    T(I)=BL
  1

```

SUB000950
SUB000960
SUB000970

SUB010000
SUB01010
SUB01020
SUB01030
SUB01040
SUB01050
SUB01060
SUB01070
SUB01080
SUB01090
SUB01100
SUB01110
SUB01120
SUB01130
SUB01140
SUB01150
SUB01160
SUB01170
SUB01180
SUB01190
SUB01200
SUB01210
SUB01220

SUB01240
SUB01250
SUB01260
SUB01270
SUB01280
SUB01290
SUB01300

SUB01310
SUB01320
SUB01330
SUB01340
SUB01350
SUB01360
SUB01370
SUB01380

RINK=RANGE/80.

TOP=BIG+RINK

CEN=BIG

BOT=BIG-RINK

KC=0

DO 7 K=1,41

IC=0

DO 6 I=1,101

ROW(I)=BL

IF((I.EQ.1).OR.(I.EQ.51).OR.(I.EQ.101))ROW(I)=PL

IF((K.EQ.1).OR.(K.EQ.41))ROW(I)=PL

IF((TOP.GE.C).AND.(BOT.LE.0.))ROW(I)=DH

IF(IC.EQ.5)GO TO 3

GO TO 4

IC=0

IF(KC.EQ.10)ROW(I)=PL

IF(KPT.LE.2)GO TO 5

IF((D(I).LE.TOP).AND.(D(I).GE.BOT))ROW(I)=ST

IF((B(I).LE.TOP).AND.(B(I).GE.BOT))ROW(I)=EX

IC=IC+1

IF(KC.EQ.5)KC=0

IF(KC.NE.0)WRITE (6,65) (ROW(I),I=1,101)

IF(KC.EQ.0)WRITE (6,68) CEN,(ROW(I),I=1,101)

TOP=TOP-2.*RINK

CEN=CEN-2.*RINK

BOT=BOT-2.*RINK

KC=KC+1

WRITE (6,66) (ST,I=1,120)

FORMAT (//,J=1,13//)

FORMAT (1X,F8.3,1X,101A1)

FORMAT (1H1,//121A1//)

FORMAT (//121A1//)

FORMAT (10X,101A1)

RETURN

END

C000018

C

SUBROUTINE INTERP (A,IM,AS,B,JM,BS)

INTERP CONVERTS A REGULAR VECTOR A OF IM POINTS TO A REGULAR VECTOR
B OF JM POINTS. OS=.5 FOR A VECTOR WITH POINTS DEFINED IN THE
CENTER OF THE INTERVAL, AS AND BS ARE THE % OF AN INTERVAL FROM THE
EDGE OF THE FIELD TO THE FIRST POINT (.0 OR .5 FOR EDGE OR CENTER
DEFINED POINTS)

DIMENSION A(IM),B(JM)

SUB01850
SUB01860
SUB01870
SUB01880
SUB01890
SUB01900
SUB01910
SUB01920
SUB01930
SUB01940
SUB01950
SUB01960
SUB01970
SUB01980
SUB01990
SUB02000
SUB02010
SUB02020
SUB02030
SUB02040
SUB02050
SUB02060
SUB02070
SUB02080
SUB02090
SUB02100
SUB02110
SUB02120
SUB02130
SUB02140
SUB02150
SUB02160
SUB02170
SUB02180
SUB02190
SUB02200
SUB02210

SUB02220
SUB02230
SUB02240
SUB02250
SUB02260
SUB02270
SUB02280
SUB02290
SUB02300


```

RIM=IM
RJM=JM
RAT=(RIM-1.+2.*AS)/(RJM-1.+2.*BS)
DO 2 I=1,JM
  BI=I
  AI=RAT*(BI+BS)-AS
  IA=AI
  F=AI-FLOAT(IA)
  IF((IA.EQ.0).OR.(IA.EQ.JM)) GO TO 1
  B(I)=A(IA)+F*(A(IA+1)-A(IA))
  GO TO 2
1 IF(IA.EQ.0) B(I)=A(1)*(F-AS)/(1.-AS)
2 IF(IA.EQ.JM) B(I)=A(JM)*F/(1.-AS)
CONTINUE
RETURN
END

```

C000019

```

SUBROUTINE SPLINE
  PURPOSE
    PROVIDES INTERPOLATED VALUE USING "CUBIC SPLINE FITTING"
  USAGE
    FIRST CALL TO SUBROUTINE:
      CALL SPLINE(X,Y,M,XINT,YINT)
    SUBSEQUENT CALLS:
      CALL SPLINN(X,Y,M,XINT,YINT)
  DESCRIPTION OF PARAMETERS
    X: MONOTONICALLY INCREASING ABSCISSA ARRAY
    Y: ONE-FOR-ONE CORRESPONDING ORDINATE ARRAY
    M: NUMBER OF X AND Y VALUES SUPPLIED < OR = 300
    XINT: VALUE OF ABSCISSA FOR WHICH CORRESPONDING ORDINATE
          IS TO BE INTERPOLATED (OR EXTRAPOLATED)
    YINT: INTERPOLATED (OR EXTRAPOLATED) ORDINATE VALUE
  REMARKS
    IF SPECIFIED X FALLS OUTSIDE OF RANGE, AN EXTRAPOLATED
    VALUE WILL BE SUPPLIED
  SUBROUTINES AND FUNCTION SUBPROGRAMS REQUIRED
    SUBROUTINE SPLICO IS INCLUDED IN SUBROUTINE SPLIN PACKAGE

```


C C C C C C C C C C C C C C C C
 MATHEMATICAL METHOD
 UPON FIRST ENTRY TO SPLIN, A CALL TO SPLICO IS MADE TO
 DETERMINE THE COEFFICIENTS TO BE USED IN PERFORMING THE
 INTERPOLATIONS. SEARCH FOR BRACKETING ABSCISSA VALUES IS
 ALWAYS MADE FROM THE REFERENCE LAST USED IN INTERPOLATING.
 REFERENCE
 PENNINGTON, RALPH H., "INTRODUCTORY COMPUTER METHODS AND
 NUMERICAL ANALYSIS", THE MACMILLAN COMPANY, NEW YORK, 1965

 SPL00320
 SPL00330
 SPL00340
 SPL00350
 SPL00360
 SPL00370
 SPL00380
 SPL00390
 SPL00400
 SPL00410
 SPL00420
 SPL00430

SUBROUTINE SPLINE(X,Y,M,XINT,YINT)
 DIMENSION X(M),Y(M),C(4,300)
 CALL SPLICO(X,Y,M,C)
 K=1
 ENTRY SPLIN(X,Y,M,XINT,YINT)
 IF(XINT-X(1)) 70,1,2
 3 70 K=1
 GO TO 7
 1 YINT=Y(1)
 RETURN
 2 IF(XINT-X(K+1)) 6,4,5
 4 YINT=Y(K+1)
 RETURN
 5 K=K+1
 IF(M-K) 71,71,3
 71 K=M-1
 GO TO 7
 6 IF(XINT-X(K)) 13,12,11
 12 YINT=Y(K)
 RETURN
 13 K=K-1
 GO TO 6
 7 PRINT 101,XINT
 101 FORMAT(8H,XINT = E18.9,32H, OUT OF RANGE FOR INTERPOLATION)
 11 YINT=(X(K+1)-XINT)*(C(1,K)-XINT)**2+C(3,K))
 YINT=YINT+(XINT-X(K))*(C(2,K)-XINT-X(K))**2+C(4,K))
 RETURN
 END
 SPL00440
 SPL00460
 SPL00470
 SPL00480
 SPL00490
 SPL00500
 SPL00510
 SPL00520
 SPL00530
 SPL00540
 SPL00550
 SPL00560
 SPL00570
 SPL00580
 SPL00590
 SPL00600
 SPL00610
 SPL00620
 SPL00630
 SPL00640
 SPL00650
 SPL00660
 SPL00670
 SPL00680
 SPL00690
 SPL00700
 SPL00710
 SPL00720


```

SUBROUTINE SPLICO(X,Y,M,C)
DIMENSION X(M),Y(M),C(4,300),D(300),P(300),E(300),A(300,3),B(300),
1 Z(300)
MM=M-1
DO 2 K=1,MM
D(K)=X(K+1)-X(K)
P(K)=D(K)/6.
2 E(K)=(Y(K+1)-Y(K))/D(K)
DO 3 K=2,MM
3 B(K)=E(K)-E(K-1)
A(1,2)=-1.-D(1)/D(2)
A(1,3)=D(1)/D(2)
A(2,3)=P(2)-P(1)*A(1,3)
A(2,2)=2.*(P(1)+P(2))-P(1)*A(1,2)
A(2,3)=A(2,3)/A(2,2)
B(2)=B(2)/A(2,2)
DO 4 K=3,MM
4 A(K,2)=2.*(P(K-1)+P(K))-P(K-1)*A(K-1,3)
B(K)=B(K)-P(K-1)*B(K-1)
A(K,3)=P(K)/A(K,2)
B(K)=B(K)/A(K,2)
Q=D(M-2)/D(M-1)
A(M,1)=1.+Q+A(M-2,3)
A(M,2)=-Q-A(M,1)*A(M-1,3)
B(M)=B(M-2)-A(M,1)*B(M-1)
Z(M)=B(M)/A(M,2)
MN=M-2
DO 6 I=1,MN
6 K=M-I
Z(K)=B(K)-A(K,3)*Z(K+1)
Z(1)=-A(1,2)*Z(2)-A(1,3)*Z(3)
DO 7 K=1,MM
7 Q=1./(6.*D(K))
C(1,K)=Z(K)*Q
C(2,K)=Z(K+1)*Q
C(3,K)=Y(K)/D(K)-Z(K)*P(K)
C(4,K)=Y(K+1)/D(K)-Z(K+1)*P(K)
RETURN
END

```

SPL00730
SPL00750
SPL00760
SPL00770
SPL00780
SPL00790
SPL00800
SPL00810
SPL00820
SPL00830
SPL00840
SPL00850
SPL00860
SPL00870
SPL00880
SPL00890
SPL00900
SPL00910
SPL00920
SPL00930
SPL00940
SPL00950
SPL00960
SPL00970
SPL00980
SPL00990
SPL01000
SPL01010
SPL01020
SPL01030
SPL01040
SPL01050
SPL01060
SPL01070
SPL01080
SPL01090
SPL01100
SPL01110
SPL01120

C000020

MET00010
MET00020
MET00030
MET00040
MET00050
MET00060

SUBROUTINE MTMPII

PURPOSE

MET00070
 MET00080
 MET00090
 MET00100
 MET00110
 MET00120
 MET00130
 MET00140
 MET00150
 MET00160
 MET00170
 MET00180
 MET00190
 MET00200
 MET00210
 MET00220
 MET00230
 MET00240
 MET00250
 MET00260
 MET00270
 MET00280
 MET00290
 MET00300
 MET00310
 MET00320
 MET00330
 MET00340
 MET00350
 MET00360
 MET00370
 MET00380
 MET00390
 MET00400
 MET00410
 MET00420
 MET00430
 MET00440
 MET00450
 MET00460
 MET00470
 MET00480
 MET00490
 MET00500
 MET00510
 MET00520
 MET00530
 MET00540

MTMPII WILL PRODUCE, ON THE PRINTER, A CONTOUR MAP OF ANY SINGLE PRECISION TWO DIMENSIONAL ARRAY.	
CALL MTMPII(Y,N,M,T,BND,AZ,BZ,AMIN,IJT,ICON)	
DESCRIPTION OF PARAMETERS	
Y - THE ARRAY TO BE CONTOURED. DIMENSIONED Y(N,M)	
N - NUMBER OF ROWS IN Y.	
M - NUMBER OF COLUMNS IN Y.	
T - ARRAY FOR PLOT TITLE. REAL*4. T(24).	
BND - BANDWIDTH FOR THE CONTOURING. IF BND IS ZERO A BANDWIDTH WILL BE CALCULATED AS FOLLOWS BND=(MAX(Y)-MIN(Y))/15.	
AZ - A LINEAR TRANSFORMATION MAYBE PERFORMED ON THE ARRAY Y OF THE FOLLOWING FORM AZ=Y+BZ. IF AZ=0 THEN AZ WILL BE COMPUTED SUCH THAT MAX(IMAX(Y)),IMIN(Y)) WILL BE LESS THAN 1, AND BZ WILL BE LEFT AS INPUT.	
BZ - SEE UNDER AZ	
AMIN - THE LEVEL AT WHICH COUTOURING WILL BEGIN. IF AMIN > MIN(Y) THEN AMIN WILL BE CALCULATED TO BE, WITH REFERENCE AT ZERO, THE NEXT LOWER CONTOUR LEVEL FROM MIN(Y) AS DETERMINED BY BND.	
IJT - IF IJT=0 AMIN WILL BE CALCULATED AS DESCRIBED IF IJT>0 AMIN WILL BE CALCULATED AS DESCRIBED IF IJT<0 AMIN WILL BE CALCULATED AS DESCRIBED	
ICON - IF ICON=0 NO CONTOURING WILL BE DONE BUT THE ARRAY Y WILL BE PRINTED IN THE PLOT FORMAT.	
REMARKS	
MTMPII REQUIRES A PRINTER WITH 132 PRINT POSITIONS. IF NECESSARY THE MAP WILL BE SEGMENTED COLUMNWISE. THE ROWS AND COLUMNS ARE NUMBERED ALONG THE EDGES. SO THAT A SEGMENTED MAP MAYBE EASILY JOINED TOGETHER. ONLY THREE SIGNIFICANT FIGURES WILL BE PRINTED AT EACH POINT. THE POSITION OF THE FIRST SIGNIFICANT DIGIT WILL BE DETERMINED BY MAX(IMAX(Y)),IMIN(Y)). THE PLOT WILL BE PRODUCED ON A INCH GRID. IT WILL BE ASSUMED THAT THE SPACING BETWEEN POINTS IN BOTH DIRECTIONS IS THE SAME AND EQUAL FOR ALL POINTS	
SUBROUTINES REQUIRED	
NONE	
METHOD	
THE CONTOUR LEVELS ARE DETERMINED BY SIMPLE LINEAR	


```

C C C C C C C
      INTERPOLATION FROM THE FOUR SURROUNDING PIONTS.
      *****
MET00550
MET00560
MET00570
MET00580
MET00590
MET00600
MET00610
MET00620

MTMPII SUBROUTINE FOR ONE-INCH GRID SPACING
OAKES CODE 5105 15 JAN 69

      *****
SUBROUTINE MTMPII(Y,N,M,T,BND,AZ,BZ,AMIN,IJT,ICON)
REAL*4 IH,KG,IJTJZ
DIMENSION A(140),B(140),C(140),D(140),IH(20),Y(N,M),TP(10),TPX(10)
Z,TPM(10),XMT(10),BTM(10),BTX(10),BT(10),KG(10),T(24)
DIMENSION E(140),F(140),G(140),H(140)

DATA DUE/4H /,EPL/4H+ /,EMI/4H- /,IH/1H0,1H /,1H1,1H /,1H2,
11H,1H3,1H /,1H4,1H,1H5,1H,1H6,1H,1H7,1H,1H8,1H /,1H9,1H /,KG/
21H0,1H1,1H2,1H3,1H4,1H5,1H6,1H7,1H8,1H9/,BLK/4H /

YMIN=Y(1,1)
YMAX=Y(1,1)
DO 20 I=1,M
DO 10 J=1,N
YMIN=AMIN1(YMIN,Y(J,I))
YMAX=AMAX1(YMAX,Y(J,I))
10 CONTINUE
20 DELY=YMAX-YMIN
IF(BND) 25,25,30
BND=DELY/15.0
25 IF (AMIN-YMIN) 31,31,32
30 IF (IJT) 33,32,33
32 PD=YMIN/BND
PF=ABS(PD-INT(PD))
IF (YMIN) 2,1,1
1 AMIN=YMIN-PF*BND
GO TO 33
2 AMIN=YMIN-(1.0-PF)*BND
33 AHLD=AZ
IF(AZ) 55,35,55
35 SM=AMAX1(ABS(YMIN),ABS(YMAX))
NS=0
40 NS=NS+1
SM=10.0*SM
IF(SM-1.0)40,50,45
45 NS=NS-1

```



```

SM=SM/10.0
IF(SM-1.0)50,50,50,45
50 AHLD=10.0*NS
55 HBND=BND/2.0
PRINT 70
PRINT 6,T
6 FORMAT(5X,24A4,/)
PRINT 57,AHLD,BZ
57 FORMAT(1H0,65H THE FOLLOWING TRANSFORMATION WAS PERFORMED ON THE IN
1 PUT MATRIX /5X,1H(,E12.5,8H*Y(I,J)+,E12.5,1H) //2X,73HAND THREE
2 DIGITS TO THE RIGHT OF THE DECIMAL POINT ARE PRINTED IN THE MAP )
MET0101010
MET0101020
MET0101030
MET0101040
MET0101050
MET0101060
MET0101070
MET0101080
MET0101090
MET0101100
MET0101110
MET0101120
MET0101130
MET0101140
MET0101150
MET0101160
MET0101170
MET0101180
MET0101190
MET0101200
MET0101210
MET0101220
MET0101230
MET0101240
MET0101250
MET0101260
MET0101270
MET0101280
MET0101290
MET0101300
MET0101310
MET0101320
MET0101330
MET0101340
MET0101350
MET0101360
MET0101370
MET0101380
MET0101390
MET0101400
MET0101410
MET0101420
MET0101430
MET0101440
MET0101450
MET0101460
MET0101470
MET0101480

C
54 PRINT 54,YMAX,YMIN
54 FORMAT(/4X,5HYMAX=,E15.7,5X,5HYMIN=,E15.7)
5 IF (ICON)5,58,5
5 PRINT 11,BND
11 FORMAT(2X,17H THE BAND WIDTH IS,E12.5,6H UNITS //4X,14H CONTOUR LEVE
1LS
I=0
YTOP=AMIN
IF(ABS(YMIN-YMAX)-100.0*BND)53,53,58
53 YB=YTOP
YTOP=YTOP+BND
I=I+1
J=MOD(I,20)
ITJZ=IH(J)
IF(YB-YMAX)59,58,58
59 PRINT 61,YB,YTOP,ITJZ
61 FORMAT(/4X,E10.3,4H TO ,E10.3,2H =,1X,A1)
GO TO 53
58 NCCP=0
NCP=0
PRINT 70
70 FORMAT(1H1)
PRINT 6,T
NLINE=0
NCCP=NCP+1
NCP=NCP+13
73 IF(NCP-M)80,80,75
75 NCP=M
80 CONTINUE
J=-2
NLINE=NLINE+1
LLINE=NLINE+1
C SET UP HEADING
85 IF(NCCP-1) 85,85,90
90 J=-1
DO 100 I = 1,135

```



```

      A(I)=BLK
      B(I)=BLK
      H(I)=BLK
100  CONTINUE
110  DO 160 L=NCCP,NCP
      J=J+8
      IF(KI-100) 130,120,120
120  LL=KI/100
      A(J)=KG(LL+1)
      KI=KI-100*LL
      GO TO 135
130  A(J)=KG(1)
135  J=J+1
      IF(KI-10) 150,140,140
140  LL=KI/10
      A(J)=KG(LL+1)
      KI=KI-10*LL
      GO TO 155
150  A(J)=KG(1)
155  J=J+1
      A(J)=KG(KI+1)
160  CONTINUE FIRST ROW OF ARRAY
      C SETUP
      GO TO 260
170  NLINE=NLINE+1
      LLINE=N-NLINE+1
      IF(NLINE-N) 180,180,380
180  DO 190 I=1,135
      A(I)=BLK
      B(I)=BLK
      C(I)=BLK
      D(I)=BLK
      E(I)=BLK
      F(I)=BLK
      G(I)=BLK
      H(I)=BLK
190  CONTINUE
195  IF (ICON)195,260,195
      NCV=NCCP-1
      J=4
      IF(NCY)200,200,210
200  J=5
210  NCV=NCV+1
      IF(NCV-NCP) 220,220,260
220  IF(NCV-M) 230,260,260
230  NLINE=NLINE-1
      YD1=Y(NLINE,NCY)-Y(NLINE+1,NCY)

```

```

MET01490
MET01500
MET01510
MET01520
MET01530
MET01540
MET01550
MET01560
MET01570
MET01580
MET01590
MET01600
MET01610
MET01620
MET01630
MET01640
MET01650
MET01660
MET01670
MET01680
MET01690
MET01700
MET01710
MET01720
MET01730
MET01740
MET01750
MET01760
MET01770
MET01780
MET01790
MET01800
MET01810
MET01820
MET01830
MET01840
MET01850
MET01860
MET01870
MET01880
MET01890
MET01900
MET01910
MET01920
MET01930
MET01940
MET01950
MET01960

```



```

YD2=Y(NLINE,NCY+1)-Y(NLINE+1,NCY+1)
TP(1)=Y(NLINE,NCY)-0.125*YD1
TPX(1)=Y(NLINE,NCY)-0.250*YD1
TPM(1)=Y(NLINE,NCY)-0.375*YD1
XMT(1)=Y(NLINE,NCY)-0.500*YD1
BTM(1)=Y(NLINE,NCY)-0.625*YD1
BTX(1)=Y(NLINE,NCY)-0.750*YD1
BT(1)=Y(NLINE,NCY)-0.875*YD1
TPX(10)=Y(NLINE,NCY+1)-0.125*YD2
TPM(10)=Y(NLINE,NCY+1)-0.250*YD2
XMT(10)=Y(NLINE,NCY+1)-0.375*YD2
BTM(10)=Y(NLINE,NCY+1)-0.500*YD2
BTX(10)=Y(NLINE,NCY+1)-0.625*YD2
BT(10)=Y(NLINE,NCY+1)-0.750*YD2
NLINE=NLINE+1
D1=0.1***(TP(10)-TP(1))
D2=0.1***(TPX(10)-TPX(1))
D3=0.1***(TPM(10)-TPM(1))
D4=0.1***(XMT(10)-XMT(1))
D5=0.1***(BTM(10)-BTM(1))
D6=0.1***(BTX(10)-BTX(1))
D7=0.1***(BT(10)-BT(1))
DO 240 I=2,9
TP(I)=TP(I-1)+D1
TPX(I)=TPX(I-1)+D2
TPM(I)=TPM(I-1)+D3
XMT(I)=XMT(I-1)+D4
BTM(I)=BTM(I-1)+D5
BTX(I)=BTX(I-1)+D6
BT(I)=BT(I-1)+D7
CONTINUE
DO 250 I=1,10
J=J+1
I1=MOD(IFIX((TP(I)-AMIN)/BND),20)+1
I2=MOD(IFIX((TPX(I)-AMIN)/BND),20)+1
I3=MOD(IFIX((TPM(I)-AMIN)/BND),20)+1
I4=MOD(IFIX((XMT(I)-AMIN)/BND),20)+1
I5=MOD(IFIX((BTM(I)-AMIN)/BND),20)+1
I6=MOD(IFIX((BTX(I)-AMIN)/BND),20)+1
I7=MOD(IFIX((BT(I)-AMIN)/BND),20)+1
A(J)=IH(I1)
B(J)=IH(I2)
C(J)=IH(I3)
D(J)=IH(I4)
E(J)=IH(I5)
F(J)=IH(I6)
G(J)=IH(I7)

```

```

MET01970
MET01980
MET01990
MET02000
MET02010
MET02020
MET02030
MET02040
MET02050
MET02060
MET02070
MET02080
MET02090
MET02100
MET02110
MET02120
MET02130
MET02140
MET02150
MET02160
MET02170
MET02180
MET02190
MET02200
MET02210
MET02220
MET02230
MET02240
MET02250
MET02260
MET02270
MET02280
MET02290
MET02300
MET02310
MET02320
MET02330
MET02340
MET02350
MET02360
MET02370
MET02380
MET02390
MET02400
MET02410
MET02420
MET02430
MET02440

```



```

250 CONTINUE
260 GO TO 210
265 NCY=NCCP-1
270 J=-2
275 IF(NCY) 265,265,270
280 J=-1
285 GO TO 330
290 NCY=NCY+1
295 IF(NCY-NCP) 280,280,310
300 J=J+7
305 THLD=AHLD*Y(NLINE,NCY)+BZ
310 IF(THLD) 285,290,290
315 H(J)=EMI
320 GO TO 295
325 H(J)=EPL
330 NUM=INT(ABS(THLD-INT(THLD)))*1000.0+0.5)
335 NDS=100
340 DO 300 KK=1,3
345 J=J+1
350 KI=NUM/NDS
355 H(J)=KG(KI+1)
360 NUM=NUM-KI*NDS
365 NDS=NDS/10
370 CONTINUE
375 GO TO 270
380 IF(NCP-M) 360,320,320
385 IF(J-127)330,330,360
390 J=J+3
395 KI=NLINE
400 IF(KI-100) 340,335,335
405 LL=KI/100
410 H(J)=KG(LL+1)
415 KI=KI-100*LL
420 GO TO 343
425 H(J)=KG(1)
430 J=J+1
435 IF(KI-10) 350,345,345
440 LL=KI/10
445 H(J)=KG(LL+1)
450 KI=KI-10*LL
455 GO TO 355
460 H(J)=KG(1)
465 J=J+1
470 H(J)=KG(KI+1)
475 J=J-5
480 IF(NCY-1) 270,270,360
485 IF(NLINE-1)362,362,368
490 PRINT 370,(A(I),I=1,132),(B(IP1),IP1=1,132),(H(IP2),IP2=1,132)

```

```

MET02450
MET02460
MET02470
MET02480
MET02490
MET02500
MET02510
MET02520
MET02530
MET02540
MET02550
MET02560
MET02570
MET02580
MET02590
MET02600
MET02610
MET02620
MET02630
MET02640
MET02650
MET02660
MET02670
MET02680
MET02690
MET02700
MET02710
MET02720
MET02730
MET02740
MET02750
MET02760
MET02770
MET02780
MET02790
MET02800
MET02810
MET02820
MET02830
MET02840
MET02850
MET02860
MET02870
MET02880
MET02890
MET02900
MET02910
MET02920

```



```

368 GO TO 170
    PRINT 370, (A(I), I=1,132), (B(IP1), IP1=1,132), (C(IP2), IP2=1,132),
    1(D(IP3), IP3=1,132), (E(IP4), IP4=1,132), (F(IP5), IP5=1,132),
    2(G(IP6), IP6=1,132), (H(IP7), IP7=1,132)
370 FORMAT(132A1)
380 GO TO 170
    DO 390 I=1,135
    A(I)=BLK
    B(I)=BLK
    C(I)=BLK
    D(I)=BLK
390 CONTINUE
    J=-2
    IF(NCCP-1) 395,395,400
    J=-1
    DO 430 L=NCCP,NCP
    J=J+8
    KI=L
    IF(KI-100) 410,405,405
    LL=KI/100
    C(J)=KG(LL+1)
    KI=KI-100*LL
    GO TO 412
    C(J)=KG(1)
    J=J+1
    IF(KI-10) 420,415,415
    LL=KI/10
    C(J)=KG(LL+1)
    KI=KI-10*LL
    GO TO 422
    C(J)=KG(1)
    J=J+1
    C(J)=KG(KI+1)
    CONTINUE
    PRINT 370, (B(IP1), IP1=1,132), (C(IP2), IP2=1,132)
    IF(NCP-M)60,500,500
500 RETURN
    END

```

```

MET02930
MET02940
MET02950
MET02960
MET02970
MET02980
MET02990
MET03000
MET03010
MET03020
MET03030
MET03040
MET03050
MET03060
MET03070
MET03080
MET03090
MET03100
MET03110
MET03120
MET03130
MET03140
MET03150
MET03160
MET03170
MET03180

```

```

MET03200
MET03210
MET03220
MET03230
MET03240
MET03250
MET03260
MET03270
MET03280
MET03290
MET03300

```

```

C000021
C .....
C SUBROUTINE GAUSS
C .....
C PURPOSE
C COMPUTES A NORMALLY DISTRIBUTED RANDOM NUMBER WITH A GIVEN
C .....
GAUS 10
GAUS 20
GAUS 30
GAUS 40
GAUS 50
GAUS 60
GAUS 70

```


CCCCCCCCCCCCCCCCCCCCCCCCCCCCCCCCCCCCCCCCCCCCCCCCCCCCCCCCCCCC

```
SUBROUTINE RANDU
PURPOSE
  COMPUTES UNIFORMLY DISTRIBUTED RANDOM REAL NUMBERS BETWEEN
  0 AND 1.0 AND RANDOM INTEGERS BETWEEN ZERO AND 2**31. EACH
  ENTRY USES AS INPUT AN INTEGER RANDOM NUMBER AND PRODUCES
  A NEW INTEGER AND REAL RANDOM NUMBER.
USAGE
  CALL RANDU(IX,IY,YFL)
DESCRIPTION OF PARAMETERS
  IX - FOR THE FIRST ENTRY THIS MUST CONTAIN ANY ODD INTEGER
  NUMBER WITH NINE OR LESS DIGITS. AFTER THE FIRST ENTRY,
  IX SHOULD BE THE PREVIOUS VALUE OF IY COMPUTED BY THIS
  SUBROUTINE.
  IY - A RESULTANT INTEGER RANDOM NUMBER REQUIRED FOR THE NEXT
  ENTRY TO THIS SUBROUTINE. THE RANGE OF THIS NUMBER IS
  BETWEEN ZERO AND 2**31
  YFL-- THE RESULTANT UNIFORMLY DISTRIBUTED, FLOATING POINT,
  RANDOM NUMBER IN THE RANGE 0 TO 1.0
REMARKS
  THIS SUBROUTINE IS SPECIFIC TO SYSTEM/360 AND WILL PRODUCE
  2**29 TERMS BEFORE REPEATING. THE REFERENCE BELOW DISCUSSES
  SEEDS (65539 HERE), RUN PROBLEMS, AND PROBLEMS CONCERNING
  RANDOM DIGITS USING THIS GENERATION SCHEME. MACLAREN AND
  MARSAGLIA, JACM 12, P. 83-89, DISCUSS CONGRUENTIAL
  GENERATION TYPE, ONE FILLING A TABLE AND ONE PICKING FROM THE
  TABLE, IS OF BENEFIT IN SOME CASES. 65549 HAS BEEN
  SUGGESTED AS A SEED WHICH HAS BETTER STATISTICAL PROPERTIES
  FOR HIGH ORDER BITS OF THE GENERATED DEVIATE.
  SEEDS SHOULD BE CHOSEN IN ACCORDANCE WITH THE DISCUSSION THAT
  GIVEN IN THE POINT RANDOM NUMBERS ARE DESIRED, AS ARE
  IF FLOATING POINT RANDU, THE RANDOM CHARACTERISTICS OF THE
  AVAILABLE FROM RANDU, ARE MODIFIED AND IN FACT THESE
  FLOATING POINT DEVIATES ARE HAVING A TRAILING LOW
  DEVIATES HAVE HIGH PROBABILITY OF HAVING A TRAILING LOW
  ORDER ZERO BIT IN THEIR FRACTIONAL PART.
SUBROUTINES AND FUNCTION SUBPROGRAMS REQUIRED
  NONE
METHOD
  POWER RESIDUE METHOD DISCUSSED IN IBM MANUAL C20-8011,
  RANDOM NUMBER GENERATION AND TESTING
```



```

C .....RAND 520
C .....RAND 530

SUBROUTINE RANDU(IX,IY,YFL)
  IY=IX*65539
  IF(IY) 5,6,6
  IY=IY+2147483647+1
5  YFL=IY
6  YFL=YFL*.4656613E-9
  RETURN
END

RAND 540
RAND 550
RAND 560
RAND 570
RAND 580
RAND 590
RAND 600

```


BIBLIOGRAPHY

1. Caulfield, H. J. and Lee, Sun, The Applications of Holography, John Wiley and Sons, 1970.
2. Ellis, B. K. and Furey, R. J., Wing-Body Interactions at a Mach Number of 9.5., Naval Ship Research and Development Center Report 2564, Aerodynamics Laboratory Research and Development Report 1133, September 1967.
3. Jagota, R. C., The Application of Holographic Interferometry to the Determination of the Flow Field Around a Right Circular Cone at Angle of Attack, Aeronautical Engineer Thesis, Naval Postgraduate School, December 1970.
4. Jagota, R. C. and Collins, D. J., "Finite Fringe Holographic Interferometry Applied to a Right Circular Cone at Angle of Attack", to be published in Journal of Applied Mechanics.
5. Kaufman, L. G. II and Meckler, L., Pressure and Heat Transfer Measurements at Mach 5 and 8 for a Fin-Flat Plate Model, Technical Documentary Report No. ASD-TDR 63-235, April 1963.
6. Kaufman, L. G. II, Pressure Distributions and Oil Film Photographs for Mach 5 Flows Past Fins Mounted on a Flat Plate, Technical Documentary Report No. ASD-TDR-63-755, September 1963.
7. Landenberg, R. W., et. al., ed., Physical Measurements in Gas Dynamics and Combustion, Princeton University Press, 1954.
8. Liepmann, H. W., and Roshko, A., Elements of Gas Dynamics, p. 165, John Wiley and Sons, Inc., 1957.
9. Maldonado, C. D., Caran, A. P., and Olsen, H. N., "New Method for Obtaining Emission Coefficients from Emitted Spectral Intensities. Part I--Circularly Symmetric Light Sources.", Journal of the Optical Society of America, Vol. 55, No. 10, pp. 1247-1254, October 1965.
10. Maldonado, C. D., "Note on Orthogonal Polynomials Which Are 'Invariant in Form' to Rotations of Axis", Journal of Mathematical Physics Vol. 6, No. 12, pp. 1935-1938, December 1965.
11. Maldonado, C. D. and Olsen, H. N., "New Method for Obtaining Emission Coefficients from Emitted Spectral Intensities. Part II--Asymmetrical Sources", Journal of the Optical Society of America, Vol 56, No. 10, pp. 1305-1313, October 1966.
12. Matulka, R. D., The Application of Holographic Interferometry to the Determination of Asymmetric Three-Dimensional Density Fields in Free Jet Flow, Ph. D. Thesis, Naval Postgraduate School, June, 1970.
13. Matulka, R. D. and Collins D. J., "Determination of Three-Dimensional Density Fields from Holographic Interferograms", Journal of Applied Physics, Vol. 42, No. 3, March 1971.

14. Okayama, H. and Emori, Y., "Polarization Effects in Holography", Applied Physics Letters, Vol. 19, No. 9, pp. 359-360, 1 November 1971.
15. Olsen, H. N., Maldonado, C. D., Duckworth, G. D., and Caron, A. P., Investigation of the Interaction of an External Magnetic Field with an Electric Arc, Aerospace Research Laboratories Report ARL 66-0016, January 1966.
16. Olsen, H. N., Maldonado, C. D., and Duckworth, G. D., "A Numerical Method for Obtaining Internal Emission Coefficients from Externally Measured Spectral Intensities of Asymmetrical Plasmas", J. Quant. Spectrosc. Radiat. Transfer, Vol. 8, pp. 1419-1430, 1968.
17. Ragent, B. and Brown, R. M., editors, Holographic Instrumentation Applications, Conference held at Ames Research Center, Moffett Field, California, NASA Sp-248, January 13-14, 1970.
18. Roe, P. L., Exploratory Flow Measurements in the Wing-Body Junction of a Possible Mach Four Vehicle, Royal Aircraft Establishment Technical Report No. 65257, November 1965.
19. Polutchko, R. J., Hypersonic Flow Field About a Blunt Slab Wing at Angle of Attack: Phase I, Aerospace Research Laboratories 64-213, December 1964.
20. Stewartson, K. and Treadgold, D. A., "Wing-Body Interference at Supersonic Speeds", Transonic Aerodynamics, AGARD Conference Proceedings No. 35, pp. 19-1--19-9, September 1968.
21. Stewartson, K., On Wing-Body Interference in Supersonic Flow, Aeronautical Research Council 27-715, 9 February 1966.
22. Stollery, J. K., Hypersonic Viscous Interaction--An Experimental Investigation of Flow over Flat Plates at Incidence and Around an Expansion Corner, Aerospace Research Laboratories 70-0125, July 1970.
23. Thomas, J. P., Investigation of the Pressure Distribution on a Blunt-Fin Blunt-Plate Combination at a Mach Number of 11.26, Aerospace Research Laboratories 66-0142, July 1966.
24. Thomas, J. P., Flow Investigation About a Fin-Plate Model at a Mach Number of 11.26, Aerospace Research Laboratories 67-0188, September 1967.
25. Weirich, R. L. and Vahl, W. A., Flow-Field Properties Near an Arrow-Wing-Body Model at Mach Numbers of 1.60, 2.36, and 2.96, NASA Technical Note D-4809, October 1968.
26. Winkelmann, A. E., "Flow Visualization Studies of a Fin Protuberance Partially Immersed in a Turbulent Boundary Layer at Mach 5", United States Naval Ordnance Laboratory NOLTR-70-93, 20 May 1970.
27. Winkelmann, A. E., "Aerodynamic Interaction Phenomena Produced by a Fin Protuberance Partially Immersed in a Turbulent Boundary Layer at Mach 5", AGARD Conference Proceedings No. 71, September 1970.

INITIAL DISTRIBUTION LIST

	No. Copies
1. Defense Documentation Center Cameron Station Alexandria, Virginia 22314	2
2. Library, Code 0212 Naval Postgraduate School Monterey, California 93940	2
3. Chairman, Department of Aeronautics Naval Postgraduate School Monterey, California 93940	1
4. Professor D. J. Collins, Code 57Co Department of Aeronautics Naval Postgraduate School Monterey, California 93940	1
5. LT Robert W. Heyer, USN 10811 Spring Lane Lemoore, California 93245	1

DOCUMENT CONTROL DATA - R & D

(Security classification of title, body of abstract and indexing annotation must be entered when the overall report is classified)

1. ORIGINATING ACTIVITY (Corporate author) Naval Postgraduate School Monterey, California 93940		2a. REPORT SECURITY CLASSIFICATION Unclassified	
		2b. GROUP	
3. REPORT TITLE Holographic Interferometry of The Flow Field Between a Fin And Flat Plate			
4. DESCRIPTIVE NOTES (Type of report and, inclusive dates) Master's Thesis; (March 1972)			
5. AUTHOR(S) (First name, middle initial, last name) Robert Ward Heyer			
6. REPORT DATE March 1972		7a. TOTAL NO. OF PAGES 178	7b. NO. OF REFS 27
8a. CONTRACT OR GRANT NO.		9a. ORIGINATOR'S REPORT NUMBER(S)	
b. PROJECT NO.			
c.		9b. OTHER REPORT NO(S) (Any other numbers that may be assigned this report)	
d.			
10. DISTRIBUTION STATEMENT Approved for public release; distribution unlimited.			
11. SUPPLEMENTARY NOTES		12. SPONSORING MILITARY ACTIVITY Naval Postgraduate School Monterey, California 93940	
13. ABSTRACT <p>This study was an attempt to map the density field in a fin-flat plate junction three-dimensionally using holographic interferometry. This investigation has extended the density studies by Matulka [12, 13] and Jagota [3, 4] to include, for the first time, interferometric fringe information obtained through a transparent model in supersonic flow. The fringe information was then inverted by a FORTRAN computer program to produce a plot of the density field around the model. The feasibility of the method was demonstrated.</p> <p>The factors which are thought to have limited the success of the experiment include vibration of the model, fluctuations of the tunnel flow and the fact that the model was somewhat too large in relation to the size of the wind tunnel test section. Schlieren photography was used to look through and around the model and to verify that the same flow was established as was reported by Thomas [23, 24] and Winkelmann [26, 27].</p> <p>The data reduction of holographic interferograms was, for the first time, accomplished using photographic enlargements. This technique is considered to be much easier and more accurate than the one used in the previous investigations. However, the data reduction step, because of the time and labor involved, is considered to be the rate controlling process of the whole analysis.</p>			

14

KEY WORDS

LINK A

LINK B

LINK C

ROLE

WT

ROLE

WT

ROLE

WT

fin-flat plate flow field

wing-root flow field

holography

three-dimensional density field

three-dimensional flow field

fin

flat plate

interferogram

flow field

fin flat plate junction

wing root junction

holographic interferometry

supersonic flow

Thesis 24 JUL 73 213550
H52635 Heyer 21616
c.1 Holographic inter-
ferometry of the flow
field between a fin and
flat plate.

Thesis 135352
H52635 Heyer
c.1 Holographic inter-
ferometry of the flow
field between a fin and
flat plate.

24 JUL 73 21616

Thesis 135352
H52635 Heyer
c.1 Holographic inter-
ferometry of the flow
field between a fin and
flat plate.

thesH52635

Holographic interferometry of the flow f



3 2768 001 91944 2

DUDLEY KNOX LIBRARY